AN ABSTRACT OF THE DISSERTATION OF

David J. Bettinardi for the degree of Doctor of Philosophy in Nuclear Engineering presented on July 31, 2020.

Title: Process Optimization in the Chemical Life Cycle of Accelerator-Produced, Low Specific Activity ^{99}Mo

Abstract approved: _____

Alena Paulenova

Global efforts to support non-uranium approaches for ^{99}Mo production, due to the proliferation risks associated with ^{235}U fission-based production methods, have recently taken huge strides towards fruition. Several linear accelerator-based methods are currently in late-stage development that can produce low specific activity ^{99}Mo from enriched $^{98/100}$Mo targets. The development of these technologies requires new chemical processing and purification schemes that emphasize low-waste recycling of the expensive, enriched Mo material. This dissertation arranges the results from three studies investigating parts of Mo chemical life cycle during accelerator-production of ^{99}Mo.

The first chapter of this work provides background information to some of the work that has already been accomplished towards production of commerical ^{99}Mo, with an emphasis on acclerator-production strategies. This chapter contextualizes the individual objectives of the dissertation within the full chemical cycle of ^{99}Mo. The subsequent chapters discuss results from three studies aimed at specific parts of this chemical cycle while including additional background information where needed for perspective. The first of these studies is a fundamental exploration into the chemical thermodynamics of Mo(VI) in aqueous solutions where high Mo concentrations are present. In this work, three polyoxometalate Mo species were identified and their thermodynamic formation constants were calculated using spectrophotometric data and equilibrium modeling. These results provide new knowledge about Mo speciation during

molybdenum recycling and purification schemes that are currently used during the recycling of enriched Mo targets.

The second and third projects of this dissertation deliver chemical flowsheets based on laboratory-scale experiments for the purification and recycling of Mo targets. In the first of these studies, two separation methods are introduced for the purification of Mo-oxide target material. Rhenium (Re), a frequent contaminant in Mo, is an especially critical element to detect and separate due the neutron activation of short-lived radioisotopes $^{186/188}$Re that interfere with the radiopurity of the ^{99m}Tc product eluted from low specific activity generators. These methods are based on solvent extraction or chromatographic extraction of Re from the dense Mo matrix. Instrument detection limits investigated and optimized to enable detection of ultratrace quantities of Re. The final project offers a strategy to recycle Mo from the solidified waste stream of some low specific activity generator designs. Recovering Mo from superabsorbant polymer waste of is crucial for maintaining the economic feasability accelerator-produced ^{99}Mo. The results of this work provide a simplified procedure for near-quantitative recovery of Mo as well as some preliminary data on its purification from organic contaminants.

Process Optimization in the Chemical Life Cycle of Accelerator-Produced, Low Specific Activity ^{99}Mo

by
David J. Bettinardi

A DISSERTATION

submitted to

Oregon State University

in partial fulfillment of
the requirements for the
degree of

Doctor of Philosophy

Presented July 31, 2020
Commencement June 2021

Doctor of Philosophy dissertation of David J. Bettinardi presented on July 31, 2020

APPROVED:

Major Professor, representing Nuclear Engineering

Head of the School of Nuclear Science & Engineering

Dean of the Graduate School

I understand that my dissertation will become part of the permanent collection of Oregon State University libraries. My signature below authorizes release of my dissertation to any reader upon request.

David J. Bettinardi, Author

ACKNOWLEDGEMENTS

I would like to express my deepest gratitude to my graduate school advisor and mentor, Dr. Alena Paulenova, who has provided me with every possible opportunity to succeed and whose unwavering support and guidance has been vital to my progress. My growth in this professional endeavor has relied on her trust and encouragement and I am extremely grateful for it.

Thank you, Dr. Peter Tkac, my mentor and employer at Argonne National Laboratory who has provided me with not only the underlying goals of my dissertation research but also with the invaluable instruction and critical oversight of my work that I needed to develop my skills as a scientist and engineer.

Thank you to my family, most especially Cheryl, Nicole, Alex, Andrea, and Mossimo (world's greatest dog), who have given me support and stability when it was needed most.

Thank you to my undergraduate mentor, Dr. Barry Alto, who has been a lasting role model for ethics in science and in life.

To my friends and colleagues, Gabi, Will, Yana, Clinton, and Stas, I was so lucky to have shared this experience with such generous and kind people who have helped at every opporunity no matter the time of day.

CONTRIBUTION OF AUTHORS

Dr. Alena Paulenova (OSU) assisted in the editing of each chapter and in the data interpretation in chapters 2 and 3.

In chapters 2, 3, and 4, Dr. Peter Tkac (ANL) edited the manuscripts and provided guidance on experimental design, modeling, and data analysis.

In chapter 3, Dr. M. Alex Brown (ANL) edited the maniscript, assisted with data interpretation, and performed parallel research on the solvent extraction system. Yifen Tsai (ANL) performed the ICP-MS analysis and contributed the instrument operating parameters for the manuscript.

Jim Byrnes (ANL) helped with obtaining radiochemical tracers used for experiments in chapters 3 and 4. Madeline Eddy (CSM) assisted during the kinetics experiments in chapter 4.

All other data collection, data visualization, modeling, and manuscript preparation was done by the author.

TABLE OF CONTENTS

TABLE OF CONTENTS (Continued)

TABLE OF CONTENTS (Continued)

LIST OF FIGURES

Figures Page

LIST OF FIGURES (Continued)

Figures Page

LIST OF FIGURES (Continued)

Figures Page

LIST OF TABLES

Tables Page

ACRONYMS AND ABBREVIATIONS

LEU	low-enriched uranium
HEU	highly-enriched uranium
DOE	U.S. Department of Energy
SPECT	single-photon emission computed tomography
AHM	ammonium heptamolybdate
SHINE	subcritical hybrid intense neutron emitter
eMo	enriched molybdenum
TD	theoretical density
SF	separation factor
DF	decontamination factor
PUREX	plutonium-uranium reduction extraction
MOEX	molybdenum extraction
LSA	low specific activity
ANL	Argonne National Laboratory
NNSA	National Nuclear Security Administration
ABEC	aqueous biphasic extraction chromatography
TBP	tri-*n*-butyl phosphate
NMR	nuclear magnetic resonance
AMUSE	Argonne's Model for Universal Solvent Extraction
NAA	Neutron activation analysis
HPGe	High-purity germanium
CCV	continuous calibration verification
O/A	organic-to-aqueous phase ratio
CSIR	coated solvent-impregnated resin
SAP	superabsorbent polymer
DR	deswelling ratio
TCE	tetrachloroethylene

This work is dedicated to my parents, Karen and David.

CHAPTER 1 LITERATURE REVIEW

1.1 Background

The ^{99m}Tc generator was first developed at Brookhaven National Labs in 1957, sparking a revolution in medical diagnostic imaging and leading ^{99m}Tc to become the most widely used isotope in nuclear medicine. Its longer-lived parent, ^{99}Mo, is used as the transportable isotope that is shipped as the source of ^{99m}Tc, where they are later radiochemically separated and administered to patients for radioimaging. ^{99m}Tc is used in approximately 80 percent of all nuclear medicine procedures performed each year, bringing worldwide demand for ^{99}Mo to about 9,000 6-day Ci per week[1] [1]. Despite the growing popularity of ^{99m}Tc in medical applications, the U.S. has struggled to establish a domestic supplier of the parent ^{99}Mo. For the last 30 years, about 95% of the global ^{99}Mo supply has come from seven research reactors. Only five target processing facilities located in Canada, Europe, Australia, and South Africa have supplied ^{99}Mo to hospitals throughout the world. Presently, six of these reactors remain operational since the shutdown Canada's National Research Universal reactor in late 2016.

Historically, the majority (75%) of the total global supply of ^{99}Mo has been produced using high-enriched uranium (HEU) targets with the remaining 25% coming from low-enriched uranium (LEU) targets [2]. Due to non-proliferation concerns, the full conversion from HEU to LEU targets is underway for ^{99}Mo manufacturers worldwide. Unfortunately, the outcome of conversion from HEU has been projected to reduce total processing capacity for ^{99}Mo [1]. Under the provisions of the American Medical Isotopes Production Act of 2012 [3], U.S. research institutions and companies were instructed to comply with the phase-out of all U.S. government exports of HEU related to medical isotope production with a goal of full conversion to LEU by 2020. The bill also includes a directive for the U.S. Department of Energy (DOE) to support non-uranium approaches for ^{99}Mo production, which has recently taken huge strides towards fruition.

[1] A "6-day Ci" measurement is defined as the remaining ^{99}Mo activity on the sixth day after leaving the processing facility, which is the average time between its end of processing (EOP) and first use.

Much of the utility of the $^{99}Mo/^{99m}Tc$ system is due to the near-ideal decay chain depicted in Figure 1-1. ^{99}Mo ($t_{1/2}$ = 65.98 hr) decays to ^{99}Tc (17.8%) and ^{99m}Tc (82.2%), the latter of which is a metastable isomer whose relaxation is accompanied by low-energy gamma rays (140.5 keV and 143 keV). The principal photon of interest has nearly the same energy as diagnostic X-rays (140.5 keV, B.R. = 88.5%), making it ideal for medical imaging applications. Its relatively short halflive ($t_{1/2}$ = 6.01 hr) allows for same-day imaging while minimizing radiation exposure to the patient.

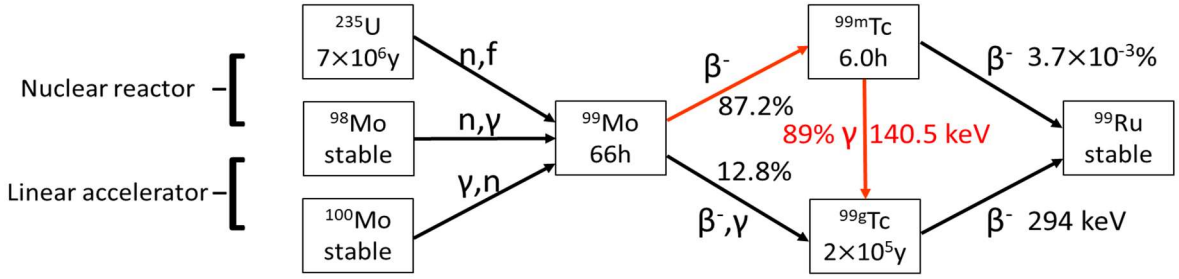

Figure 1-1. Decay scheme of ^{99}Mo and its daughters

In nuclear medicine, single-photon emission computed tomography (SPECT) is applied to visualize the ^{99m}Tc gamma emissions. SPECT is able to construct 3-dimensional images and can be applied *in vivo* for imaging of infections, cancers, ulcers, and other forms of disease [4]. ^{99m}Tc can be introduced directly to the patient body as sodium pertechnetate ($Na^{99m}TcO_4$), where the pertechnetate ion ($^{99m}TcO_4^-$) distributes throughout the body and equilibrates with extracellular space to allow for the real-time imaging of various physiological processes [4]. Furthermore, the chemical labeling of desired molecules with ^{99m}Tc is used to produce a wide array of radiopharmaceuticals with selective and targeted organ-specific behavior. Since the development of the ^{99m}Tc generator, the use $Na^{99m}TcO_4$ and ^{99m}Tc-radiopharmaceuticals has continued to grow in popularity due to its simplicity of usage and clinical effectiveness.

1.2 ^{99}Mo Production

The optimal strategy for $^{99}Mo/^{99m}Tc$ isotope production remains to be seen. While cyclotrons and compact linear accelerators are a reliable and mature technology for on-demand production, high-flux nuclear reactors can produce large quantities of high specific activities of

^{99}Mo. An expanded list of current and developing methods to produce ^{99}Mo/^{99m}Tc is provided in *Table 1-1*.

Table 1-1. Uranium and non-uranium methods to produce ^{99}Mo, data from Ref. [8-10]

Process	Nuclear Reaction	Cross-section
^{235}U production		
• High-enriched UO_2 • Low-enriched UO_2 • Natural U • U_3O_8 microspheres (NWMI) • Selective gas extraction (GA) • Superconducting e$^-$ beam (Niowave) • Tantalum neutron generator • U_3Si_2 • Subcritical Hybrid Intense Neutron Emitter (SHINE)	$^1n + {}^{235}\mathrm{U} \rightarrow {}^{99}\mathrm{Mo} + \mathrm{FP} + 2.5\ {}^1n$	σ_f = 568 b (Yield = 6.1%)
Non-uranium production		
• ^{98}Mo neutron activation (Northstar)	$^1n + {}^{98}\mathrm{Mo} \rightarrow {}^{99}\mathrm{Mo}$	σ_a = 0.14 b
• Photo-fission of ^{235}U	$\gamma + {}^{238}\mathrm{U} \rightarrow {}^{99}\mathrm{Mo} + \mathrm{FP} + 2\ {}^1n$	σ_f = 0.16 b
• Photo-transmutation neutron knockout (Northstar)	$\gamma + {}^{100}\mathrm{Mo} \rightarrow {}^{99}\mathrm{Mo} + {}^1n$	σ_f = 0.16 b
• Proton-induced reaction	$^2p + {}^{100}\mathrm{Mo} \rightarrow {}^{99}\mathrm{Mo} + {}^2p + {}^1n$	σ_a = 0.15 b
• Direct production of ^{99m}Tc	$^2p + {}^{100}\mathrm{Mo} \rightarrow {}^{99m}\mathrm{Tc} + 2\ {}^1n$	σ_a = 0.20 b

The traditional. uranium-based approach to ^{99}Mo production involves the thermal-neutron induced fission of ^{235}U, given by the reaction:

$$^{235}\mathrm{U} + {}^{1}\mathrm{n}_{\mathrm{thermal}} \rightarrow {}^{236}\mathrm{U}^* \rightarrow {}^{99}\mathrm{Mo} + {}^{134}\mathrm{Sn} + 3\ {}^1n \quad (1)$$

^{235}U fission generates a bimodal distribution of waste fission products (A = 80 to 160). Used as a means of producing ^{99}Mo, this method requires complex purification schemes to remove fission products and fission gasses (Kr and Xe). Immediately following irradiation, these highly radioactive targets must be cooled prior to shipment and still contain significant quantities of non-fissioned ^{235}U, raising proliferation concerns.

In a typical processing scheme for HEU and LEU targets (e.g. U_3Si_2, UO_2), the target meat is dissolved along with its Al cladding material using aqueous NaOH (~3M) solution [5]. The solution is filtered, collecting non-fissioned uranium, and this residue is dissolved using H_2O_2 and NaOH to collect the remaining Mo. During the alkaline dissolution, H_2O_2 is used as an oxidant to convert insoluble elemental Mo to the soluble oxidized MoO_4^- anion. Alkaline filtrates are run through a series of ion exchange columns before final conversion to solid ammonium heptamolybdate (AHM). Whether alkaline or acidic dissolution processes are used, the production of H_2 gas, fission gasses, and large waste volumes pose significant both safety and technological challenges for fission-based ^{99}Mo production routes [6,7].

^{99}Mo can also be produced through LEU fission without the use of a nuclear reactor [11]. The Subcritical Hybrid Intense Neutron Emitter (SHINE) system uses an accelerator-based, high output D-T (fusion) neutron generator as its neutron source to maintain subcritical neutron multiplication in aqueous LEU uranyl sulfate solutions [12]. The hybrid aspect of the approach combines the accessibility of accelerators with the high ^{99}Mo yield and specific activity of aqueous reactor technology. Despite these advantages, the purification of ^{99}Mo from aqueous reactors remains a challenge, due in part to the formation of fission gasses and the necessity of complex microfluidics equipment and protocols. A second aqueous reactor-based approach to nuclear reactor-free LEU fission uses a tantalum neutron generator. In this system, an electron accelerator incident on a solid Ta-converter generates Brehmsstrahlung photons with the concomitant release of neutrons by the (γ, n) and (γ, 2n) photonuclear reactions [11,13]. In addition to the considerations of the previously mentioned liquid reactor systems, the production of high energy photons must be accounted for in the device shielding.

Several non-uranium alternatives for production of ^{99}Mo are still under development, including direct production of ^{99m}Tc on-location with small medical cyclotrons using the ^{100}Mo(p, 2p)^{99m}Tc reaction [14,15]. After two 6-hour bombardments using medium-energy cyclotrons suitable for hospitals (200 μA and 15-30 MeV), approximately 70 Ci of ^{99m}Tc can be produced [16,17]. Two other non-uranium approaches that have recently become more commercially feasible are the electron accelerator-based production via bremsstrahlung photonuclear reaction ^{100}Mo(γ,n)^{99}Mo or the neutron capture ^{98}Mo(n,γ)^{99}Mo reaction. Neutron capture production

requires a large target due to the low neutron cross-section (σ_a = 0.14 b). Current estimates state that standard research reactor with a flux of 5x10^{13} n/cm^2·s can produce about 0.8 Ci/h of ^{99}Mo per 500 g of target [17]. Feasability studies for the neutron knockout method performed at Argonne National Laboratory achieved up to 3.6 mCi/kW-h-g for 99% enriched ^{100}Mo [17]. In either of these alternatives, enriched Mo (eMo; i.e. ^{98}Mo or ^{100}Mo) are required to produce significant activities of ^{99}Mo economically. Next to the economic advantages and proliferation-resistance of these methods, the use of non-uranium targets requires simpler and faster purification schemes and produces lower volumes of less radiotoxic waste.

1. 3 eMo Target Fabrication

The two main methods of interest for non-uranium production of ^{99}Mo are the ^{100}Mo(γ,n)^{99}Mo and ^{98}Mo(n,γ)^{99}Mo reactions. The former is performed using an electron accelerator and isotopically enriched ^{100}Mo sintered (29mm x 0.5mm or 26mm x 1.0mm) disk targets. Post-irradiation processing of these targets necessitates rapid target dissolution procedures to minimize the ^{99}Mo loss due to decay, which occurs at a rate of ~1% per hour [18]. However, high atom densities of eMo disks are important to achieve optimal irradiation yields. So the fast dissolution of a target due to its high porosity would typically be accompanied by a reduction in the target's theoretical density (TD). This problem was investigated to some extent in a series of studies at Argonne National Lab [18] but new target designs continue to be tested. This work is an important part in designing the fabrication conditions of the Mo targets.

Sintered eMo disk (wafer) targets for can be fabricated using the spray-dried powder technique [19]. This technique requires three main steps to accomplish:

(i) reduction of precursor Mo(VI) to elemental Mo
(ii) powder processing and spraying
(iii) pressing and sintering of powder into disks

The result is a high-density consolidated metal powder disks with tunable TD and porosity.

Powder metallurgy has numerous advantages over machining in the case of ^{100}Mo target preparation. First, very little material is wasted during fabrication which is important when

handling expensive eMo material. Traditional target manufacturing involves punching circular disks from sheet metal, followed by grinding and lapping until dimensional specifications are met. Conversely, the spray-dried powder method provides tight control of metal application, reducing material loss negligible quantities. The level of control available in powder metallurgy can pose challenges to ensuring that accelerator target specifications are met. Irradiation targets must meet a series of strict specifications including dimensional (thickness, diameter), morphological (flatness), and material (green density, porosity) characteristics. However, since powder metallurgy is in fact the most common method of producing Mo metal products, its optimization for meeting demanding manufacturer specifications has been studied in great detail [20].

Perhaps the most critical advantage of powder metallurgy is the ability to finely tune the porosity and particle size of the final product [21], since these are the factors most influencing dissolution kinetics. Preliminary results show that spray-dried Mo disks using 44 ± 149 μm size Mo metal particles can produce a 90% theoretical density (TD) sintered Mo disk with 5% open porosity, which is near the goal of 90% TD with 8-10% open porosity [18]. Spray-dried Mo disks showed very good dissolution rates up to 3 g/min, indicating that ideal properties are achievable.

Example spray-dried protocol:

1) Process $(NH_4)_6MoO_{24}{\cdot}4H_2O$ into MoO_3
    - Characterize, mill and sieve precursor powder
2) Reduce to MoO_3 to MoO_2 (Mo(VI) → Mo(IV))
    - Characterize, mill and sieve dioxide powder
3) Reduce MoO_2 to Mo metal (Mo(IV) → Mo(0))
    - Characterize, mill and sieve metal powder
4) Spray dry metal powder
    - Characterize and sieve spray-dried metal powder
5) Pre-sinter disk (~1500-1600ºC)
    - Characterize disks for dimensional specifications
6) Lubricate and press disk (1000 MPa)
    - Characterize disks for density and dimensional specifications
7) Sinter disk (~1500-1600ºC)
    - Characterize disks for density and dimensional specifications

Spheroidization of Mo metal particles, which improves flow characteristics, is also being investigated to facilitate the use of additive manufacturing (3D-printing). However, Mo disks have

been successfully produced with >90% TD, making them usable as electron accelerator irradiation targets and likely candidates for $^{100}Mo(\gamma,n)$ production of ^{99}Mo.

1.4 Post-irradiation Target Processing

To avoid ^{99}Mo loss due to decay (~1% per hour), it is important that post-irradiation processing of the targets occurs as quickly as possible, with a desired dissolution rate of >0.7 g/min [18]. The two main factors affecting dissolution time in Mo targets are the Mo particle size and open porosity. However, other factors such as pre-sinter and sinter conditions and pressing conditions also play a role [22]. Spray-dried Mo disks have the advantage of tunable porosity and particle sizes. The overall balance between porosity vs density ultimately impacts the dissolution time and irradiation time. For example, disks with very high packing densities may require less irradiation time but may not fully dissolve even after prolonged periods of time. Therefore, it is important that these factors are investigated with regard to the disk dissolution properties, as this will provide feedback on the feasibility of Mo targets.

Dissolution procedures of Mo disks occurs by oxidation with 30% or 50% H_2O_2 (70ºC) in a reaction kettle, forming peroxymolybdic(VI) acid [22]. Higher concentrations of H_2O_2 sharply increase the dissolution current ($I_0' >> I_0$) meaning that dissolution occurs more rapidly and violently at higher H_2O_2 [23]. A 50% H_2O_2 solution requires a stabilizer (such as Sn^{2+}) to prevent the spontaneous decomposition of hydrogen peroxide which is thermodynamically unstable at high concentrations (ΔH^0= -98.2 kJ/mol, ΔS = 70.5 J/mol·K). While adding a stabilizer allows higher peroxide concentration and therefore more rapid dissolution of Mo, its role as a potential impurity downstream must be taken into account.

The oxidation reaction is strongly exothermic, requiring active cooling with ethylene glycol to prevent boil-over or over-pressurization of the vessel due to O_2 release.

Simplified half-reactions:

$$Mo(0) - 6e^- \rightarrow Mo(VI) \quad (2)$$

$$3(H_2O_2 \rightarrow 2H^+ + O_2 + 2e^-) \quad (3)$$

Overall reaction:

$$2Mo_{(s)} + 10H_2O_2 \rightarrow [Mo_2O_3(O_2)_4(H_2O)_2]^{2-} + 2H_3O^+ + 5H_2O \quad (4)$$

Dissolution rates of Mo-disks also depend on the disk morphology and fabrication history. For example, high sintering factors and high theoretical densities can greatly reduce the dissolution rates, due to pore size and grain growth. In one report [22], the best conditions for quick dissolutions include high pre-sintering and low sintering temperatures, with the authors note that that there must be a compromise between high density targets and quick dissolution times. Upon complete dissolution of the Mo target, the solution is then heated to destroy and evaporate the remaining peroxide. Then potassium hydroxide (KOH) is added to the molybdate solution to precipitate Mo as K_2MoO_4:

$$2[Mo_2O_3(O_2)_4(H_2O)_2]^{2-} + 8KOH \rightarrow 4K_2MoO4^{-}\cdot(H_2O)_2 + 5O_2 \quad (5)$$

This precipitate is filtered under vacuum (~15 min) until dry. The sample is re-dissolved in KOH solution to prepare 0.2 g-M/mL K_2MoO_4 in 5M KOH. Processing times for the overall procedure at the Missouri Research Reactor (MURR) currently take about 5-6 hours to complete. However, this time was recently reduced in large-batch, lab-scale testing [18]. Total processing time for 50% H_2O_2 dissolution takes between 1-2 hours whereas that of 30% H_2O_2 takes 3-4 hours.

Prior to shipment, Mo solution must be purified to fit specifications. Significant quantities of impurities such as Zr and Nb are byproducts generated during the production of ^{99}Mo from irradiated Mo targets. This can be accomplished through coprecipitation with magnetite followed by filtration [24]. The presence of impurities in the final product may affect the decontamination factor of the ^{99m}Tc generator and purity of the final ^{99m}Tc product so they must be accounted for in each step.

1. 5 ^{99}Mo and ^{99m}Tc Separation and ^{99m}Tc Generator Systems

The separation factor (SF) for ^{99m}Tc/^{99}Mo in a generator must be as high as possible to avoid radiotoxic exposure to ^{99}Mo, which emits several medium-energy beta particle emissions during its decay. NRC regulations for the maximum administered dose to patients are 0.15 uCi of

^{99}Mo per mCi of ^{99m}Tc (10 C.F.R. § 35.204). The initial design of the ^{99}Mo/^{99m}Tc generator system developed in 1957 at Brookhaven National Laboratory consisted of a simple column apparatus containing the amphoteric absorbent material alumina (Al_2O_3) to retain Mo and Tc. Both the Tc and Mo form stable anionic species in mildly acidic aqueous solutions. A dilute nitric acid (HNO_3) was used to elute pertechnetate (TcO_4^-), while the molybdate (MoO_4^{2-}) species was retained on the column. The innovation of replacing dilute nitric acid with saline solution was the first milestone in the development towards modern generator designs, as it reduced the steps required for the safe intravenous administration of the ^{99m}Tc product [25].

Alumina's uptake capacity for molybdate ions, ~20 mg Mo per g Al_2O_3, introduced some limitations to this type of generator. When the specific activity of the ^{99}Mo is low (~10^3 Ci/g or 37 TBq/g) but a certain final activity of ^{99m}Tc activity is still required, larger alumina columns must

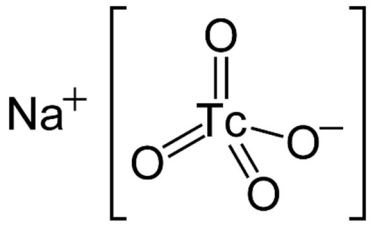

Figure 1-2. Coordination structure of the TcO_4^- anion with sodium counterion

be used to accommodate the larger volumes of Mo/Tc feed solution introduced to the column. Larger columns in turn require larger volumes of saline solution to elute Tc, which leads to a reduction in the activity concentration of the final ^{99m}Tc eluate. To avoid lengthy concentration steps of the rapidly-decaying product, the source of ^{99}Mo used with the alumina column must yield the highest specific activity of ^{99}Mo available [17]. Only the fission-produced ^{99}Mo (fission yield = 6%) was able to reach high enough specific activities, on the order of 10^4 Ci/g (370 TBq/g), suitable for alumina generator designs. Years later, a method for concentrating of ^{99m}Tc eluate was successfully developed for Tc/Mo generators, but the movement towards reducing the total number of steps required has so far precluded its mainstream adoption. Further approaches to optimization ^{99m}Tc generator performance involved resin-based research, such as the application of nanocrystalline γ-Al_2O_3 [26] or DOWEX [27] resins with higher sorption capacities.

Column chromatographic separation of Mo/Tc remains the method of choice for modern generator designs due to its overall simplicity, rapidity, cost, and very high decontamination factor (DF). Several alternative separation materials have been introduced over the years, including methyl-ethyl-ketone extraction, solid-phase column extraction, Zr-molybdate gel extraction, and electrochemical separation. Further research is required to make these methods feasible for routine operation.

1. 6 Molybdenum Extraction (MOEX) Process

Two main modes of production for use with the low specific activity (LSA) generator are the $^{100}Mo(\gamma,n)^{99}Mo$ and $^{98}Mo(n,\gamma)^{99}Mo$. Enriched ^{100}Mo or ^{98}Mo are required in both cases to produce significant activities of ^{99}Mo economically. Due to the high cost of enriched material ($500-1000/g for kilogram quantities), efficient recycling strategies for molybdenum need to be developed. The principle goals of the Mo recycle process are to maintain (i) high recovery yields, (ii) purity specifications, and (iii) recycled targets with similar properties of density, porosity, and dissolution rates.

Some Mo recycle processes have been suggested for which relatively poor recovery yields (85% [14], 87% [28]) were achieved. A precipitation technique was used on Mo targets irradiated at MURR and achieved 95% Mo recovery yields [29]. However, this methodology involves many steps and would be difficult to adapt as an automated chemical process. A new, high-efficiency method called the molybdenum extraction (MOEX) process has recently been developed at Argonne National Lab [17] [30] and implemented as a viable recycling strategy. The MOEX system relies on extraction of Mo dissolved in HCl using the neutral extracting ligand tri-*n*-butyl phosphate (TBP).

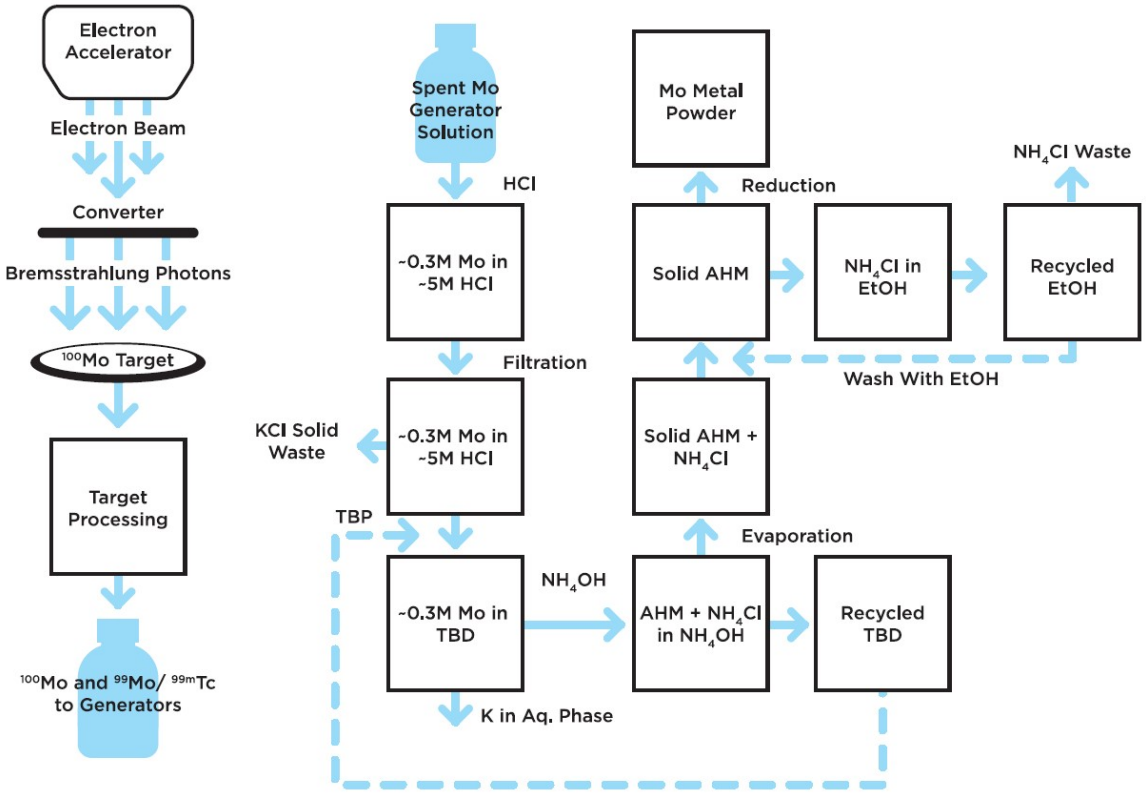

Figure 1-3. Diagram of electron accelerator production using ^{100}Mo (left) followed by the MOEX flowsheet (right), adapted from Ref. [17]

The extractability of metals by TBP, used primarily in the plutonium-uranium reduction extraction (PUREX) process for used nuclear fuel, was adapted for Mo extraction in spent generator solutions by Tkac *et al* [17]. Mo(VI) does not extract from nitric acid, but the ability of molybdic acid to associate with free chloride ions in HCl allows for the formation of neutral di-chloro species:

$$MoO_2^{2+} + 2Cl^- \leftrightarrow MoO_2Cl_2 \quad (6)$$

MOEX uses 30%-50% TBP in organic solvent to extract Mo(VI) in HCl followed by stripping of the metal back into the aqueous phase. Very high extraction yields were observed at 5M HCl and 0.45M Mo solution (95-97%) accompanied by low co-extraction of potassium.

In the next step, the Mo is stripped into a fresh aqueous phase using NH_4OH to produce ammonium heptamolybdate, $(NH_4)_6Mo_7O_{24}$. It was found that 5-20 seconds of contact in

centrifugal contactors was adequate to strip >99.8% of Mo from the organic phase. The solution containing ammonium heptamolybdate is dried in a rotary evaporater. The resulting solid is washed with EtOH to selectively dissolve the corrosive byproduct NH_4Cl, leaving solid ammonium heptamolybdate precipitate ready to be sent for processing at the target fabrication facility.

1. 7 Mo(VI) Aqueous Chemistry

Recent investigations of the extraction process indicate that the primary extracted Mo(VI) species by TBP is the di-chloro molybdenyl species MoO_2Cl_2. [31] However, the possibility of other extracted species exists, especially at high Mo concentrations where polynuclear species are known to form under lower acid conditions. A better understanding of Mo(VI) speciation at high Mo and HCl concentrations could help illuminate the extraction mechanisms involved in TBP-Mo extraction and lead to design improvements in the MOEX process.

Molybdenum's chemistry in aqueous media is notoriously complex, forming several mono- and polynuclear complexes concurrently. Mo is a group VI transition metal with most stable oxidation +6, which allows for relatively high degree of coordination in aqueous solutions [32]. The formation of the molybdate anion, MoO_4^{2-}, occurs at neutral and alkaline pH and provides high mobility of the metal in water. This characteristic imparts high bioavailablity of Mo which has led to its utility as an important biological catalyst for humans and other forms of life [33,34]. As the acidic proton concentrations in solution increase, molybdate begins to form various polyoxometalate species consisting of high-nuclearity complexes containing 7, 8, 24, or more monomer units. These structures are produced by Brønsted acid-base condensation-addition processes [35]. Figure 1-7 shows a speciation diagram for 10 mM Mo in a non-complexing acid, as calculated by thermodynamics constants.

The formation constants and equilibria of Mo in non-complexing acidic solutions are well-characterized by various authors. A summary of these, calculated by Cruywagen et al. [34,35], can found in Table 1-2.

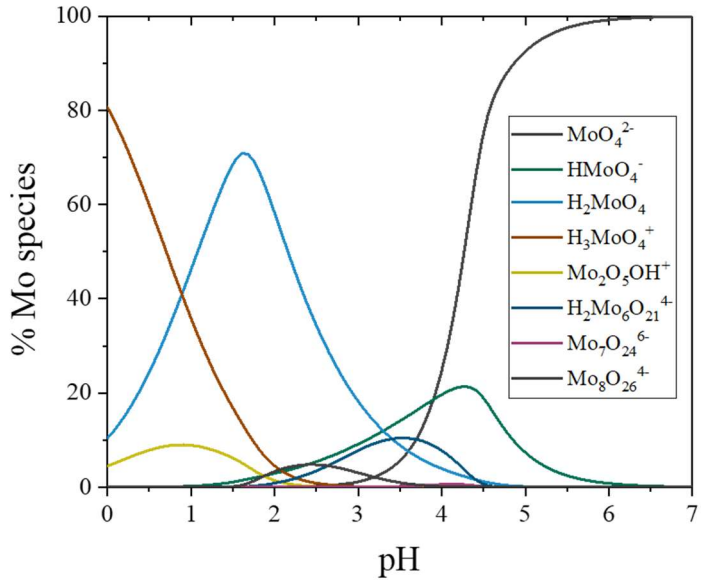

Figure 1-4. Example speciation diagram for ~0.01M Mo(VI) in $HClO_4$ as a function of pH

Table 1-2. Stability constants on Mo(VI) species in $HClO_4$ reported by [48]

Equilibrium	Log K_n
$MoO_4^{2-} + 3H^+ \leftrightarrow H_3MoO_4^+$	Log K_1 = 8.44
$MoO_4^{2-} + 3H^+ \leftrightarrow MoO_2OH^+ + H_2O$	Log K_2 = 8
$2MoO_4^{2-} + 5H^+ \leftrightarrow Mo_2O_5OH^+ + 2H_2O$	Log K_3 = 18
$2MoO_4^{2-} + 6H^+ \leftrightarrow Mo_2O_2(OH)_6^{2+}$	Log K_4 = 19
$7MoO_4^{2-} + 8H^+ \leftrightarrow Mo_7O_{24}^{6-} + 4H_2O$	Log K_5 = 52
$8MoO_4^{2-} + 12H^+ \leftrightarrow Mo_8O_{26}^{4-} + 6H_2O$	Log K_6 = 71
$18MoO_4^{2-} + 32H^+ \leftrightarrow Mo_{18}O_{56}^{4-} + 16H_2O$	Log K_7 = 171
$MoO_4^{2-} + H^+ \leftrightarrow HMoO_4^-$	Log K_8 = 3.57
$7MoO_4^{2-} + 9H^+ \leftrightarrow HMo_7O_{24}^{5-} + 4H_2O$	Log K_9 = 57
$7MoO_4^{2-} + 10H^+ \leftrightarrow H_2Mo_7O_{24}^{4-} + 4H_2O$	Log K_{10} = 60
$7MoO_4^{2-} + 11H^+ \leftrightarrow H_3Mo_7O_{24}^{3-} + 4H_2O$	Log K_{11} = 62
$7MoO_4^{2-} + 7H^+ \leftrightarrow Mo_7O_{24}^{7-} + 3H_2O$	Log K_{12} = 46
$6MoO_4^{2-} + 8H^+ \leftrightarrow H_2Mo_6O_{21}^{4-} + 3H_2O$	Log K_{13} = 49
$8MoO_4^{2-} + 11H^+ \leftrightarrow H_3Mo_8O_{28}^{5-} + 4H_2O$	Log K_{14} = 67
$13MoO_4^{2-} + 21H^+ \leftrightarrow HMo_{13}O_{42}^{5-} + 10H_2O$	Log K_{15} = 119
$MoO_4^{2-} + 2H^+ \leftrightarrow MoO_3$	Log K_{16} = 7.2
$MoO_4^{2-} + 2H^+ \leftrightarrow H_2MoO_4$	Log K_{17} = 7.36

The interactions of Mo(VI) with complexing acids such as HCl leads to the formation of monomeric chloro-complexes where the molybdic acid fragment MoO_2^{2+} (molybdenyl cation) is preserved throughout successive chlorination and protonation reactions [37]:

$$[MoO_2(OH)(H_2O)_3]^+ + Cl^- \leftrightarrow MoO_2(OH)Cl(H_2O)_2 \quad (7)$$

$$MoO_2(OH)Cl(H_2O)_2 + H^+ + Cl^- \leftrightarrow MoO_2Cl_2 + 3H_2O \quad (8)$$

$$MoO_2Cl_2 + Cl^- \leftrightarrow [MoO_2Cl_3]^- \quad (9)$$

Equilibrium constant values show that the prevailing mononuclear species from 1-3M HCl is $[MoO_2(OH)(H_2O)_3]^+$ and from 3-11M HCl is MoO_2Cl_2. With the notable exception of the tetrahedral MoO_4- anion, Mo(VI) oxo-complexes typically have octahedral coordination. As the total molybdate concentration increases from 0.1 mM to 100 mM, interactions between molybdenum subunits cause the formation of dinuclear species ($Mo_2O_5(OH)\cdot(H_2O)_5^+$, $Mo_2O_5\cdot(H_2O)_6^{2+}$, $Mo_2O_4(OH)\cdot(H_2O)_6^{3+}$) which are known to occur in perchloric acid [36]. Formulations were created under the assumption that a single oxo-bridge is formed between molybdate units through hydrolysis. These structures have been supported through Raman, XANES, and EXAFS spectroscopic evidence [38].

In the solvent extraction of metals, the distribution value of a metal depends on its affinity to complex with the extracting ligand. Since complexation affinity depends on the metal species, the aqueous equilibria and thermodynamic constants are critical to understanding and potentially improving the behavior of solvent extraction methods like MOEX. Relatively few studies have been done that investigate the speciation of Mo(VI) in HCl compared to the non-complexing acids such as $HClO_4$. This research will be an important step forward to understanding the solvent extraction of high Mo concentrations (>0.1M) in HCl by TBP.

1. 8 Low specific activity ^{99}Mo

The ^{235}U-fission–produced Mo production requires careful monitoring to prevent U/Pu scavenging through the formation of $UO_2Mo_2O_7\cdot(nH_2O)$ and $(PuMoO_4)\cdot 2H_2O$ [39]. Therefore,

parallel research on development of non-uranium production, based on two ^{98}Mo (neutron-activation) and ^{100}Mo (neutron knock-out) nuclear reactions:

$$^{1}n + {}^{98}\text{Mo} \rightarrow {}^{99}\text{Mo} \quad (10)$$

$$\gamma + {}^{100}\text{Mo} \rightarrow {}^{99}\text{Mo} + {}^{1}n \quad (11)$$

In early 2018, a novel low specific activity (LSA) generator was introduced to the market to process accelerator-produced ^{99}Mo from eMo targets. This work was developed in collaboration with Argonne National Laboratory (ANL) and supported by the National Nuclear Security Administration's Office of Material Management and Minimization (NNSA M^3). This approval simultaneously marks the first U.S. domestic supplier of ^{99}Mo in 30 years and reduces the U.S. reliance on HEU.

The multicolumn generator (Figure 1-9) concept differs from traditional ^{99m}Tc generators principally because Tc is retained on the column while Mo is eluted through. The concept of the multicolumn selectivity inversion generator is used to produce a highly pure daughter product. [40] This is achieved using a pertechnetate-selective aqueous biphasic extraction chromatography (ABEC) resin comprising monomethylated polyethylene glycol (PEG) covalently attached to polystyrene. The selective removal of the daughter allows for the use of low-specific activity ^{99}Mo without diluting the final ^{99m}Tc activity concentration. After elution of the column, the final product is equivalent to elute from HEU and LEU (traditional) ^{99m}Tc generators, yielding ~5mL of ^{99m}Tc sodium pertechnetate.

Table 1-3. Comparison of a traditional vs LSA model generator

	Traditional Generator	**LSA Generator**
Column resin:	Alumina	ABEC (PEG)
^{99}Mo source:	Uranium (high sp. activity)	Non-uranium (low sp. activity)
Eluate:	Na^{99m}TcO4	Na^{99m}TcO4
Elution time:	2-3 min	75 min

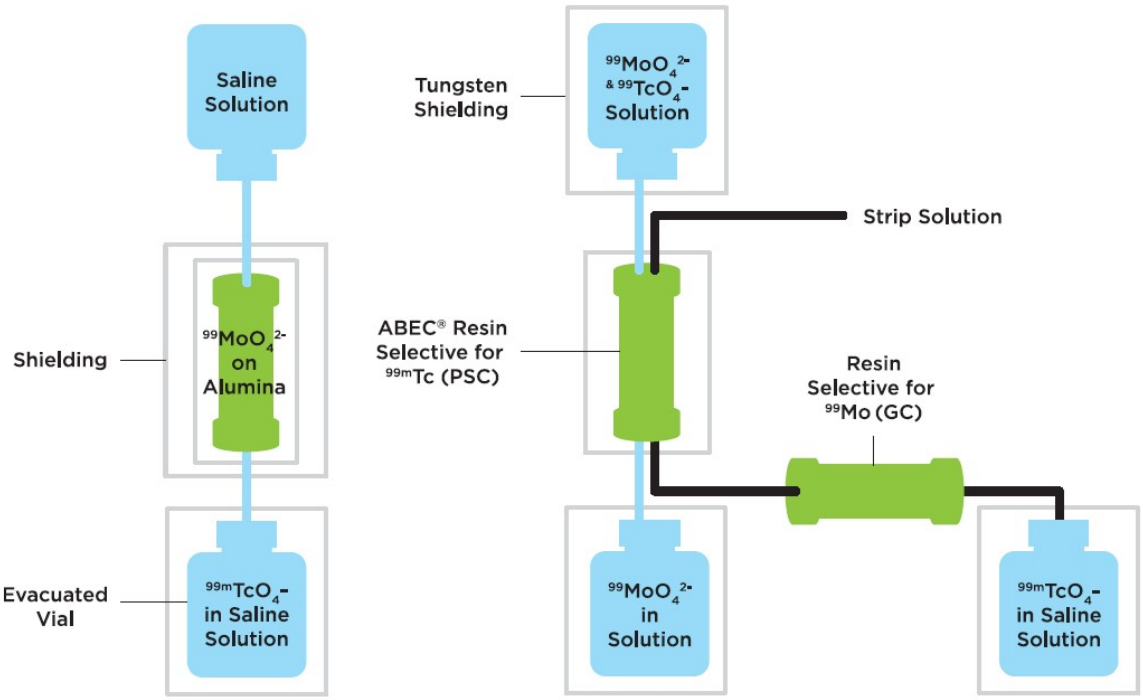

Figure 1-5. Comparison of traditional ion-exchange column and a generic multicolumn selectivity inversion generator, adopted from [40]

Modern LSA generator systems are large, fully-shielded and automated closed system. It has a maximum possession limit of 7.5 Ci $^{99}Mo/^{99m}Tc$ per week, including waste and decay source vessels [41]. It is approved for both ^{98}Mo (neutron-activation) and ^{100}Mo (neutron knock-out) sources. The system is essentially the same as a traditional generator design, as it is still alumina column. However, these LSA generator designs include the addition of the ABEC column to first separate Tc. The preconcentration of ^{99m}Tc is what allows a low specific activity of ^{99}Mo to be used.

LSA ^{99m}Tc elution protocol [41]:

- Rinse the system with hydrogen peroxide (H_2O_2)
- Precondition the primary separation cartridge (PSC) with 5M KOH
- Source solution passes through PSC (5mL x7)
- PSC rinsed with 5M KOH
- PSC rinsed with Na-acetate
- Rinse with 0.9% NaCl to elute ^{99m}Tc

The Mo waste stream is composed of 5 M NaOH and NaCl (saline) solution and contains small amounts of K_2MoO_4 in 5 M KOH. The solution comprises about 1.8 kg-K/kg-Mo which far exceeds the required purity specifications of MoO_3 powder (<100 mg-K/kg-Mo) required for the manufacturing of new targets. Proper chemical recycling methods must be employed to treat the waste solution if the enriched material is to be reused. Prior to shipment back to the processing facility, the Mo waste stream is solidified in a waste using a proprietary superabsorbent polymer. Recycling of the enriched materials must incorporate steps to dissolve this polymer and liberate Mo for the fabrication of new targets.

1.9 Goals and Objectives of this research work

The goals of this dissertation are related to the optimization and improvement of various aspects of the ^{99}Mo chemical lifecycle derived from accelerator-produced, low specific activity ^{99}Mo sources. The scope of my work can be outlined into three objectives.

Objective 1. Building a thermodynamic model for Mo(VI) complexation on chloride solutions.

Recent investigations of the Mo solvent extraction (MOEX) process indicate that the primary extracted Mo(VI) species by TBP is the di-chloro molybdenyl species MoO_2Cl_2. However, at higher Mo concentrations, UV and NMR spectroscopic evidence shows the possibility of additional species at high HCl. It is proposed that a comprehensive thermodynamic model of Mo in HCl is built to identify the potential polymerization of Mo in the high HCl conditions. When Mo is dissolved in HCl, it has been shown that TBP primarily extracts the di-chloro species, MoO_2Cl_2 [42] [31]:

$$MoO_2(OH)Cl(H_2O)_2 + H^+ + Cl^- + 2TBP \leftrightarrow MoO_2Cl_2{\cdot}TBP_2 + 3H_2O$$

This is evidenced by the higher extraction yield at 1M HCl (~30%) compared to 5M HCl (99%). However, at higher concentrations of Mo (>0.1M), there are indications of the potential formation of new species at high HCl. This result is supported by UV and NMR spectroscopic results that suggest the presence of additional species in the TBP extracts at higher HCl.

Applying quantitative spectrophotometric techniques, we will measure the absorption spectra and calculate the stability constants of the prevalent monomeric and dimeric Mo(VI) species in 0.5-11 M HCl solutions from 0.0001 – 0.3 M. The diversity of mono- and polynuclear molybdenum species that exist simultaneously in chloride media poses a great challenge to understanding the broader behavior, distribution and extractability of these species in a two-phase system. Therefore, model building requires careful analytical chemical techniques and refined numerical processing of data.

Hence, the first objective of this dissertation is identification and characterization of the Mo species distribution in the aqueous phase used during the MOEX process (~0.3 M Mo) to create a better understanding of the aqueous environment during extraction. Through chemometric analysis of UV spectrophotometric data, major Mo species in a wide range of Mo and HCl concentrations were identified and these results are presented in chapter 2.

Objective 2. Purification and detection of ultratrace Re in Mo target material

The production of very pure molybdenum is extremely important in meeting target purity specifications during the production of ^{99}Mo for medical applications. Rhenium (Re), whose similar chemistry and co-occurrence in Mo ores makes it a common impurity in commercial Mo, is an especially critical element to detect and separate from Mo target material. Its two naturally occurring isotopes ^{185}Re (37.5%) and ^{187}Re (62.6%) have large thermal neutron absorption cross sections and produce short-lived neutron-activation products ^{186}Re ($t_{1/2}$ = 90.6 hr) and ^{188}Re ($t_{1/2}$ = 16.9 hr), thus even low concentrations of Re impurities in bulk Mo powders can pose a great challenge to meeting strict radiopurity requirements during neutron-activation production of ^{99}Mo from Mo targets. ^{186}Re and ^{188}Re impurities have been observed in irradiated samples of ^{nat}Mo and eMo, but due to the strict timeline post-irradiation and the challenges associated with handling highly radioactive material, Mo target material should be purified prior to irradiation.

Two methods for the detection and removal of ultratrace Re in Mo powders were developed. The results and flowsheets for these processes is provided in chapter 3 and the statistical

and procedural approach to determining the method detection limits by inductively coupled plasma mass spectrometry (ICP-MS) is discussed in detail.

Objective 3. Minimizing enriched-Mo losses in generator waste streams.

Despite during each milking, generator systems can lose roughly ~1% of eMo into waste stream, netting a cumulative loss of ~20-30% of eMo material into the waste. Typically, the waste stream is composed of NaOH and saline (NaCl) solution with small amounts of K_2MoO_4 in 5M KOH. This waste stream is solidified in a waste container using a proprietary "superabsorbent polymer". Due to a significant fraction of enriched Mo material lost to this waste stream, it is of great importance to recover Mo, as it is a valuable and expensive material suitable for recycling in fresh targets. This is not a problem when natural Mo targets are used, but the high cost of enriched Mo material (^{100}Mo or ^{98}Mo) requires that the Mo in the waste stream be efficiently recycled into fresh targets.

Options to recover the enriched Mo from the polymeric gel were investigated and a near-quantitative (90-95%) recovery process was developed using common chemicals and simple chemical techniques. A flowsheet for this process was developed and is discussed in chapter 4, where preliminary data for Mo purification from the polymer is also described.

1. 10 References

[1] O. N. E. A. (NEA), "The Supply of Medical Radioisotopes: 2016 Medical Isotope Supply Review on 99Mo/99mTc Market Demand and Production Capacity Projection 2016-2021," no. March, 2011.

[2] Molybdenum-99 for Medical Imaging. National Academies Press, 2016.

[3] 112th Congress. American Medical Isotopes Production Act of 2011. H.R. 4310, Public Law 112-239, 2013

[4] L. De Silva et al., "Characterization, optimization, and in vitro evaluation of Technetium-99m-labeled niosomes," International Journal of Nanomedicine, vol. Volume 14, pp. 1101–1117, Feb. 2019, doi: 10.2147/ijn.s184912.

[5] P. R. Cristini, H. J. Cols, R. Bavaro, M. Bronca, R. Centurión, and D. Cestau, "Production of molybdenum-99 from low enriched uranium targets," Proc. 2002 Int. Meet. Reduc. Enrich. Res. Test React. San Carlos Bariloche, Argentina, pp. 7–9, 2002.

[6] G.F.Vandegrift, J.L. Snelgrove, S. and Aase, "Converting targets and processes for fission-product molybdenum-99 from high- to low-enriched uranium", (IAEA-TECDOC-1065), International Atomic Energy Agency (IAEA), 1999

[7] Z. I. Kolar and H. T. Wolterbeek, "Making of fission 99Mo from LEU silicide: A radiochemist's view," no. November, pp. 8–11, 2004.

[8] Committee on Medical Isotope Production without Highly Enriched Uranium, National Research Council of the National Academies. *Medical Isotope Production Without Highly Enriched Uranium*. Washington, DC: The National Academies Press, **2009**.

[9] S. C. van der Marck, A. J. Koning, and K. E. Charlton, "The options for the future production of the medical isotope 99Mo," European Journal of Nuclear Medicine and Molecular Imaging, vol. 37, no. 10, pp. 1817–1820, Jun. 2010.

[10] S. M. Qaim, Nuclear Data for Science and Technology: Proceedings of the International Conference on Nuclear Data for Science and Technology, 1991.

[11] A. J. Youker et al., "Fission-Produced 99 Mo Without a Nuclear Reactor," Journal of Nuclear Medicine, vol. 58, no. 3, pp. 514–517, Sep. 2016.

[12] G. R. Piefer, K. M. Pitas, and E. N. Van Abel, "Mo-99 Production Using a Subcritical Assembly," 1st Annu. Molybdenum-99 Top. Meet., vol. 235, 2011.

[13] Y. O. Lee, T. Fukahori, and J. Chang, "Evaluation of photonuclear reaction data on tantalum-181 up to 140MeV," J. Nucl. Sci. Technol., vol. 35, no. 10, pp. 685–691, 1998.

[14] C. Economou et al., "Direct Production of 99mTc via 100Mo(p,2n) on Small Medical Cyclotrons," Phys. Procedia, vol. 66, pp. 383–395, 2015.

[15] A. Boschi, P. Martini, M. Pasquali, and L. Uccelli, "Recent achievements in Tc-99m radiopharmaceutical direct production by medical cyclotrons," Drug Dev. Ind. Pharm., vol. 43, no. 9, pp. 1402–1412, 2017.

[16] M. R. A. Pillai, A. Dash, and F. F. Knapp, "Sustained Availability of 99mTc: Possible Paths Forward," J. Nucl. Med., vol. 54, no. 2, pp. 313–323, 2012.

[17] P. Tkac, M. A. Brown, A. Momen, K. E. Wardle, J. M. Copple, and G. F. Vandegrift, "MOEX: Solvent extraction approach for recycling enriched 98Mo/100Mo material," Sep. Sci. Technol., vol. 53, no. 12, pp. 1856–1863, 2018.

[18] J. H. Peter Tkac, David Rotsch, Dominique Stepinski, Vakhtang Makarashvili, George Vandegrift, "Optimization of the Processing of Mo Disks," 2016.

[19] R. A. Lowden, S. D. Nunn, and J. O. Kiggans, Powder Metallurgy Fabrication of Molybdenum Accelerator Target Disks, no. July. 2015.

[20] J. A. Shields, Applications of Molybdenum Metal and its Alloys. 2013.

[21] R. G. FREY and J. W. HALLORAN, "Compaction Behavior of Spray-Dried Alumina," J. Am. Ceram. Soc., vol. 67, no. 3, pp. 199–203, 1984.

[22] P. Tkac, G. Vandegrift, and J. Harvey, "Dissolution of Sintered Mo Disks," 2012.

[23] V. P. Guro, "Molybdenum dissolution in mixtures of H2O2 and concentrated HNO3 and H2SO4 in the presence of tungsten," Inorg. Mater., vol. 44, no. 3, pp. 239–243, 2011.

[24] A. J. Bakel et al., "Parametric Studies on the Use of In Situ Formed Magnetite for the Removal of Sr and Actinides from Tank Waste at the Savannah River," 2002.

[25] N. Ramamoorthy, "Production and Availability of 99m Tc Generators and of 99 Mo: Technology Considerations and the IAEA's Contributions," Proc. NUCAR-2007, DAE-BRNS, India, vol. 3746, no. 1958, pp. 24–32, 2007.

[26] C. Gervais et al., "Nanocrystalline Mesoporous γ-Alumina Powders 'UPMC1 Material' Gathers Thermal and Chemical Stability with High Surface Area," Chem. Mater., vol. 18, no. 22, pp. 5238–5243, 2006.

[27] S. Chattopadhyay, M. K. Das, S. K. Sarkar, P. Saraswathy, and N. Ramamoorthy, "A novel Tc-99m delivery system using (n,gamma)Mo-99 adsorbed on a large alumina column in tandem with Dowex-1 and AgCl columns," Appl. Radiat. Isot., vol. 57, no. 1, pp. 7–16, 2002.

[28] K. Gagnon et al., "Cyclotron production of 99mTc: Recycling of enriched 100Mo metal targets," Appl. Radiat. Isot., vol. 70, no. 8, pp. 1685–1690, 2012.

[29] M. Gumiela, J. Dudek, and A. Bilewicz, "New precipitation method for isolation of 99mTc from irradiated 100Mo target," J. Radioanal. Nucl. Chem., vol. 310, no. 3, pp. 1061–1067, 2016.

[30] P. Tkac and G. F. Vandegrift, “Recycle of enriched Mo targets for economic production of99Mo/99mTc medical isotope without use of enriched uranium,” J. Radioanal. Nucl. Chem., vol. 308, no. 1, pp. 205–212, 2016.

[31] P. Tkac, M. A. Momen, A. T. Breshears, M. A. Brown, and G. F. Vandegrift, “Molybdenum(VI) Coordination in Tributyl Phosphate Chloride Based System,” Ind. Eng. Chem. Res., vol. 57, no. 16, pp. 5661–5669, 2018.

[32] M. L’Annunziata, Handbook of Radioactivity Analysis (Google eBook), 2nd Ed. Academic Press, 2012.

[33] T. Wichard, B. Mishra, S. C. B. Myneni, J. P. Bellenger, and A. M. L. Kraepiel, “Storage and bioavailability of molybdenum in soils increased by organic matter complexation,” Nat. Geosci., vol. 2, no. 9, pp. 625–630, 2009.

[34] M. L. Kirk, “Metal Ions in Biological Systems. Volume 39. Molybdenum and Tungsten: Their Roles in Biological Processes Edited by Astrid Sigel and Helmut Sigel (University of Basel). 2002. ix + 810 pp. $250.00. ISBN 0-8247-0765-6.,” J. Am. Chem. Soc., vol. 125, no. 1, pp. 305–306, 2003.

[35] J. J. Cruywagen, A. G. Draaijer, J. B. B. Heyns, and E. A. Rohwer, “Molybdenum(VI) equilibria in different ionic media. Formation constants and thermodynamic quantities,” Inorganica Chim. Acta, vol. 331, no. 1, pp. 322–329, 2002.

[36] J. J. Cruywagen and J. B. B. Heyns, “Molybdenum(VI) equilibria at high perchloric acid concentration,” Polyhedron, vol. 19, no. 8, pp. 907–911, 2000.

[37] I. A. Dement’ev, A. O. Kozin, Y. V. Kondrat’ev, D. V. Korol’kov, and A. A. Proyavkin, “Mononuclear, polynuclear, and cluster complexes of molybdenum and their reactions as models of biochemical systems and processes,” Russ. J. Gen. Chem., vol. 77, no. 5, pp. 822–843, 2007.

[38] K. H. Tytko, G. Baethe, and J. J. Cruywagen, “Equilibrium studies of aqueous polymolybdate solutions in 1 M sodium chloride medium at 25 degree C,” Inorg. Chem., vol. 24, no. 20, pp. 3132–3136, 2005.

[39] Y. Pokhitonov, V. Aleksandruk, B. Bibichev, G. Novikov, V. Riazantsev, and V. Saprykin, “Composition of insoluble residues generated during spent fuel dissolution,” in WM’02 Conference, 2002.

[40] E. P. Horwitz and A. H. Bond, “Purification of radionuclides for nuclear medicine: The multicolumn selectivity inversion generator concept,” Czechoslov. J. Phys., vol. 53, no. S1, pp. A713–A716, 2007.

[41] T. W. S. Sijabat, “RadioGenix Molybdenum-99/Technetium-99m Generator System,” 2018.

[42] P. Tkac and A. Paulenova, “Speciation of molybdenum (VI) in aqueous and organic phases of selected extraction systems,” Sep. Sci. Technol., vol. 43, no. 9–10, pp. 2641–2657, 2008.

[43] J. J. Cruywagen and E. F. C. H. Rohwer, “Coordination number of Molybdenum(VI) in Monomeric Molybdic Acid,” Inorg. Chem., vol. 14, no. 12, pp. 3136–3137, 1975.

CHAPTER 2 SPECIATION OF MOLYBDENUM(VI) IN CHLORIDE MEDIA AT ELEVATED MOLYBDENUM CONCENTRATIONS

This text is a modified version of an accepted publication in ACS Omega.

2. 1 Abstract

Speciation of Mo(VI) in chloride media (0.5–11M HCl) at elevated Mo concentration (0.1–300mM Mo) was investigated using UV spectroscopy. In addition to five major monomeric species, H_2MoO_4, $H_3MoO_4^+$, H_3MoO_4Cl, MoO_2Cl_2, and $MoO_2Cl_3^-$, chemometric analysis of UV spectra suggests the presence of three cationic dinuclear species that predominate in solutions of 1–4.5M HCl at >20mM Mo concentrations. Thermodynamic values and molar absorptivity spectra were calculated from UV spectrophotometric data using refined numerical methods. The stability constants determined for three Mo dimers are log $\beta = 3.53 \pm 0.05$ ($H_2Mo_2O_5^{2+}$), log $\beta = 3.60 \pm 0.04$ ($H_3Mo_2O_5^{3+}$), and log $\beta = 2.91 \pm 0.03$ ($H_3Mo_2O_6Cl^{2+}$).

2. 2 Introduction

The radionuclide ^{99m}Tc is used in approximately 80 percent of all nuclear medicine procedures performed worldwide [1]. The short half-life of the metastable ^{99m}Tc (6.0 h) precludes its chemical separation at the production site. Instead, the longer-lived parent ^{99}Mo (66-h half-life) is sent to radiopharmacies, where the grown-in ^{99m}Tc is separated from Mo and used immediately for diagnostics. Traditionally, production of ^{99}Mo was obtained through the fissioning of >90% high-enriched uranium (HEU) targets. A shift in U.S. policy occurred with the 2011 American Medical Isotopes Production Act, which was aimed at establishing a reliable domestic supply of ^{99}Mo while eliminating the use of HEU in the various medical isotope supply chains [2, 3]. In accordance with these goals and those put forth by the International Atomic Energy Agency, most manufacturers of fission-made ^{99}Mo have converted research reactors and medical isotope production facilities worldwide to less proliferation-sensitive low-enriched uranium (<20% ^{235}U) sources [4]. However, several novel non-uranium alternatives for producing ^{99}Mo are also gaining attention, such as accelerator-based production via the bremsstrahlung photonuclear reaction $^{100}Mo(\gamma,n)^{99}Mo$ or use of neutron capture $^{98}Mo(n,\gamma)^{99}Mo$. In both cases, enriched ^{100}Mo or ^{98}Mo

is often required to produce significant activities of ^{99}Mo economically. Because of the high cost of enriched material ($500–1000/g for kilogram quantities), efficient recycling strategies for Mo must be developed.

The recycling of enriched Mo into fresh target material involves the conversion of aqueous Mo(VI) solutions, typically in alkaline media (e.g. KOH, NaOH), to Mo(0) metal powders. Important qualities of a recycle process include high recovery yields, high throughput, meeting purity specifications, and obtaining recycled target characteristics similar to those of the original material. A Mo solvent extraction (MOEX) process has recently been proposed as a viable option for recycling enriched Mo material [5]. The MOEX system relies on extraction of high concentrations of Mo (~0.3M) in HCl by tri-n-butyl phosphate (TBP) to achieve decontamination from Na, K, and other impurities. However, there is limited understanding of the aqueous Mo chemistry occurring in this system. Recent investigations indicate that the aqueous Mo species primarily extracted by TBP is the di-chloro molybdenyl species MoO_2Cl_2 [6], occurring as an adduct with two TBP molecules. But insights into Mo(VI) polyoxometalate chemistry suggest that polynuclear complexes may constitute a significant fraction of Mo species under these conditions [7].

The diversity of mono- and polynuclear Mo species existing simultaneously in acid solutions poses a great challenge to understanding and predicting their aqueous distribution at high Mo concentrations. The simple tetrahedral molybdate ion MoO_4^{2-} is the well-known dominant species in alkaline solutions. Mononuclear metal oxide forms of Mo(VI) persist when Mo concentrations are low (<0.1mM). Table 2-1 shows the monomeric equilibria of Mo(VI) species, which follow a series of protonation steps and complexation with chlorides. Between pH 0 and 1, the predominant species of Mo(VI) is H_2MoO_4. Molybdic acid is protonated to form the $H_3MoO_4^+$ cation. In HCl, this is followed by a rapid, two-step complex formation with a first-order dependence on both $[H^+]$ and $[Cl^-]$ to form the first chlorinated monomer species, H_3MoO_4Cl [8]. A second chlorination step leads to the formation of the neutral complex MoO_2Cl_2 containing the molybdenyl $[MoO_2]^{2+}$ moiety, which then predominates throughout acid concentrations >5M in coordination with chloride ions.

Table 2-1. Formation Constants of the Mononuclear Mo(VI) Complexes in HCl [8]

Equation	*log K*
$MoO_4^{2-} + H^+ \leftrightarrow HMoO_4^-$	4.21 ± 0.04
$HMoO_4^- + H^+ \leftrightarrow H_2MoO_4$	4.00 ± 0.04
$H_2MoO_4 + H^+ \leftrightarrow H_3MoO_4^+$	0.934 ± 0.01
$H_3MoO_4^+ + Cl^- \leftrightarrow H_3MoO_4Cl$	-0.89 ± 0.04
$H_3MoO_4Cl + H^+ + Cl^- \leftrightarrow MoO_2Cl_2 + 2H_2O$	-1.42 ± 0.02
$MoO_2Cl_2 + Cl^- \leftrightarrow MoO_2Cl_3^-$	-2.64 ± 0.09

There is a favorable enthalpy change (dH = -47 kJ/mol) for the $MoO_4^{2-}/HMoO_4^-$ reaction, owing to the bond energy gained from an increase in coordination number upon protonation of molybdate [9]. As such, the changes in formulation from four-coordinate MoO_4^{2-} to six-coordinate $MoO(OH)_5^-$ and $Mo(OH)_6$ are typically used to emphasize the thermodynamic driving forces behind complex formation. The true structure of molybdic acid has been identified by various authors after extensive experimental and DFT analyses to take the form of the octahedral $MoO_3(H_2O)_3$ complex [9, 10]. To reduce the confusion that often occurs around hydrated formulations, this paper employs general formulas (e.g., H_2MoO_4) for all species.

The ability of tetrahedral MoO_4^{2-} to expand its coordination sphere from 4 to 6 allows molybdate subunits to condense to various electron-dense isopolymolybdate complexes in weakly acidic media (pH 1 to 5). These arrangements are facilitated by Mo-O π-bonding of MoO_6 subunits sharing edges and vertices. Mo-O bond lengths in isopolyanions of Mo are shorter because of π-bonding, resulting in distinct UV spectra compared to dinuclear cations, which contain the σ-bonded Mo-O-Mo bridge. Examples of the isopolyanions of Mo(VI) include $[Mo_7O_{24}]^{6-}$, $[Mo_8O_{26}]^{4-}$, $[Mo_{36}O_{112}]^{8-}$, and their protonated variants that form large 3-dimensional frameworks whose nuclearity and equilibria have been fairly well characterized [7]. Polymolybdate assembly is produced through Brønsted acid-base condensation-addition processes. Partial reduction of Mo(VI) can lead to covalent self-assembly of Mo into nano-sized, mixed-valence Mo^{VI}-O-Mo^{V} entities such as $[MO^{VI}_{126}Mo^{V}_{28}O_{426}H_{14}(H_2O)_{70}]^{14-}$ [11]. The unique nature and various applications of transition-metal polyoxometalate chemistry has made it a principal focus of aqueous Mo research.

In contrast to the tendency of most isopolymolybdate clusters to occur as anions in aqueous solutions, the dinuclear complexes of Mo(VI) are predominantly cationic. One exception is the singly charged $HMo_2O_7^-$ anion, whose existence between pH 2 and 6 is so far supported only by quantitative treatment of spectrophotometric evidence [12]. Dimerization of Mo in non-complexing acids such as $HClO_4$ is strongly promoted by medium effects, namely by an increase in ionic strength and decrease in water activity [13]. In these conditions, Mo condensation can occur at relatively low Mo concentrations (~1mM) with rapid kinetics [14]. Previous spectroscopic and calorimetric investigations of Mo(VI) revealed the presence of three oxocation dimers, $HMo_2O_6^+$, $Mo_2O_5^{2+}$, and $HMo_2O_5^{3+}$ [12–15], which begin to form just above 0.1mM Mo. The dimerization reaction was shown to be enthalpy-driven (K_D = -30 kJ/mol) which is derived from the formation of a free water molecule to form $Mo_2O_5^{2+}$, coupled with an unfavorable entropy change due to an increase in molecular order [16].

$$2HMoO_3^+ \leftrightarrow Mo_2O_5^{2+} + H_2O \quad (1)$$

$$HMo_2O_6^+ + H^+ \leftrightarrow H_2Mo_2O_6^{2+} \leftrightarrow Mo_2O_5^{2+} + H_2O \quad (2)$$

$$Mo_2O_5^{2+} + H^+ \leftrightarrow HMo_2O_5^{3+} \quad (3)$$

The major dimeric species in 1M $HClO_4$ solutions is the divalent cation $Mo_2O_5^{2+}$ [15, 16]. Dimeric Mo(VI) cations notably show a characteristic peak at ~245 nm which has been attributed to the unique Mo-O-Mo oxygen bridge joining two octahedral Mo units in the $[Mo_2O_5]^{2+}$ moiety. This peak is absent in spectra of isopolyanions, where μ-oxo bridging is not present and bonding is instead composed of edge- and vertex-sharing MoO_4^{2-} [17]. The $[Mo_2O_5]^{2+}$ structure has been verified by Raman and EXAFS spectroscopies as a constituent of various cationic dimers having a bond angle of ~125 degrees [17]. Because of the unique bonding nature of the dimeric species, UV spectrophotometry can readily distinguish Mo dinuclear cations from its mononuclear or anionic polynuclear forms.

Mo(VI) condensation has been observed under strong acid conditions in both complexing (HCl) and non-complexing ($HClO_4$) media; however, the main body of research has focused almost entirely on the latter [10, 18]. To the best of our knowledge, the nature of polynuclear

Mo(VI) complexes in HCl has hitherto not been identified. It is likely that the formation of dinuclear species would occur in HCl and that additional species complexed with chlorides are also possible.

Applying UV spectrophotometric techniques, we have measured the absorption spectra and identified the major Mo(VI) species in 0.5–11M HCl solutions using refined numerical processing. Stability constants at varying ionic strengths were estimated by accounting for activity coefficients using the modified Bromley theory [19]. In this work, we seek to identify mono- and polynuclear species of Mo present in the aqueous phase during the MOEX solvent extraction process.

2. 3 Experimental

Trace metal grade HCl and 18 MΩ·cm H_2O (MilliQ) were used to prepare solutions. A series of Mo stocks were prepared from MoO_2Cl_2 (Sigma Aldrich) in volumetric flasks. Mo samples were prepared in batch experiments by mixing stocks to achieve the desired HCl concentration (0.5–11M HCl). Samples were prepared over a wide range of Mo concentrations (0.1–300mM Mo). NaCl was used in experiments where it was desired to maintain acid concentration but increase [Cl^-]. Concentrations of Mo and Na were determined via inductively coupled plasma mass spectroscopy (ICP-MS). Hydronium concentrations of all samples were determined through triplicate titration with a standardized solution of NaOH. In the calculation of total proton concentrations, an allowance was made for the conversion of molybdenyl to molybdate upon neutralization to pH 7:

$$MoO_2^{2+} + 2H_2O \leftrightarrow MoO_4^{2-} + 4H^+ \quad (4)$$

A Cary 5000i (Agilent) double-beam spectrophotometer was used for absorption measurements in dual-beam mode to correct for fluctuations due to electrical noise. Quartz cuvettes of path length 0.01 mm, 0.1 mm, 1.0 mm, and 10 mm (Starna Cells) were used for measuring 0.3M, 20mM, 2mM, and 0.1mM Mo samples, respectively. Each sample was measured at room temperature (20°C) against a blank reference solution with the corresponding HCl concentration to correct for the solvent absorbance peak exhibited just below 200-nm wavelength. It is important to note that the published tolerances of very-low-path-length open-cell cuvettes can

be very high (10 μm ± 3 μm), posing a significant challenge to quantitative analysis. The path length of the "10-μm" cuvette was measured interferometrically, and the actual path length was 7.86 μm ± 0.5 μm.

The concentrations of chemical components that were determined by ICP-MS and acid-base titration were used to calculate ion activities. Since thermodynamic data are based on activities, special care was taken to relate concentrations of chemicals to their thermodynamic activity. The complexities surrounding this relation are often avoided by performing experiments at constant, high ionic strength through the addition of nonparticipating ions to the solution. Such a simplification is not practical at the wide range of acid concentrations covered in these experiments. Therefore, activity coefficients were calculated for each solution using a modified semi-empirical Bromley method to allow stability constants to be calculated in reference to the infinite dilution standard state (I = 0M) [19]. The Argonne AMUSE (Argonne's Model for Universal Solvent Extraction) code was used for this purpose [20].

Equilibrium constants and molar absorptivity spectra were calculated from the spectrophotometric data using the HypSpec program, which solves the non-linear simultaneous mass balance equations using the Newton-Raphson method [21]. The stability of a complex in solution refers to the associations between the metal (M) and ligand (L) at equilibrium, such that for the reaction $M + L \leftrightarrow ML$ the stepwise stability constant (K) is given as $K_1 = [ML] / [M][L]$ and $K_2 = [ML_2] / [ML][L]$, etc. Successive stepwise equilibria may be related by their cumulative stability constant (β) so that $\beta_1 = K_1 = [ML] / [M][L]$ and $\beta_2 = K_1K_2 = [ML_2] / [M][L]^2$, which are provided as logarithm values for the convenience that $\log \beta_n = \log K_1 + \log K_2 + \ldots + \log K_n$.

A unit weighting scheme was applied to all spectrophotometric data. Data fitting was achieved by determining the parameters for which the objective function is minimized. Experimental error was estimated by the root mean square σ of the residual r values:

$$\sigma = \sqrt{\frac{\sum_i r_i^2}{n-m}} \qquad (5)$$

where n is the number of data points and m is the number of parameters. The expectation value of σ in this case is zero, providing a universal index of goodness of fit. Speciation diagrams with known constants were modeled using HySS, which belongs to the same HYPERQUAD program suite. Spectral data from previous authors used for comparison were extracted and interpolated (where necessary) by the cubic spline method using scikit-image [22].

2. 4 Results and Discussion

2. 4. 1 Mononuclear Mo(VI) species

UV spectra of solutions collected from 0.5–11M HCl with 0.1, 2, 20, and 300mM Mo are shown in Figure 2-1. At 0.1mM Mo, the concentrations of Mo(VI) polynuclear species are known to be below 1% [10]. The first step of the analysis was to compare these absorbance spectra to those collected by previous authors who studied the monomeric Mo(VI) system. The 0.1mM spectra show that a dominant peak with a maximum near 226 nm increases with acid concentration. At high HCl concentrations, a shoulder region forms in the interval of wavelengths between 250 and 270 nm. These spectra show strong agreement with previous authors [8, 24], including the tangential contact of the shoulder at 256–274 nm, supporting the conclusion that it does not constitute an isosbestic region. The high-HCl spectra appear nearly identical across all Mo concentrations, indicating that little to no speciation differences occur under these conditions. However, significant spectral changes appear in the more weakly acidic region between approximately 0.5 and 5M HCl (brown-black lines in Figure 2-1) as Mo concentration increases.

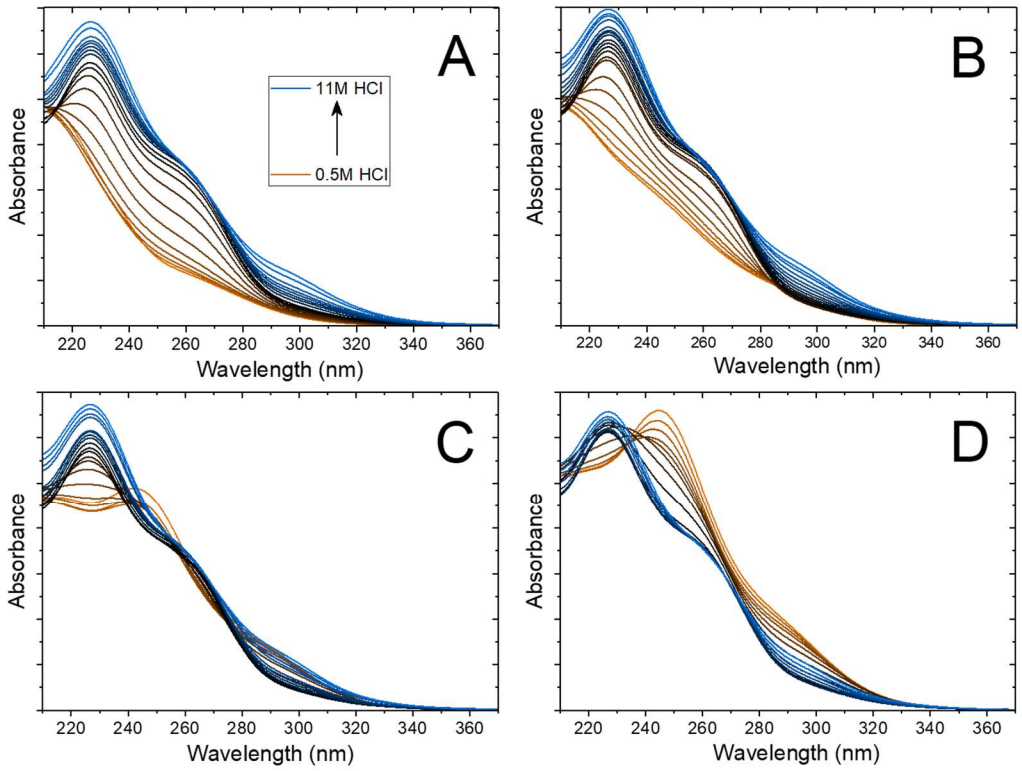

Figure 2-1. UV-vis absorption spectra collected for 0.1mM (A), 2mM (B), 20mM (C), and 300mM (D) Mo in 0.5–5M HCl (brown-black) and 5.5–11M HCl (black-blue). Spectra were recorded in quartz cuvettes of path length 10, 1.0, 0.1, and 0.01 mm, respectively.

To explore the monomeric equilibrium model, the 0.1mM Mo spectra were evaluated using the HypSpec program. A set of cumulative stability constants (log β) for monomeric Mo(VI) species in chloride media determined in previous work (Table 2-1) were applied as the initial estimates. The comparison between calculated and experimental spectra resulted in an excellent fit ($\sigma = 3.6x10^{-3}$), confirming that the data are adequately described by monomeric species. The calculated stability constants compared to literature data are summarized in Table 2-2, and molar absorptivity spectra for the monomeric species identified are shown in Figure 2-2. High absorbance near 210 nm is due to the presence of protonated molybdic acid species that become chlorinated at higher HCl concentrations. The shoulder region at ca. 260–270 nm (Figure 2-1) is due to the formation of MoO_2Cl_2 and $MoO_2Cl_3^-$ species, which show equivalent extinction coefficient values at these wavelengths (Figure 2-2).

Table 2-2. Equilibrium Stability Constants (log β) of Monomeric Mo(VI) Species in HCl Solutions

Equation	*log β (this work)*	*log β [8]*
$H_2MoO_4 + H^+ \leftrightarrow H_3MoO_4^+$	0.94 ± 0.02	0.934 ± 0.01
$H_3MoO_4^+ + Cl^- \leftrightarrow H_3MoO_4Cl$	0.09 ± 0.02	0.044 ± 0.04
$H_3MoO_4Cl + H^+ + Cl^- \leftrightarrow MoO_2Cl_2 + 2H_2O$	-1.31 ± 0.02	-1.38 ± 0.02
$MoO_2Cl_2 + Cl^- \leftrightarrow MoO_2Cl_3^-$	-3.52 ± 0.02	-4.02 ± 0.09

Discrepancies between experimental stability constants determined here and those from the literature are most likely the result of different assumptions regarding the calculation of activity coefficients. Activities for H_3O^+ and Cl^- ions, which in this study were obtained by Bromley's method [19], differ from literature data [7] mostly at higher acid concentrations where even small changes in activity coefficients lead to more pronounced differences in activities. This conclusion is supported by the observation that stability constants for the low-acid species $H_3MoO_4^+$ and H_3MoO_4Cl are within experimental error, and only the constants for Mo species that predominate at higher HCl concentrations, MoO_2Cl_2 and $MoO_2Cl_3^-$, show more pronounced differences.

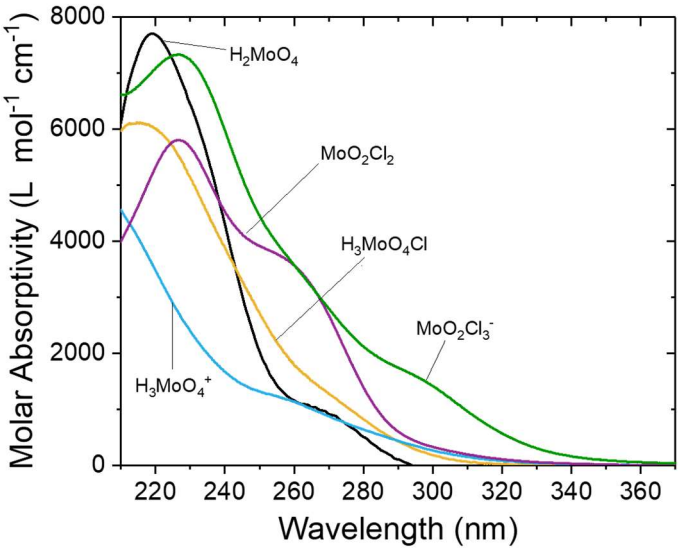

Figure 2-2. Molar absorptivity spectra for monomeric Mo(VI) species in HCl determined from 0.1mM Mo absorbance spectra

Figure 2-3 shows the speciation diagram for monomeric Mo based on experimentally determined stability constants (Table 2-2). The diagram confirms that at 0.5M HCl, the protonation of molybdic acid is already ~80% complete. A concentration of roughly 4M HCl is required for 50% conversion to the MoO_2Cl_2 species. The maximum abundance of MoO_2Cl_2 is about 85% and occurs at ~5M HCl. Then at HCl concentrations >6M, the absorbance spectra are satisfactorily described with only the di- and tri-chloro molybdate complexes. Similarities observed in absorption spectra at high HCl (>6M) across all Mo concentrations investigated (Figure 2-1) indicate that only monomeric MoO_2Cl_2 and $MoO_2Cl_3^-$ species are present. This observation will be further discussed in more detail.

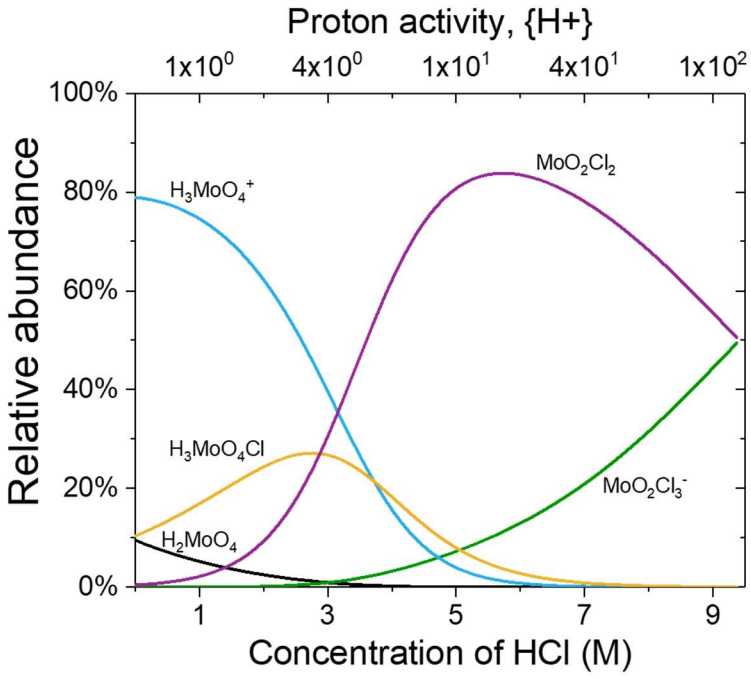

Figure 2-3. Speciation diagram of monomeric Mo(VI) in 0.5–11M HCl obtained using stability constants determined in this work

The speciation diagram and individual molar absorptivity spectra calculated from the experimental UV data in this work are nearly identical to those produced in the work of Cruywagen & Rohwer [7]. In particular, molar absorbance spectra of the H_2MoO_4 and $H_3MoO_4^+$ species that occur in 0.5–5M acid concentrations agree very well with those reported previously [7, 23]. Allowing for identification of molar absorptivity spectra and stability constants for mononuclear Mo species greatly reduces the number of unknowns that need to be resolved when analyzing the absorption spectra at higher Mo concentrations with the presence of dimeric Mo species. Therefore, experimentally determined molar absorptivity spectra and stability constants from the refinement of 0.1mM Mo spectra for monomeric Mo species were set as known values in the remaining models for the purpose of refining spectra at higher Mo concentrations.

2. 4. 2 Dinuclear Mo(VI) species

Absorption spectra for various Mo concentrations (Figure 2-1) at lower HCl concentrations indicate several changes in spectral features as the Mo concentrations increase. In the 2mM and 20mM Mo spectra, significant deviations from monomeric spectra occur below 5M HCl (brown lines). This observation correlates well with the expectation for Mo dimerization, which was previously confirmed in non-complexing $HClO_4$ media [14]. Spectra collected across the Mo concentration range from 2 to 300mM were added to the 0.1mM Mo analysis and evaluated for their fit to the monomeric model. As expected, the poor fit obtained indicates that the presence of only monomeric Mo species at 0.1mM Mo does not sufficiently describe the absorbance spectra at higher Mo concentrations. Evidence for this was also observed by Cruywagen at Mo concentrations greater than 0.1mM, where the extinction of Mo(VI) solutions began to deviate from Beer's law [7]. Therefore, addition of dimeric Mo species needs to be considered to properly analyze spectra at >0.1mM Mo concentrations.

Individual spectral features of 300mM Mo in 1.0M HCl were identified using Gaussian peak-fitting to determine peak positions and intensities. The results are compared with 0.1mM Mo spectra and displayed in Figure 2-4, showing that the 300mM Mo absorbance spectrum can be described as the sum of three peaks at 210 nm, 245 nm, and 274 nm ($R^2 = 0.99999$). The absorption peaks near 210 nm are a common feature of many aqueous Mo species, as is apparent from the

molar absorptivity spectra. Previous literature utilizing molecular orbital calculations have ascribed the absorbance peaks between roughly 200 and 240 nm to ligand-to-metal charge transfer transitions ($O^{2-} \rightarrow Mo^{6+}$) from terminal oxygen atoms [23, 25]. At 0.1mM Mo, absorbance at 210 nm is primarily governed by the monomeric equilibria involving $H_3MoO_4^+$, which is the dominant species between 0.5 and 3M HCl (Figure 2-2). As Mo concentration increases, the growth of the absorption band at 245 nm indicates that the polynuclear equilibria are increasingly important. As previously stated, it is well documented that Mo dimers contain the μ-oxo bridge (Mo-O-Mo) responsible for the characteristic absorption feature at 245 nm. The formation of this peak in Mo spectra shows that Mo-O-Mo bridging occurs in solutions with ≥2mM Mo. This finding strongly suggests that the changes in the absorption spectra at high Mo concentrations are most likely due to formation of cationic dimers.

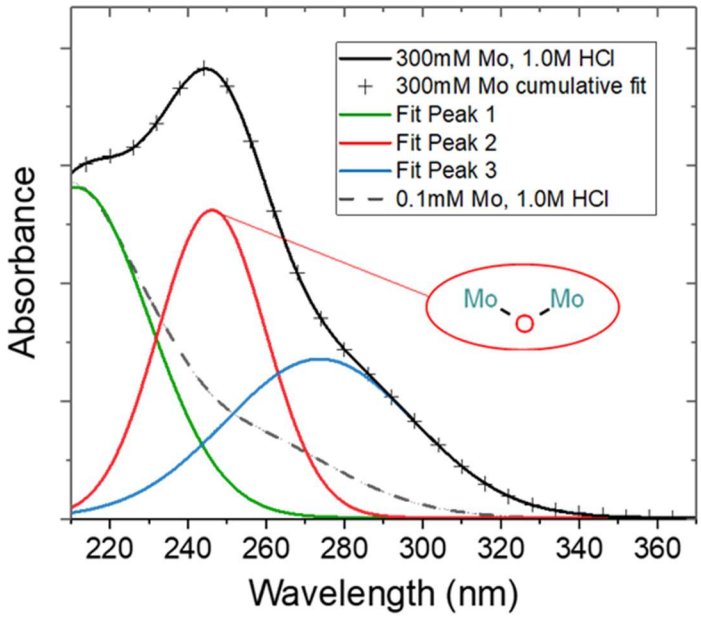

Figure 2-4. Peak fitting of the absorbance spectrum at 300mM Mo and 1M HCl (0.01-mm path length) showing the characteristic feature of Mo dimer at 245 nm. The absorbance at 0.1mM Mo (dashed gray line) is shown for reference (10-mm path length); no 245-nm peak is present

To gain insight into the number of dimers that may be present, factor analysis via singular value decomposition was performed on the absorbance data. This analysis was applied to all three

datasets, i.e., 2mM, 20mM, and 300mM Mo (~20 spectra at each Mo concentration) and on the 0.1mM Mo and 20mM Mo data sets separately. The goal of this analysis was to identify the number of major absorbing species contributing to the overall absorbance. The number of significant eigenvalues obtained from 0.1mM Mo spectra indicates the presence of 5 species, which is consistent with the monomeric model previously determined. The ≥2mM Mo data revealed the presence of 8 factors from these datasets. This result suggests that 3 new species form between 0.1mM and 2mM Mo.

Three known dimeric species could be expected in HCl, on the basis of previous investigations in perchloric acid: $HMo_2O_6^+$, $Mo_2O_5^{2+}$, and $HMo_2O_5^{3+}$ [13-16]. However, the ionization constant of the singly protonated form $HMo_2O_6^+$ is predicted to be too low for it to occur in significant concentrations under these conditions. The presence of a third dimeric species revealed by factor analysis could be explained by the presence of chlorinated Mo dimeric species. To explore these proposed scenarios, 2mM and 20mM Mo datasets were analyzed by the HypSpec program. Models incorporating known dimeric $HMo_2O_6^+$, $Mo_2O_5^{2+}$, and $HMo_2O_5^{3+}$ species were first examined. Indeed, the exclusion of the singly charged dimer was supported after it showed a poor fit to the data in all models. In this study, an allowance was made for various protonation and chlorination states of dimeric species, tentatively formulated as $H_mMo_2O_5Cl_n^{(2+m-n)+}$, and these were evaluated for their fit to spectrophotometric data. Results from these various models indicate that in addition to two oxocation dimers previously reported in $HClO_4$ [9], it was necessary to include a chlorinated dimer with the formula $HMo_2O_5Cl^{2+}$ to explain all absorbing features in the UV spectra. Incorporating the presence of all three dimers, $Mo_2O_5^{2+}$, $HMo_2O_5^{3+}$, and $HMo_2O_5Cl^{2+}$, into the HypSpec model with all previously determined monomeric species (Table 2-2) provided an excellent fit to experimental data. Numerical refinement converged with $\sigma = 9.3x10^{-3}$ for all spectra between 0.1 and 20mM Mo. The model was then applied to treat the 300mM Mo spectra, with which it provided excellent agreement.

Stability constants of the dimeric complexes were calculated from UV spectra and are listed in Table 2-3. The proposed dimeric Mo species were found to adequately describe the dimerization equilibria of Mo(VI) in HCl at 0.1–300mM Mo. A plot of the 300mM Mo speciation diagram, depicted in Figure 2-5, shows how the dimeric species predominate in solution between 2 and

4.5M HCl. The chlorinated Mo dimer $HMo_2O_5Cl^{2+}$ species (red line) appears to be stable in up to ~4–5M HCl, together with other monomeric chlorinated species. As the Mo concentration increases, the $HMo_2O_5Cl^{2+}$ prevails over H_3MoO_4Cl (yellow line) and to a lesser extent over MoO_2Cl_2 (purple line), especially at <4M HCl. The decrease in relative abundance of MoO_2Cl_2 in 5M HCl at 2mM Mo (85%) versus 55% at 300mM Mo demonstrates the effect of Mo concentration on speciation even at high HCl concentrations. This effect can be better observed by direct comparison of spectra collected with 5M HCl (Figure 2-6) and different Mo concentrations, showing how the Mo spectra change abruptly at 300mM Mo because of the presence of the $HMo_2O_5Cl^{2+}$ species.

Table 2-3. Suggested Dimeric Formulas and Their Calculated Equilibrium Values

Mo dimer species (general formula)	log β
$Mo_2O_5^{2+}$	3.53 ± 0.05
$HMo_2O_5^{3+}$	3.60 ± 0.04
$HMo_2O_5Cl^{2+}$	2.91 ± 0.03

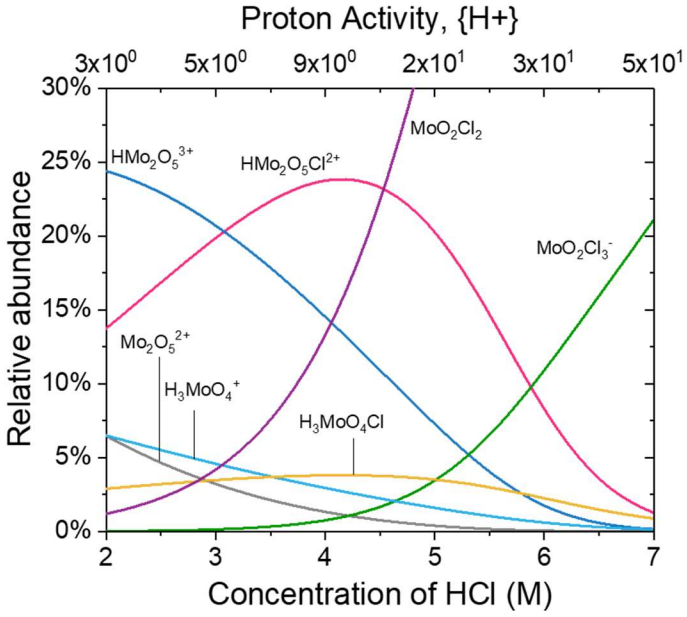

Figure 2-5. Speciation diagram of 300mM Mo in 2–7M HCl obtained using stability constants determined in this work

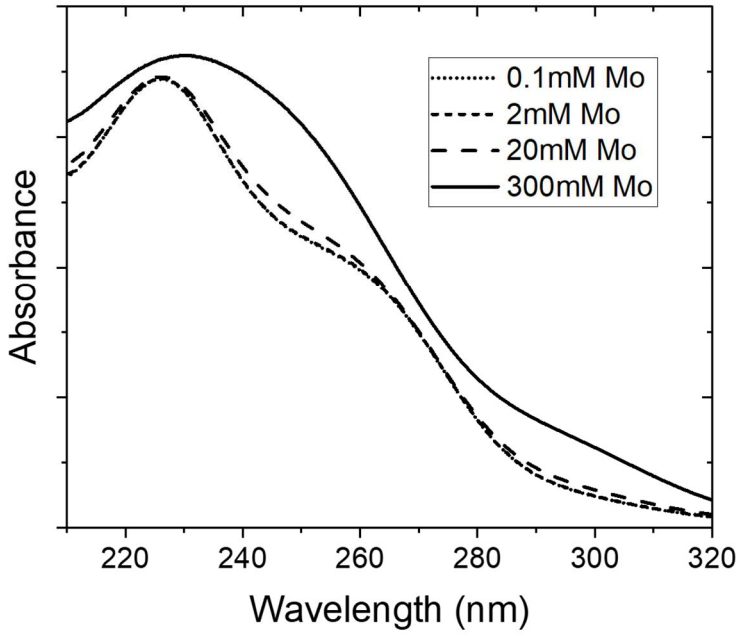

Figure 2-6. Comparison of 0.1, 2, 20, and 300mM Mo UV spectra at 5M HCl showing the major changes of spectral shape at 300mM Mo and the increase in absorbance at 245 nm

2. 4. 3 Dependence on chloride concentration

The proposed dimeric Mo species were further validated by analysis of 20mM Mo spectra at 1M HCl concentration and varying total chloride concentrations (achieved by adding NaCl). From the trends in the speciation diagram of dimeric Mo species (Figure 2-5), it is apparent that at 1.0M HCl, all three postulated dimeric Mo species will coexist. The collected absorbance spectra for 20mM Mo in 1M HCl and total chloride concentrations of 0–4M are presented in Figure 2-7. The overall trend is an increase in absorbance with increasing NaCl concentration at nearly all wavelengths. This result contrasts with spectra of increasing HCl concentration, where an isosbestic point occurs at ca. 240 nm (Figure 2-1C and 2-1D). The broad peak developing at ~230 nm resembles spectra of 20mM Mo obtained at 3–4M HCl, where there are six major species present: $H_3MoO_4^+$, H_3MoO_4Cl, MoO_2Cl_2, $Mo_2O_5^{2+}$, $HMo_2O_5^{3+}$, and $HMo_2O_5Cl^{2+}$. The overall increase in absorbance indicates that the concentration of dimeric species is greater at 1M HCl and 4M NaCl than at 5M HCl. However, owing to the presence of many species in this region, the

characteristic spectral feature for Mo dimer at 245 nm is obscured, so analysis of spectra was performed using the equilibrium modeling software. HypSpec analysis of 20mM Mo spectra in 1M HCl and varying NaCl concentrations is summarized in Table 2-4.

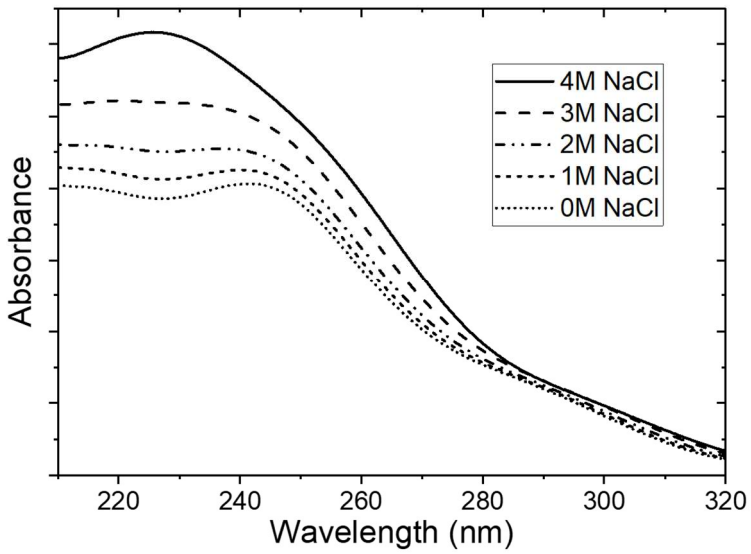

Figure 2-7. UV spectra of 20mM Mo in 1.0M HCl at increasing chloride concentration due to addition of 0–4M NaCl

Table 2-4. Species Abundance of Dinuclear Cations at 20mM Mo + 1.0M HCl with Increasing Chloride Concentration

[NaCl]	$Mo_2O_5^{2+}$ + $HMo_2O_5^{3+}$	$HMo_2O_5Cl^{2+}$
0	37%	12%
1.0	31%	19%
2.0	25%	23%
3.0	20%	27%
4.0	18%	28%

The results show that an increase in concentration of NaCl from 0 to 4M leads to ~16% increase of $HMo_2O_5Cl^{2+}$ species. This increase is accompanied by a ~19% decrease in the presence of non-chlorinated Mo dimers. These results indicate that an increase in total Cl^- concentration leads to a shift in the dimeric equilibria towards promotion of the chlorinated form while

maintaining a near-constant total Mo dimer concentration in the investigated range of 0–4M NaCl and 1M HCl. This finding provides good support for the existence of $HMo_2O_5Cl^{2+}$ by showing that the formation of an absorbing species not present in the molar absorptivity spectra for monomeric Mo shown in Figure 2-3 follows a clear dependence on [Cl^-] and thus is best explained by a chlorinated polynuclear complex. Analysis of the experimental spectra in the absence of a chlorinated dimer would not provide a satisfactory description of the increase in total absorbance at all wavelengths from 1 to 5M Cl^-. With the observation that the total dimer concentration in this region of HCl is maintained as the concentration of total chloride increases, the changes in spectral features presented in Figure 2-7 could only be supported by the increase in abundance of chlorinated dimers with higher molar absorptivity in the 220- to 260-nm region.

2. 5 Conclusions

Through chemometric analysis of UV spectrophotometric data, we have identified major Mo species in a wide range of Mo and HCl concentrations. In addition to previously reported monomeric Mo species present in HCl, the data suggest three dimeric Mo species present at concentrations above 0.1 mM Mo in HCl media. This study suggests the existence of a previously unreported chlorinated, cationic dimeric species stable at up to ~6M HCl at 300mM Mo, with the general formula $HMo_2O_5Cl^{2+}$.

At 0.1mM Mo and 0.5–11 M HCl, monomeric Mo(VI) species predominate, with the contribution from dimeric species below 1%. As the Mo concentration increases up to 300mM, absorbance spectra show the characteristic peak attributed to O-Mo-O bridging of cationic Mo dimers. Equilibrium modeling and factor analysis revealed three major dimeric species present in HCl, doubly and triply charged $Mo_2O_5^{2+}$ and $HMo_2O_5^{3+}$ cations stable at lower (<4M) HCl concentrations, and a singly chlorinated dinuclear cation $HMo_2O_5Cl^{2+}$ which is present in relevant concentration even at 6M HCl at 300mM Mo. It was also demonstrated that for MOEX-relevant conditions at 300mM Mo and 5M HCl, about 40% of Mo atoms exist in dinuclear form.

2. 6 Acknowledgements

Work supported by the U.S. Department of Energy, NNSA's Material Management and Minimization office, under Contract DE-AC02-06CH11357. Argonne National Laboratory is operated for the U.S. Department of Energy by UChicago Argonne, LLC.

2. 7 References

[1] National Academies of Sciences, Engineering, and Medicine, *Molybdenum-99 for Medical Imaging.* Washington, DC: The National Academies Press, 2016.

[2] 112th Congress. *American Medical Isotopes Production Act of 2011*. H.R. 4310, Public Law 112-239, 2013.

[3] Committee on Medical Isotope Production without Highly Enriched Uranium, National Research Council of the National Academies. *Medical Isotope Production Without Highly Enriched Uranium*. Washington, DC: The National Academies Press, 2009.

[4] International Atomic Energy Agency. *Non-HEU Production Technologies for Molybdenum-99 and Technetium-99m*. Nuclear Energy Series No. NF-T-5.4. Vienna: IAEA, 2013.

[5] Tkac, P.; Brown, M. A.; Momen, A.; Wardle, K. E.; Copple, J. M.; Vandegrift, G. F. MOEX: Solvent Extraction Approach for Recycling Enriched ^{98}Mo/^{100}Mo Material. *Sep. Sci. Technol.* 2018, 53, no. 12, 1856–1863, DOI: 10.1080/01496395.2017.1287739.

[6] Tkac, P.; Momen, A.; Breshears, A. T.; Brown, M. A.; Vandegrift, G. F. Molybdenum(VI) Coordination in Tributyl Phosphate Chloride Based System. *Ind. Eng. Chem. Res.* 2018, 57, no. 16, 5661–5669, DOI: 10.1021/acs.iecr.8b00590.

[7] Cruywagen, J. J. Protonation, Oligomerization, and Condensation Reactions of Vanadate(V), Molybdate(VI), and Tungstate(VI). *Adv. Inorg. Chem.* 2000, 49, 127–182, DOI: 10.1016/S0898-8838(08)60270-6.

[8] Cruywagen, J. J.; Rohwer, E.F.C.H. Monomeric Chloro-complexes of Molybdenum(VI). *Journal of the South African Chemical Institute* 1966, XI, no. 7, 11–23.

[9] Cruywagen, J. J.; Rohwer, E.F.C.H. Coordination Number of Molybdenum(VI) in Monomeric Molybdic Acid. *Inorg. Chem.* 1975, 14, no. 12, 3136–3137, DOI: 10.1021/ic50154a061.

[10] Oyerinde, O. F.; Weeks, C. L.; Anbar, A. D.; Spiro, T. G. Solution Structure of Molybdic Acid from Raman Spectroscopy and DFT Analysis. *Inorganica Chim. Acta* 2008, 361, no. 4, 1000–1007, DOI: 10.1016/j.ica.2007.06.025.

[11] Yin, P.; Wu, B.; Li, T.; Bonnesen, P. V.; Hong, K.; Seifert, S.; Porcar, L.; Do, C.; Keum, J. K. Reduction-Triggered Self-Assembly of Nanoscale Molybdenum Oxide Molecular Clusters. *Journal of the American Chemical Society* 2016, 138, no. 33, 10623–10629, DOI: 10.1021/jacs.6b05882.

[12] Cruywagen, J. J.; Heyns, J. B. B. Equilibria and UV Spectra of Mono- and Polynuclear Molybdenum(VI) Species. *Inorg. Chem.* 1987, 26, no. 16, 2569–2572, DOI: 10.1021/ic00263a003.

[13] Esbelin, E.; Gareil, P.; Masson, M.; Emin, J. L. Investigation of Mo(VI) Monomer–Dimer Equilibrium in Highly Acidic Solutions by UV Absorbance Spectroscopy Using Refined Numerical Processing. *Analytica Chimica Acta* 2001, 433, 299–310, DOI: 10.1016/S0003-2670(01)00782-6.

[14] Ojo, B. J. F.; Taylor, R. S.; Sykes, A. G. Kinetics of Rapid Monomer-Dimer Equilibrium of Mo in Aqueous Perchloric Acid. *J.C.S. Dalton* 1973, vi, 500–505.

[15] Cruywagen, J. J.; Heyns, J. B. B.; Rohwer, E. F. C. H. Dimeric Cations of Molybdenum(VI). *J. Inorg. Nucl. Chem.* 1978, 40, 53–59, DOI: 10.1016/0022-1902(78)80306-6.

[16] Cruywagen, J. J.; Heyns, J. B. B.; Molybdenum(VI) Equilibria at High Perchloric Acid Concentration. *Polyhedron* 2000, 19, no. 8, 907–911, DOI: 10.1016/S0277-5387(00)00331-4.

[17] Yokoi, K.; Matsubayashi, N.; Miyanaga, T.; Watanabe, I.; Ikeda, S. Studies on the Structure of Mo(VI) in Acidic Solutions by XANES and EXAFS. *Polyhedron* 1993, 12, no. 8, 911–914, DOI:10.1016/S0277-5387(00)81545-4.

[18] Dement'ev, I. A.; Kozin, A. O.; Kondrat'ev, Y. V.; Korol'kov, D. V.; Proyavkin, A. A. Mononuclear, Polynuclear, and Cluster Complexes of Molybdenum and their Reactions as Models of Biochemical Systems and Processes. *Russ. J. Gen. Chem.* 2007, 77, no. 5, 822–843, DOI: 10.1134/S1070363207050040.

[19] Bromley, L. A. Thermodynamic Properties of Strong Electrolytes in Aqueous Solutions. *AIChE J.* 1973, 19, 313, DOI:10.1002/aic.690190216.

[20] Regalbuto, M. C.; Copple, J. M.; Leonard, R.; Pereira, C.; Vandegrift, G. F. Solvent Extraction Process Development for Partitioning and Transmutation of Spent Fuel. *Eighth*

Inf. Exch. Meet. Actin. Fission Prod. Partitioning Transmutation 2004, Las Vegas, NV, Nov. 9–11, no. 6, 1–12.

[21] Gans, P.; Sabatini, A.; Vacca, A. Investigation of Equilibria in Solution: Determination of Equilibrium Constants with the HYPERQUAD Suite of Programs. *Talanta* 1996, 43, no. 10, 1739–1753, DOI: 10.1016/0039-9140(96)01958-3.

[22] van der Walt, S.; Schönberger, J. L.; Nunez-Iglesias, J.; Boulogne, F.; Warner, J. D.; Yager, N.; Gouillart, E.; Yu, T.; & scikit-image contributors. Scikit-image: Image Processing in Python. *PeerJ* 2014, 2014, no. 1, 1–18, DOI: 10.7717/peerj.453.

[23] Thielemann, J. P.; Ressler, T.; Walter, A.; Tzolova-Müller, G.; Hess, C. Structure of Molybdenum Oxide Supported on Silica SBA15 Studied by Raman, UV–Vis and X-ray Absorption Spectroscopy. *Applied Catalysis A-General* 2011, 399, 28–34, DOI:10.1016/j.apcata.2011.03.032.

[24] Neumann, H. M.; Cook, N. C. Species of Molybdenum(VI) in Hydrochloric Acid. *J. Am. Chem. Soc.* 1957, 79, no. 12, 3026–3030, DOI: 10.1021/ja01569a012.

[25] Nagazi, I.; Haddad, A. Synthesis, Crystal Structure and Physicochemical Proprieties of a Cytosine Selenomolybdate Based on Strandberg-Type [Se2Mo5O21]4−Polyanion. *Journal of Cluster Science* 2014, 25, no. 2, 627–638, DOI:10.1007/s10876-013-0658-0.

CHAPTER 3 SEPARATION OF RHENIUM/MOLYBDENUM FOR THE DETERMINATION OF ULTRATRACE RHENIUM CONTENT

This text is a modified version of a publication submitted to Separation Science & Technology.

3. 1 Abstract

The production of very pure molybdenum, free of Re even at ultratrace levels, is extremely important in meeting target purity specifications during the production of ^{99}Mo for medical applications. Here we propose two methods for separating ultratrace levels of Re from an Mo matrix: using either solvent extraction or extraction chromatography, coupled with inductively coupled plasma quadrupole mass spectrometry (ICP-MS) detection. Re is quantitatively (>99%) extracted from solutions in sulfuric acid as a complex with tri-*n*-butyl phosphate. Scrubbing and washing steps result in total decontamination factors for Mo, up to 1,700 for solvent extraction and 3,500 for extraction chromatography. Re is stripped into a 3-M NH_4OH matrix and analyzed by ICP-MS. Detection (L_D) and quantification (L_Q) limits were optimized by matrix-matching to allow detection of Re in strip solutions at levels of L_D = 0.1 ng Re/g-Mo and L_Q = 0.3 ng Re/g-Mo in Mo powder samples. By employing these two extraction methods, excellent recoveries of Re from bulk Mo were achieved, and the L_Q was improved by a factor of 5×10^4.

3. 2 Introduction

Molybdenum (Mo) is a corrosion-resistant refractory metal that sees an ever-increasing demand for its use in alloys, catalysts, and metal oxides [1–5]. Obtaining highly purified Mo is also important during the production of the radioisotope ^{99}Mo, the parent nuclide of ^{99m}Tc, which is used in diagnostic medical procedures. Recent ^{99}Mo production methods have focused on using enriched Mo target material for accelerator-based production via the bremsstrahlung photonuclear reaction ^{100}Mo(γ,n)^{99}Mo or the use of neutron capture ^{98}Mo(n,γ)^{99}Mo reaction [6].

Rhenium (Re), whose similar chemistry and co-occurrence in Mo ores makes it a common impurity in commercial Mo, is an especially critical element to detect and separate from Mo target

material. Its two naturally occurring isotopes ^{185}Re (37.5%) and ^{187}Re (62.6%) have large thermal neutron absorption cross sections and produce short-lived neutron-activation products ^{186}Re ($t_{1/2}$ = 90.6 hr) and ^{188}Re ($t_{1/2}$ = 16.9 hr); even low concentrations of Re impurities in bulk Mo powders can pose a great challenge to meeting strict radiopurity requirements during neutron-activation production of ^{99}Mo from Mo targets. This challenge is further amplified as domestic and international producers of ^{99}Mo use these technologies more frequently.

The importance of detecting and removing Re from Mo target material was previously reported in [7], where ^{186,188}Re impurities were observed in the final product; this resulted in the first batch of ^{99m}Tc being rejected. The neutron activation analysis (NAA) of Re impurities in Mo shows excellent sensitivity (~1 ng Re/g Mo) [11]; however, detection by gamma spectroscopy requires Re and Mo to be separated, so NAA is preferred when Re is separated from Mo prior to neutron activation. As ^{99}Mo technologies progress, efficient separation and detection methods must be established to ensure that the Re content in Mo batches is at acceptable levels.

Currently, commercially available Mo powders typically have the highest purity requirements in the metallic and superalloy industries; these include Mo metal powder (99.95%), high-density Mo metal powder (99.5%), and Mo metal briquettes (99.8%) [8]. Re is always present as a minor constituent, even in the ultrahigh-purity Mo (>99.9%) that is currently available. Therefore, to achieve purity requirements suitable for production of Mo irradiation targets, enhanced Mo/Re detection and separation methods are required.

Trace-level (ppm, mg/L) elemental analysis in liquid solutions is commonly performed by inductively coupled plasma quadrupole mass spectrometry (ICP-MS). It is often a preferred method for routine measurements because its sample preparation procedures are fast and simple, it is highly sensitive, and its linearity working range. Modern instruments employ automated sampling, which improves the speed, consistency, and convenience of sample measurements.

Ultratrace-level (ppb, μg/L and below) determination often involves the use of preconcentration steps, which contributes to the cost and time associated with sample analysis [9]. Extensive sample preparation procedures have been prepared for the ICP-MS detection of rare

earth elements and trace-level transition metals in geological samples [10]. However, these procedures often involve high-temperature and high-pressure digestion procedures to assist in the decomposition of refractory metals, which is arduous and not ideal for routine analysis.

The main challenge in determining trace levels of impurities by ICP-MS in bulk samples of Mo is due to the spectral and non-spectral inferences that arise from high concentrations of matrix substituents in the sample [10]. To reduce the deleterious effects of matrix constituents, samples must be diluted 500–1,000 times (commonly into 2% HNO_3 + 0.1% HF); this results in Re concentrations that are well below the instrument's detection limits (ng/L). The very low concentrations of Re (pg/g) coupled with the complex solubility characteristics of Mo in weak acids mean that highly concentrated Mo matrices must be partitioned from Re to allow accurate detection. Furthermore, the sample must be eluted into relatively small volumes to avoid diluting Re below detectable concentrations.

Re(VII) exists exclusively as the perrhenate anion (ReO_4^-) between pH 0 and 13, which has traditionally made it difficult to separate from MoO_4^{2-} and the polyoxoanions of Mo at higher concentrations. Conventional separation methods include volatilization of Re_2O_7 from hot acid solutions, precipitation of Re_2S_7 in alkaline sulfide solutions, or precipitation of Mo by α-benzoinoxime or 8-hydroxyquinoline, or strong/weak anion exchange resins [11]. However, these methods do not lend themselves well to analytically determining very small quantities of Re. A combined precipitation/ion exchange procedure developed specifically to remove Re from Mo and Tc employs the use of a Re carrier and thus impedes analytical determination of trace Re [11].

Much of the literature regarding Mo/Re separations focuses on Re extraction from acidic wash solutions during industrial molybdenite processing, which is done using ion exchange, precipitation, volatilization, or solvent extraction methods [12–15]. Industrial solutions have compositions on the order of ~0.4 mM Re and ~1–2 M Mo in nitric or sulfuric acids [16]. Separation of Re from Mo by solvent extraction is advantageous because it is highly selective toward recovery of Re from Mo-acidic matrix, but is also typically performed when Re is present at relatively high concentrations. These procedures may be suitable for the analytical determination of ultratrace Re in Mo powders, but such methodologies have not been described in the literature.

Some wet chemical strategies to extract Re from Mo are based on their chemistry in highly acidic media where Mo and Re speciation differ at very low pH values (pH < 0) [29]. MoO_4^{2-} becomes positively charged as mono- and dinuclear cations while ReO_4^- protonates to form neutral perrhenic acid [17]:

$$ReO_4^- + H^+ \rightarrow HReO_4 + H_2O \qquad \Delta G° = -1465.8 \text{ kJ/mol} \qquad (1)$$

$$H_2MoO_4 + 2H^+ \leftrightarrow MoO_2^{2+} + 2H_2O \qquad \Delta G° = -2.79 \text{ kJ/mol} \qquad (2)$$

Solvent extraction of $HReO_4$ from strong acid solutions has been performed using the neutral extractant tri-*n*-butyl phosphate (TBP), both alone and in synergistic mixtures with basic extractants such as bis-(3,5-dimethylhexyl-4- methylhexyl) amine (N298) or trialkyl amines (TAA) such as trioctylamine (TOA) [18-22]. In sulfuric acid, Re extracts quantitatively in the form of $HReO_4 \cdot 3TBP$ or $HReO_4 \cdot 4TBP$ adducts [19, 20]. However, the molybdenyl cations form sulfate complexes, such as $MoO_2SO_4 \cdot 3TBP$ or $H_2Mo_2O_5(SO_4)_2 \cdot 3TBP$, which extract poorly under such conditions (pH < -0.5) [23,29].

In this work, we propose two separation methods for detecting ultratrace Re from bulk Mo material, where Re is selectively extracted from Mo in H_2SO_4. Results of our analysis indicate that sufficient removal of Mo to trace levels facilitates the ICP-MS detection of about 0.1 ppb Re/g Mo (ng Re/g Mo) in Mo. The ICP-MS detection limit of Re was improved with a matrix-matching technique using a standard curve based on a metal-free blank of the sample matrix.

3. 3 Materials and Methods

3. 3. 1 Chemicals and sample preparation

Sulfuric acid and all other chemicals used were of trace-metal grade or optima-grade quality. Solutions were prepared with MilliQ H_2O (<18 MΩ-cm^2 conductivity). MoO_3 was purchased from Acros Organics or Sigma Chemicals Co. High-purity laboratory stock solutions of MoO_3 (<1 ppm Re/Mo) were used to evaluate the method we used for ultratrace Re detection.

Preparation of Mo samples for its purification from Re followed a two-step dissolution procedure. First, MoO_3 was dissolved in 3 M NH_4OH ($NH_{3(aq)}$-basis) with stirring and heating at 80°C on a hot plate. Alkaline dissolution of MoO_3 follows the reaction:

$$MoO_{3\,(cr)} + 2OH^- \rightarrow MoO_4^{2-} + H_2O \quad (3)$$

Complete dissolution of 1 g of MoO_3 in 10 mL of 3 M NH_4OH takes up to 30 minutes and results in a solution near pH 9.4. The predominant species of Mo under these conditions is the molybdate oxoanion MoO_4^{2-} (>99%). In the second step, concentrated H_2SO_4 was added to the chilled ammoniacal solutions to adjust to the desired H_2SO_4 concentration. This resulted in a solution volume of approximately 10–15 mL.

Hydrogen ion concentrations were determined by titration with a standardized solution of NaOH or HCl. In the calculation of total proton concentrations of acid solutions, allowance was made for the conversion of molybdenyl to molybdate upon neutralization to pH 7:

$$MoO_2^{2+} + 2H_2O \leftrightarrow MoO_4^{2-} + 4H^+ \quad (4)$$

3. 3. 2 Solvent extraction

The organic phase comprised 50% (v/v) tri-*n*-butyl phosphate (TBP) in *n*-dodecane. Following the results of Cheema et al. [19], the organic (*O*) and aqueous (*A*) phases were contacted in the 3:1 *O*/*A* volume ratio in all solvent extraction steps (including scrubs and strips). Organic phases were not pre-equilibrated with an aqueous phase prior to contact with the solution of Mo in sulfuric acid. Phase mixing was accomplished using continuous vortexing on a multi-tube vortexer for 10 minutes, unless otherwise stated. Phases were separated by centrifugation at 2,000 rpm for 5 minutes.

Distribution ratio (*D*) values of metals (*M*) between the organic and aqueous phase were determined as ratios of their analytical concentration in both phases. The *D* values are expressed as follows:

$$D = \frac{[M]_{org}}{[M]_{aq}} \quad (5)$$

3. 3. 3 Column chromatography

TBP resin obtained from Triskem International was used for chromatographic separation. The stationary phase of this resin consists of TBP impregnated (400 mg TBP/g resin) to an inert methacrylic polymeric support matrix without added diluent. The column cartridges had a measured void volume of approximately 0.3 mL and contained 300–500 mg of loosely prepacked resin with a particle size of 50–100 µm. Resin was pre-equilibrated in H_2SO_4 for at least 1 hour to allow proper wetting. Applying the same conditions as in solvent extraction studies, 2-mL samples of feed solution composition of around 1 M Mo in 4 M H_2SO_4 were loaded on the column (0.5 mL/min), washed with 4 mL of 4 M H_2SO_4 (0.5 mL/min), and eluted with 2 mL of 3 M NH_4OH solution (3 mL/min).

3. 3. 4 Detection methods

The solvent extraction experiments with the ^{99}Mo radiotracer were performed using ^{99}Mo obtained from a commercial ^{99}Mo/^{99m}Tc generator (Lantheus Medical Imaging). We took 3-mL aliquots of the aqueous and organic extraction phases for gamma counting on a high-purity germanium (HPGe) detector (ORTEC) using the ^{99}Mo 739.5 keV peak. Where applicable, the sulfur content was measured by ICP-OES (inductively coupled plasma optical emissions spectroscopy) using the PerkinElmer Optima 8300 analyzer.

Samples for ICP-MS were analyzed using a PerkinElmer NexION 2000 ICP-MS spectrometer. The instrument was calibrated with reference samples prepared by diluting the National Institute of Standards and Technology (NIST)-traceable standard solutions procured from Ultra Scientific (North Kingstown, Rhode Island, USA). Typical instrument operating conditions are listed in Table 3-1. All data collection and analysis were performed in ICP-MS standard mode using Syngistix software. The accuracy of the sample measurements were established through the

analysis of continuous calibration verification (CCV) standards. The analyte recoveries were within 10% of the true values.

Table 3-1. ICP-MS optimal instrumental operating conditions (PerkinElmer NexION 2000)

Parameter	Value
Cooling Gas	Argon
Nebulizer	Type C PFA ST3 Nebulizer
Spray Chamber	PFA Barrel Spray Chamber
Injector	Sapphire Injector 2.0 mm i.d.
Cones	Ni
Plasma Gas Flow	15 L/min
Auxiliary Gas Flow	1.2 L/min
Nebulizer Flow	0.91 L/min
Sample Delivery Rate	0.80 mL/min
RF Power	1600 W
Scan Mode	Peak Hopping
Dwell Time per amu	25 ms

The ICP-MS detection limit (L_D) and quantification limit (L_Q) for Re were calculated according to the Eurachem guide for *Fitness for Purpose of Analytical Methods* [24]. L_D provides an estimate of the minimum analyte concentration that is detectable above background (within 3 standard deviations), and L_Q is the minimum concentration of analyte that can be quantitatively determined with acceptable performance (within 10 standard deviations). The standard deviation (s'_0) used to calculate L_D and L_Q is given by the following equation:

$$s'_0 = s_0 \sqrt{\frac{1}{n} + \frac{1}{n_b}}, \quad (6)$$

where s_0 is the standard deviation of m number replicate measurements of blank solutions with analyte concentrations at or near zero, n is the number of replicate measurements for the sample, and n_b is the number of blank observations used for blank correction of the sample. L_D and L_Q are then simply determined as follows:

$$L_D = 3 \times s'_0 \quad (7)$$

$$L_Q = 10 \times s'_0 \quad (8)$$

3. 4 Results and Discussion

3. 4. 1 Solvent Extraction

Quantitative retention of Re in the organic phase is necessary for analytical determination of its concentration. To establish the necessary experimental conditions to reach Re extraction equilibria, several parameters were optimized to obtain maximum removal of Mo and recovery of Re for its detection at ultratrace levels.

3. 4. 2 Mixing time

During the extraction stage, the contacted phases were mixed for 5, 20, and 60 minutes using a vortex mixer in order to estimate the optimal contact time to obtain maximal yields of Re. The results presented in Table 3-2 show quantitative extraction of Re for all contact times examined in this study. Extraction yields, calculated as the ratio of the recovered to the initial amount of Re, were always above 99.7%; this confirms that the partitioning equilibria are achieved within 5 minutes of vigorous agitation. Scrubbing of the organic phases resulted in negligible Re losses; such losses contained less than 10 μg/L Re, equating to <0.5% of the total amount.

Table 3-2. Extraction kinetics of Re by 50% TBP/n-dodecane from 4 M H_2SO_4 containing 35 µmol Re + 0.2 M Mo at varying mixing times

	Yield			
Step	5 min agitation	20 min agitation	60 min agitation	Aqueous Phase
Extraction	>99.7%	>99.7%	>99.7%	4 M H_2SO_4
Scrub	<0.5%	<0.4%	<0.4%	4 M H_2SO_4

3. 4. 3 Sulfuric acid dependence

The H_2SO_4 concentration's dependence on the extraction behavior of both metals was investigated to maximize their separation factor (SF, i.e., the ratio of their *D* values under the same conditions), *SF = D(Re)/D(Mo*). Mo solutions were acidified with H_2SO_4 to between 0 and 6 M H_2SO_4 from ammoniacal solutions (~pH 9.4). Figure 3-1 shows that Re extraction by TBP increases with the sulfuric acid concentration and that Mo/Re separation is better at higher H_2SO_4

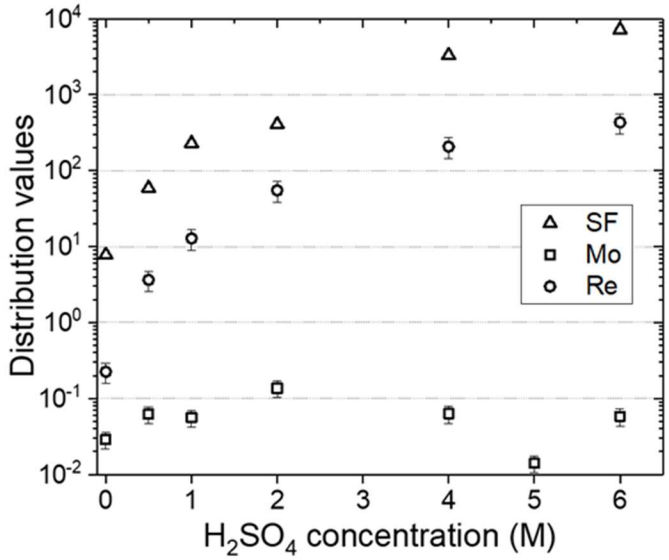

Figure 3-1. Re/Mo D values and SF for extraction in 0–6 M H2SO4 by 50% TBP in n-dodecane, an O/A ratio of 3:1, and 15-minute mixing times

concentrations; SF is equal to 3280 (4 M H_2SO_4) and 7150 (6 M H_2SO_4), owing to increased Re extraction, while extraction of Mo stays very low, D(Mo) < 0.1.

D values for Mo remain low, falling mostly below 0.1 for the whole studied range of H_2SO_4 concentrations. The trend is in agreement with the research of Alamdari and Sadrnezhaad [23], who demonstrated that extraction of Mo by TBP in the acid range 0.4–2 M H_2SO_4 is low and D values do not exceed 0.1 at [H_2SO_4] ≥ 0.3 M. The extractability of Re improves with increasing acid concentrations and is approximately linear with log [H^+] (R^2 = 0.97). D values of >200 for Re were observed for H_2SO_4 concentrations above 4 M, representing quantitative extraction from Mo in 3:1 O/A extraction.

3. 4. 4 Mo removal and Re recoveries

Solvent extraction profiles were collected to compare results from a five-stage solvent extraction procedure at 2 and 4 M H_2SO_4 (extraction, two scrubs, two strips). The results depicted in Figure 3-2 show that removal of Mo follows a similar trend at both concentrations, indicating that there is no discernable effect of H_2SO_4 concentration on Mo extraction or scrubbing under these conditions. The total Mo concentration in strip solutions collected after two scrub steps were 22.7 ± 2.9 mg/L (2 M H_2SO_4) and 21.9 ± 3.2 mg/L (4 M H_2SO_4), which equates to about 0.05% of the initial Mo concentration.

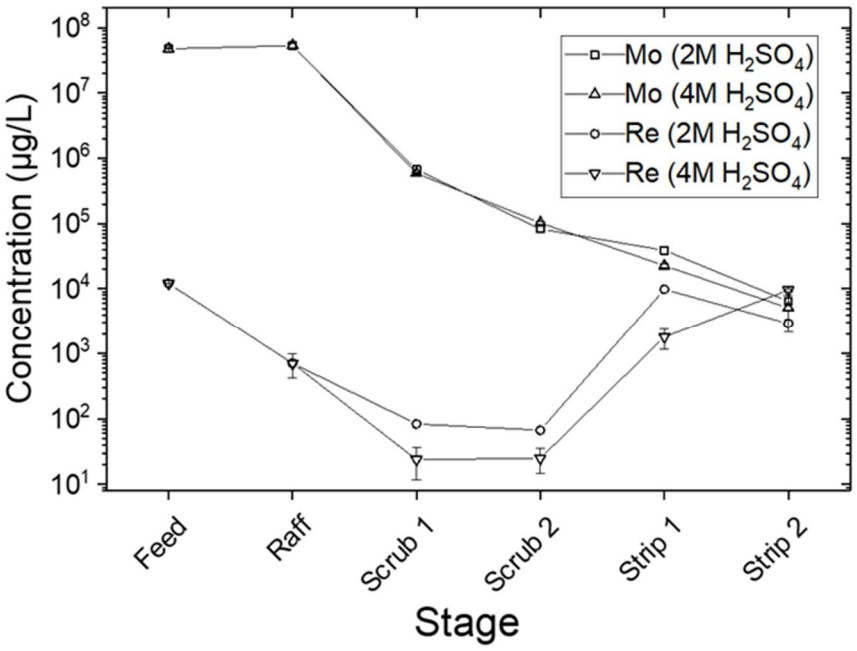

Figure 3-2. Stage profile of Mo/Re separation during solvent extraction at 2 or 4 M H2SO4 extraction and scrub and ~1 M NH4OH strip. The organic phase was 50% TBP in n-dodecane at an O/A ratio of 3:1 with 15-minute mixing times between stages

Re extraction exceeded 99% from both H_2SO_4 concentrations. Less than 1% total Re was lost in the scrub steps, but slightly more Re was lost in 2 M H_2SO_4 (0.63% ± 0.22%) than in 4 M H_2SO_4 (0.20% ± 0.09%). The main distinction in Re behavior occurred in the elution profile that used ~1 M NH_4OH. The first strip organic phase from the 4 M H_2SO_4 treatment showed very low Re recovery (14.8% ± 5.0%) compared to that of the 2 M H_2SO_4 treatment (81.4% ± 4.1%). The majority of Re from the 4 M H_2SO_4 treatment was collected in the second strip. This effect is best explained by a significant difference in the amount of H_2SO_4 extracted to the organic phase at higher H_2SO_4 concentrations, which results in partial neutralization of the strip phase and subsequently lower extraction yields. In spite of this, overall Re recovery after two strips was excellent for both 2 M H_2SO_4 (105% ± 4.5%) and 4 M H_2SO_4 (94% ± 4.3%).

These results show that maximum Re retention in the organic phase occurs from 4 M H_2SO_4, and excellent Re recovery is achieved and is reproducible between batches to within 5%.

Furthermore, the method can be improved by adding scrub steps to increase Mo removal and modifying strip steps to enhance Re recovery.

Further investigation focused on improving the scrubbing and stripping profiles of the separation process. Figure 3-3 shows the aqueous metal concentrations during four scrub stages with 4 M H_2SO_4. After four scrubbing stages, total Re losses to the aqueous phases equated to roughly 1–3% and total Mo breakthrough was about 0.01%. Increased loss of Re began on the fourth scrub step (1.3%). For stripping Re with ammonium hydroxide, a higher concentration (3 M) was applied to neutralize the coextracted H_2SO_4. The stripping profile in Figure 3-4 shows that total Re recovery from the organic phase is achieved in three contacts with 3 M NH_4OH, with 77.0% ± 3.3% Re in the first strip, 15.9% ± 0.7% in the second, and 1.11% ± 0.05% in the third strip. The recovery yields were calculated as the fraction of the mass of Re in the organic phase over the initial mass of Re in the sample, and are summarized in the Table 3-3.

Figure 3-5 shows that Mo removal improves with the number of scrubs performed, while Re recovery is minimally affected. Removal of Mo from the sample may be quantified by the decontamination factor (DF), which is calculated as the proportion of the initial ratio of metal concentrations to its ratio after treatment:

$$DF\ (Mo) = \left(\frac{[Mo]}{[Re]}\right)_{Aq,initial} \Big/ \left(\frac{[Mo]}{[Re]}\right)_{Aq,final} \quad (9)$$

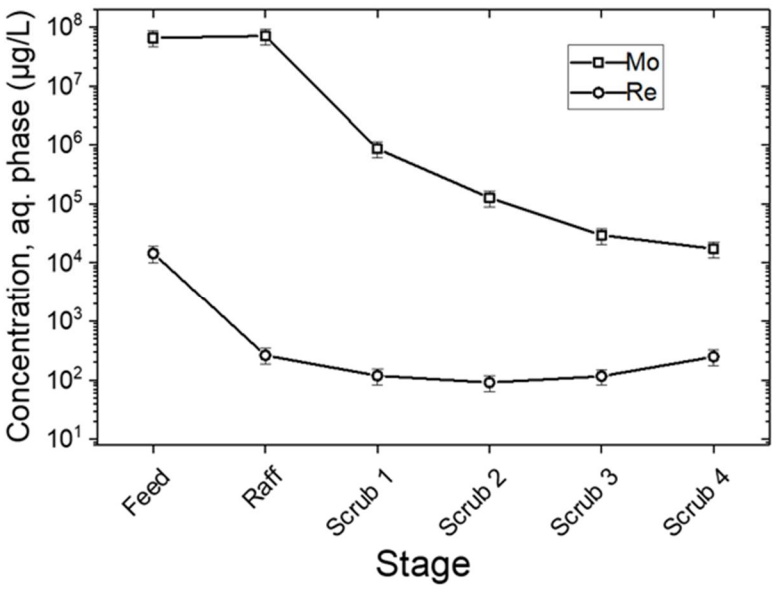

Figure 3-3. Stage profile of Mo/Re separation during solvent extraction using 4 M H2SO4 extraction and scrub, 50% TBP in n-dodecane organic phase, an O/A ratio of 3:1, and 15-minute mixing times

The DF for Mo (Eq. 14) in the strip solutions achieved values of 530 after one scrub; 1,130 after two scrubs; 1,320 after three scrubs; and finally, 1,730 after four scrubs. These results demonstrate that solvent extraction achieves excellent Mo decontamination while maintaining high Re recovery. A small percentage of Re is lost during scrub steps; however, the advantage of this tradeoff in improving Mo removal will become apparent later in this discussion.

Table 3-3. Analysis of Re in Mo samples by solvent extraction method. The final sample is from ultrahigh-purity MoO_3 stock

MoO_3(g)	Mo recovered (µg)	Re added (µg)	Re recovered (µg)	Re recovery
1.480	64.6	14.53	14.39	95.56%
1.480	81.8	14.53	13.88	99.06%
1.470	45.3	12.05	12.19	101.1%
1.470	40.9	12.05	12.75	105.8%
1.131	37.8	12.01	11.55	96.13%
1.131	33.6	12.01	11.81	98.30%
1.410	39.5	13.32	13.03	97.82%
0.921	28.0	0	0.0284	

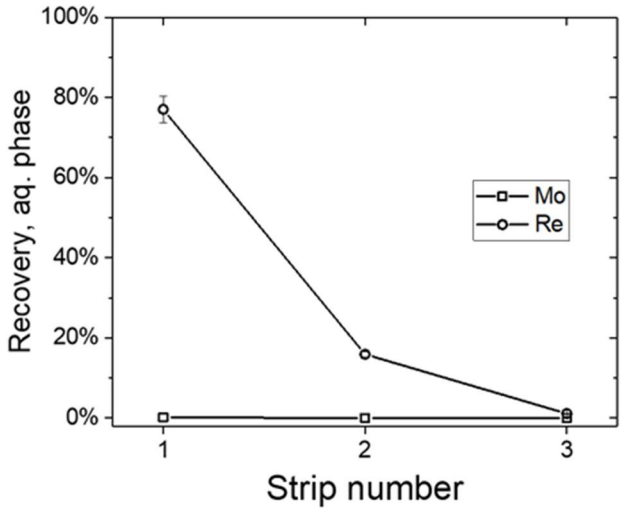

Figure 3-4. Stripping profile of Mo and Re using 3 M NH4OH from 50% TBP/dodecane

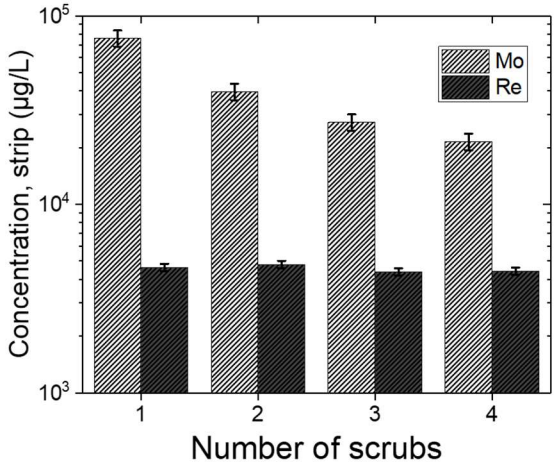

Figure 3-5. Cumulative metal concentrations after three strips steps from samples scrubbed between one and four times with 4 M H2SO4

Phase separation steps in bench-scale solvent extraction procedures place some limitations on the ability to fully recover Re from the initial sample. Following equilibration, liquid phases are separated by centrifugation and then transfered by disposable pipet. The result of these handling steps is inevitable and nonreproducible loss of sample in the pipet, on the sides of the vial, or by cross contamination of phases. Sample aliquots taken by micropipette can help reduce the error, but this modification introduces a requirement for larger initial sample volumes. A further consideration for solvent extraction as a quantitative method is that small volume changes arise in each phase after equilibration; these changes can serve to either concentrate or dilute the sample, thereby complicating recovery yields calculations. These issues represent the main practical disadvantages of using solvent extraction to analytically determine trace metal concentrations: doing so affects both precision and accuracy of results. The overall reliability of the proposed method, schematically represented in Figure 3-6, was tested with eight samples spiked with different amounts of Re, including and one blank sample of ultrahigh-purity Mo. Their recovery values are summarized in Table 3-3.

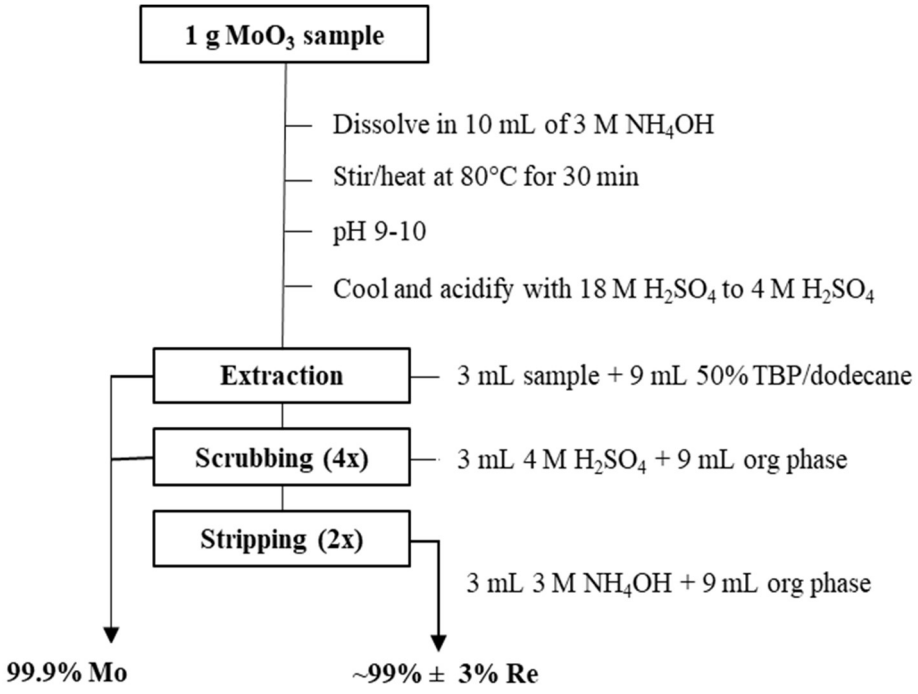

Figure 3-6. Schematic representation of proposed procedure using solvent extraction to analyze Re in Mo samples

The proposed method uses 1 g MoO_3 starting material dissolved into NH_4OH, from which subsamples may be taken for solvent extraction. Aqueous phases from extraction and scrub steps are removed between stages by transfer pipet and discarded. The total time from dissolution to recovery is approximately 3–4 hours. The final eluate contains roughly 0.3 M SO_4^{2-} + 3 M NH_4^+ + 5–10 mg/L Mo. Using this method, an unspiked sample of high-purity Mo target material was tested for Re content resulting in a value of 46.0 ± 1.5 ng Re/g Mo when applying the average recovery yield from Table 3-3.

3. 4. 5 Extraction chromatography

Separation using a chromatographic column was explored as an alternative approach to solvent extraction because it has several benefits over solvent extraction for routine measurements, especially where protocol standardization is concerned. A recent study by Ma et al. [25] concluded that quantitative Re adsorption on a TBP coated solvent-impregnated resin (TBP-CSIR) with polyvinyl alcohol coating resulted in 97.57% Re recoveries and separation from Cu, Fe, Ni, and As (SF = 93, 412, 348, 72, and 51, respectively). A TBP-impregnated resin containing TBP

(Triskem Inc.) was used and the results from the solvent extraction method were applied (discussed in Section 3.1).

Figure 3-7 shows the Mo/Re separation profile on the column. About 95% of Mo passes through the column to the eluate. Mo elution was excellent after three column washes with 4 M H_2SO_4. The final Mo concentration in the strip was 5.1 mg/L Mo (0.008% Mo breakthrough), equating to a DF of 3,480.

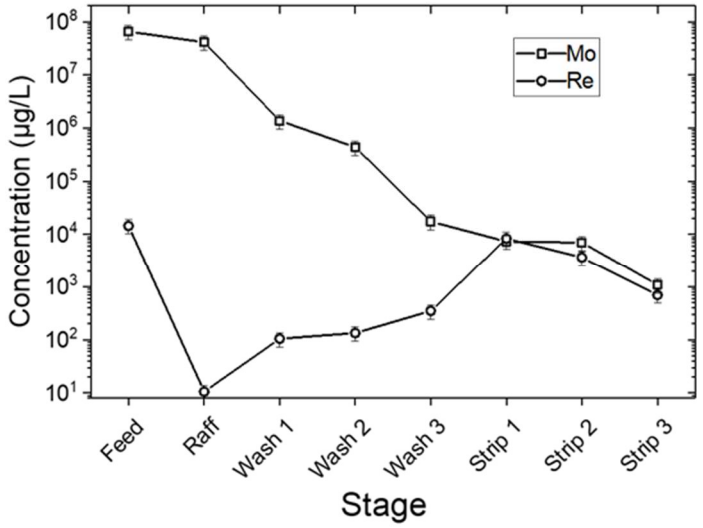

Figure 3-7. Stage profile of Mo/Re separation during column chromatography using 4M H_2SO_4 feed solution, TBP extractant resin (Triskem Inc.), and a flow rate of 0.5 mL/minute

Retention of Re from the feed solution was >99% with no detectable Re content in the eluate. Re losses amounted to roughly 3.0% in the first two column washes and a total of 4.8% after three washes. Loss of Re during wash steps might be explained by nonequilibrium Re extraction resulting from slow sorption kinetics. This explanation is consistent with investigations of TBP-impregnated resins, which showed that sorption kinetics for U(VI) and Th(IV) is diffusion limited [26]. Another possible factor that contributes to Re losses is TBP leakage from the resin the stationary phase. TBP leakage has been observed in TBP-impregnated resins on SiO_2-P supports at room temperature ranging from 100 to 1,000 mg/L, which is in accordance with TBP solubility in the selected media (HNO_3) [27]. This result correlates well to the study by Ma et al.

[25], which showed over the course of successive regeneration cycles that TBP-CSIRs (coated with polyvinyl alcohol crosslinked with boric acid) had excellent stability in H_2SO_4/NH_4OH compared to uncoated TBP-impregnated resins, in which TBP leakage may occur. Despite the small volumes used by the method in this work, TBP leakage at ~1,000 mg/L could constitute a significant fraction of the extractant lost. Nevertheless, the procedure described yields excellent Mo/Re separation that can provide an alternative solvent extraction. Results for separate samples tested using TBP resin chromatography are shown in Table 4.

Table 3-4. Analysis of Re in Mo samples by column chromatography using TBP resin. The final sample is from ultrahigh-purity MoO3 stock

MoO_3 (g)	Mo recovered (μg)	Re added (μg)	Re recovered (μg)	Re recovery
1.121	31.1	25.05	26.40	105.4%
1.039	19.4	14.53	13.75	94.67%
1.018	19.0	19.34	18.99	98.18%
1.102	17.8	0	0.0368	

The method depicted in Figure 3-8 follows the sample dissolution and acidification steps as described in the solvent extraction method (Figure 3-6). However, a smaller subsample volume is required because of simplifications in handling steps; therefore, this method may be modified to require less initial MoO_3. The total time from dissolution to recovery is approximately 2–3 hours. An unspiked sample of high-purity Mo target material was tested for Re content; a value of 49.8 ± 2.2 ng Re/g Mo was found after applying the average recovery yield from Table 3-4. This is comparable to the value obtained for the identical sample via solvent extraction procedure, 46.0 ± 1.5 ng Re/g Mo; this indicates close agreement between methodologies.

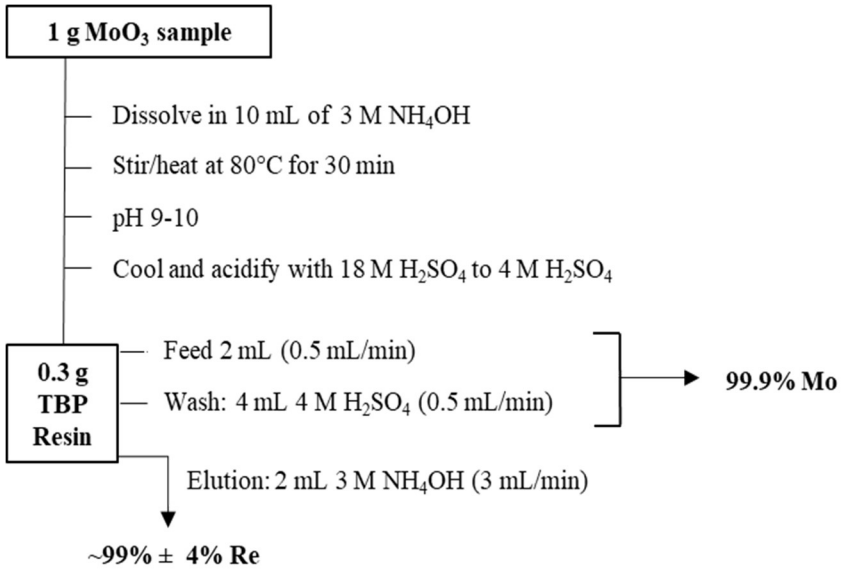

Figure 3-8. Schematic representation of proposed procedure for analysis of Re in Mo samples by column chromatography

3. 4. 6 ICP-MS detection

The limit of ICP-MS detection of a metal is strongly influenced by the chemical matrix of the sample solution. Interference from matrix elements, also known as non-spectroscopic interference, is often alleviated by sample dilution. The standard dilution procedure in ICP-MS sample preparation uses a 2% HNO_3 matrix, which helps to prevent gradual deposition of dissolved matrix components onto the nebulizer and torch injector tips. Where trace analysis is concerned, sample dilution effectively increases instrument detection limits according to the dilution factor used. One technique that can be used to avoid dilution of the analyte is to run calibration standards in a matrix-matched solution (i.e., the identical matrix of the sample excluding the analyte). However, good accuracy and precision must be experimentally confirmed for each unique sample matrix. The matrix-matching technique's effectiveness at improving detection limits for Re was investigated in solutions consisting of either blank (5% NH_4SO_4) or reference/standard solution (5 mg/L of Mo in 2% HNO_3 with 0.1% HF) to assess their individual contributions to non-spectroscopic inferences.

Table 3-5 shows the L_D and L_Q limits for Re in complex matrices resembling the strip phases from chromatographic and solvent extraction separation of Re from Mo. Matrix constituents in strip solutions are shown to provide a comparison between sources of interferences. Sulfate concentration in strip solutions of 0.3 M was determined by ICP-OES, indicating co-extraction of H_2SO_4 to the organic phase which then follows Re into the NH_4OH strip.

Monitoring the area peak for ^{187}Re (62.6% isotopic abundance) showed that the detection limit (3σ) for Re went down to <4 ng/L in 5 ppm Mo and 2 ng/L in 5% $(NH_4)_2SO_4$. The relative difference between matrix interferences derived from elevated Mo content versus that of $(NH_4)_2SO_4$ in blank solutions was roughly a factor of 2. The sum of these interferences provides an overall estimate of L_D = 5.9 ng Re/L. The aqueous concentration of a 1-g sample of MoO_3 containing 0.1 ng Re/g Mo (ppb) in 10 mL represents 7 ng Re/L in 10^9 ng/L of Mo. Provided that ~90–100% Re recoveries in the strip solutions are obtained with removal of Mo to 5 mg/L, the evaluation of this sample applying the matrix-matching technique enables detection of Re in Mo samples of L_D = 0.1 ng Re/g Mo and L_Q = 0.3 ng Re/g Mo.

Table 3-5. Evaluation of matrix effects on Re detection limits by ICP-MS

$[Mo]_{blank}$ (mg/L)	Matrix $_{blank}$	Isotope	I_{blank} (CPS)	RSD $_{blank}$ (%)	SD $_{blank}$ (µg/L)	L_D (ng/L)	L_Q (ng/L)	L_D (pg Re/g MoO_3)	L_Q (pg Re/g MoO_3)
5.0	2% HNO_3 + 0.1% HF	^{187}Re	3728	2.8	0.002	3.9	13.2	39.5	131.7
0	5% $(NH_4)_2SO_4$	^{187}Re	195	11.1	0.001	2.0	6.6	19.7	65.8

3. 5 Conclusion

Two methods for the detection of ultratrace Re in Mo powders were developed. Using solvent extraction or extraction chromatography, Re dissolved in 4 M H_2SO_4 can be quantitatively removed from Mo with a separation factor of about 3,300. For the solvent extraction using TBP, Mo distribution ratios from 2 to 6 M H_2SO_4 were less than 0.1, following no discernable trend. Extraction of Re increased with H_2SO_4 concentration, reaching a distribution ratio of 207 at 4 M H_2SO_4. Owing to excellent Re extraction, SF for Re/Mo increased with acid concentration from 100 to 1000 between 1 and 2 M H_2SO_4 to >1,000 for 4 M H_2SO_4 and above.

The developed chromatographic method provides improved separation of Re from Mo, compared to solvent extraction. Mo is removed by wash/scrub steps to trace amounts (5–10 mg/L), corresponding to a DF for Mo of up to 1,700 for solvent extraction and about 3,500 for extraction chromatography. Although Mo removal improved with chromatographic separation, some Re loss (<5%) indicates that there is a possibility of slow Re(VII) adsorption kinetics, leakage of extractant from the TBP resin, or a combination of these factors. In spite of Re losses, the excellent separation of Re from Mo achieved with the TBP chromatographic column merits a fuller investigation into TBP resins for the selective extraction of Re from Mo.

Ultrahigh-purity MoO_3 powder samples were tested in roughly 1-g quantities by solvent extraction and column chromatography. Results from the chromatographic procedure (49.8 ± 2.2 ng Re/g Mo) compares well to the value obtained for the identical sample by solvent extraction procedure (46.0 ± 1.5 ng Re/g Mo), indicating close agreement between these methodologies. Detection limits in ICP-MS analysis were improved using matrix-matching to result in final values of L_D = 0.1 ng Re/g Mo and L_Q = 0.3 ng Re/g Mo for Re in bulk Mo samples. These values offer greatly enhanced detection of Re in solid Mo target material by a factor of about 5×10^4.

3. 6 Acknowledgments

This work was supported by the U.S. Department of Energy, National Nuclear Security Administration's Material Management and Minimization office, under Contract DE-AC02-06CH11357. Argonne National Laboratory is operated for the U.S. Department of Energy by UChicago Argonne, LLC.

3. 7 References

[1] T. R. Crompton, "Metals in Surface, Ground, and Mineral Waters," in Determination of Metals in Natural Waters, Sediments and Soils, Elsevier, 2015, pp. 161–178.

[2] D. A. John, "Rhenium: a rare metal critical in modern transportation," Fact Sheet. US Geological Survey, 2015.

[3] T. Hong et al., "Selective recovery of Rhenium from industrial leach solutions by synergistic solvent extraction," Separation and Purification Technology, vol. 236, p. 116281, Apr. 2020.

[4] T. A. Lasheen, M. E. El-Ahmady, H. B. Hassib, and A. S. Helal, "Molybdenum Metallurgy Review: Hydrometallurgical Routes to Recovery of Molybdenum from Ores and Mineral Raw Materials," Mineral Processing and Extractive Metallurgy Review, vol. 36, no. 3, pp. 145–173, Nov. 2014, doi: 10.1080/08827508.2013.868347.

[5] G. Tölg, "Bedeutung und Möglichkeiten der Reinststoffanalytik in der Metallforschung," in Achtes Kolloquium über Metallkundliche Analyse mit Besonderer Berücksichtigung der Elektronenstrahl- und Ionenstrahl-Mikroanalyse Wien, 27. bis 29. October 1976, Springer Vienna, pp. 1–26, 1977.

[6] Molybdenum-99 for Medical Imaging. National Academies Press, 2016.

[7] K. Dadachova, K. La Riviere, and P. Anderson, "Improved processes of molybdenum-99 production," Journal of Radioanalytical and Nuclear Chemistry, vol. 240, no. 3, pp. 935–938, Jun. 1999, doi: 10.1007/bf02349877.

[8] T. A. Lasheen, M. E. El-Ahmady, H. B. Hassib, and A. S. Helal, "Molybdenum Metallurgy Review: Hydrometallurgical Routes to Recovery of Molybdenum from Ores and Mineral Raw Materials," Mineral Processing and Extractive Metallurgy Review, vol. 36, no. 3, pp. 145–173, Nov. 2014, doi: 10.1080/08827508.2013.868347.

[9] B. Zawisza, K. Pytlakowska, B. Feist, M. Polowniak, A. Kita, and R. Sitko, “Determination of rare earth elements by spectroscopic techniques: a review,” Journal of Analytical Atomic Spectrometry, vol. 26, no. 12, p. 2373, 2011.

[10] F. G. Pinto, R. E. Junior, and T. D. Saint’Pierre, “Sample Preparation for Determination of Rare Earth Elements in Geological Samples by ICP-MS: A Critical Review,” Analytical Letters, vol. 45, no. 12, pp. 1537–1556, Aug. 2012, doi: 10.1080/00032719.2012.677778.

[11] National Research Council. 1961. The Radiochemistry of Rhenium. Washington, DC: The National Academies Press. https://doi.org/10.17226/21549

[12] B. Zhang, H.-Z. Liu, W. Wang, Z.-G. Gao, and Y.-H. Cao, “Recovery of rhenium from copper leach solutions using ion exchange with weak base resins,” Hydrometallurgy, vol. 173, pp. 50–56, Nov. 2017, doi: 10.1016/j.hydromet.2017.08.002.

[13] Z. Ma, X. Guo, D. Li, and Q. Tian, “Adsorption of Re(VII) from sulfuric acid solutions by coated impregnated resins containing TBP,” Separation Science and Technology, pp. 1–9, Dec. 2019, doi: 10.1080/01496395.2019.1706577.

[14] T. Hong et al., “Selective recovery of Rhenium from industrial leach solutions by synergistic solvent extraction,” Separation and Purification Technology, vol. 236, p. 116281, Apr. 2020, doi: 10.1016/j.seppur.2019.116281.

[15] Y. Wang and C. Wang, “Recent advances of rhenium separation and enrichment in China: Industrial processes and laboratory trials,” Chinese Chemical Letters, vol. 29, no. 3, pp. 345–352, Mar. 2018.

[16] A. Kholmogorov et al., “Ion exchange recovery and concentration of rhenium from salt solutions,” Hydrometallurgy, vol. 51, no. 1, pp. 19–35, Jan. 1999, doi: 10.1016/s0304-386x(98)00064-4.

[17] J. J. Cruywagen, “Protonation, Oligomerization, and Condensation Reactions of Vanadate(V), Molybdate(vi), and Tungstate(vi),” in Advances in Inorganic Chemistry, Elsevier, pp. 127–182, 1999.

[18] T. Hong et al., “Selective recovery of Rhenium from industrial leach solutions by synergistic solvent extraction,” Separation and Purification Technology, vol. 236, p. 116281, Apr. 2020.

[19] H. A. Cheema, S. Ilyas, S. Masud, M. A. Muhsan, I. Mahmood, and J. Lee, “Selective recovery of rhenium from molybdenite flue-dust leach liquor using

solvent extraction with TBP," Separation and Purification Technology, vol. 191, pp. 116–121, Jan. 2018, doi: 10.1016/j.seppur.2017.09.021.

[20] D. J. Pruett and D. R. McTaggart, "The solvent extraction behavior of rhenium," Journal of Inorganic and Nuclear Chemistry, vol. 43, no. 9, pp. 2109–2112, Jan. 1981.

[21] L. Karagiozov and C. Vasilev, "Extraction of molybdenum from weak acid rhenium-containing solutions," Hydrometallurgy, vol. 12, no. 1, pp. 111–116, Feb. 1984, doi: 10.1016/0304-386x(84)90051-3.

[22] D. Fang, X. Gu, Y. Xiong, S. Yue, J. Li, and S. Zang, "Thermodynamics of Solvent Extraction of Rhenium with Trioctyl Amine," Journal of Chemical & Engineering Data, vol. 55, no. 1, pp. 424–427, Jan. 2010, doi: 10.1021/je900402w.

[23] E. K. Alamdari and S. Sadrnezhaad, "Thermodynamics of extraction of MoO4(2−) from aqueous sulfuric acid media with TBP dissolved in kerosene," Hydrometallurgy, vol. 55, no. 3, pp. 327–341, Apr. 2000, doi: 10.1016/s0304-386x(99)00090-0.

[24] B. Magnusson and U. Örnemark (eds.), Eurachem Guide: The Fitness for Purpose of Analytical Methods – A Laboratory Guide to Method Validation and Related Topics, (2nd ed. 2014). ISBN 978-91-87461-59-0. Available at www.eurachem.org.

[25] Z. Ma, X. Guo, D. Li, and Q. Tian, "Adsorption of Re(VII) from sulfuric acid solutions by coated impregnated resins containing TBP," Separation Science and Technology, pp. 1–9, Dec. 2019.

[26] M. W. Abdel Raouf and A. M. El-Kamash, "Kinetics and thermodynamics of the sorption of uranium and thorium ions from nitric acid solutions onto a TBP-impregnated sorbent," Journal of Radioanalytical and Nuclear Chemistry, vol. 267, no. 2, pp. 389–395, Jan. 2006.

[27] L. Jelinek, Y. Wei, and M. Kumagai, "Separation of Electrochemically Generated Ce(IV) from Rare Earths(III) in Nitric Acid Media by TBP Impregnated Resin," Solvent Extraction and Ion Exchange, vol. 24, no. 5, pp. 765–779, Oct. 2006, doi: 10.1080/07366290600846182.

[28] R. R. Srivastava, J. Lee, and M. Kim, "Complexation chemistry in liquid-liquid extraction of rhenium," Journal of Chemical Technology & Biotechnology, vol. 90, no. 10, pp. 1752–1764, May 2015, doi: 10.1002/jctb.4707.

[29] E. Keshavarz Alamdari, D. Darvishi, D. F. Haghshenas, N. Yousefi, and S. K. Sadrnezhaad, “Separation of Re and Mo from roasting-dust leach-liquor using solvent extraction technique by TBP,” Separation and Purification Technology, vol. 86, pp. 143–148, Feb. 2012, doi: 10.1016/j.seppur.2011.10.038.

CHAPTER 4 RECYCLING ISOTOPICALLY ENRICHED MOLYBDENUM FROM ^{99M}TC GENERATOR WASTE STREAM

This text is a modified version of a technical report published by the Chemical & Fuel Cycles Technologies Division at the Argonne National Laboratory Library.

4. 1 Abstract

Modern low specific activity (LSA) generator designs utilize an aqueous biphasic extraction chromatography column to separate Tc from low-specific-activity ^{99}Mo. During this separation process, a fraction of the source Mo material can be found in the waste. This is not of concern when natural Mo targets are used. However, the introduction of isotopically enriched ^{98}Mo for neutron capture or ^{100}Mo for accelerator-based production requires recovery of this valuable enriched Mo material. The generator waste is absorbed and solidified in a superabsorbent hydrogel polymer. In this contribution, we report results from our small-scale experimental study on development of a separation process for recovery of molybdenum from the polymeric gel waste using common chemicals and simple chemical techniques.

Our investigation confirms that the acidic deswelling of the alkaline hydrogel with concentrated hydrochloric acid converts the occluded molybdate to a neutral molybdenyl dichloride species that is freely released from the gel. Mo can then be concentrated on a commercial tri-*n*-butyl phosphate resin, eluted with ammonium hydroxide, and crystallized as ammonium heptamolybdate for conversion back to Mo metal. Typical Mo recoveries are 90–95%.

4. 2 Introduction

The development and implementation of alternative technologies to produce ^{99}Mo/^{99m}Tc without the use of ^{235}U has recently attracted a lot of interest; these technologies include i) ^{100}Mo(γ,n)^{99}Mo via photonuclear reaction with a photon source from bremsstrahlung, ii) ^{100}Mo(n,2n)^{99}Mo using fast neutrons, and iii) neutron capture on

^{98}Mo. These approaches offer a less-expensive alternative to fission-made ^{99}Mo, but with a lower yield. The main advantage of these alternative technologies is the minimal amount of low-level waste generated, owing to minimal purification requirements. However, to produce several kCi of ^{99}Mo, enriched ^{98}Mo or ^{100}Mo targets are required (enriched ^{100}Mo is available in kg quantities for ~ $1000/g). One of the difficulties with production of low specific-activity ^{99}Mo/high-specific-activity ^{99m}Tc is the need for a different generator designed to accommodate the low specific activity of ^{99}Mo.

Some modern ^{99m}Tc generators are designed for separation of ^{99m}Tc from low-specific-activity ^{99}Mo in highly alkaline solution. These designs uses a Tc-selective aqueous biphasic extraction chromatography (ABEC) resin in a multicolumn design (Figure 4-1). Small amounts of Mo that pass through the ABEC column can partition to the waste stream, where the solution is absorbed and solidified in a superabsorbent polymer. This is not a problem when natural Mo targets are used, but the high cost of enriched Mo material (^{100}Mo or ^{98}Mo) requires that the Mo in the waste stream be efficiently recycled into fresh targets.

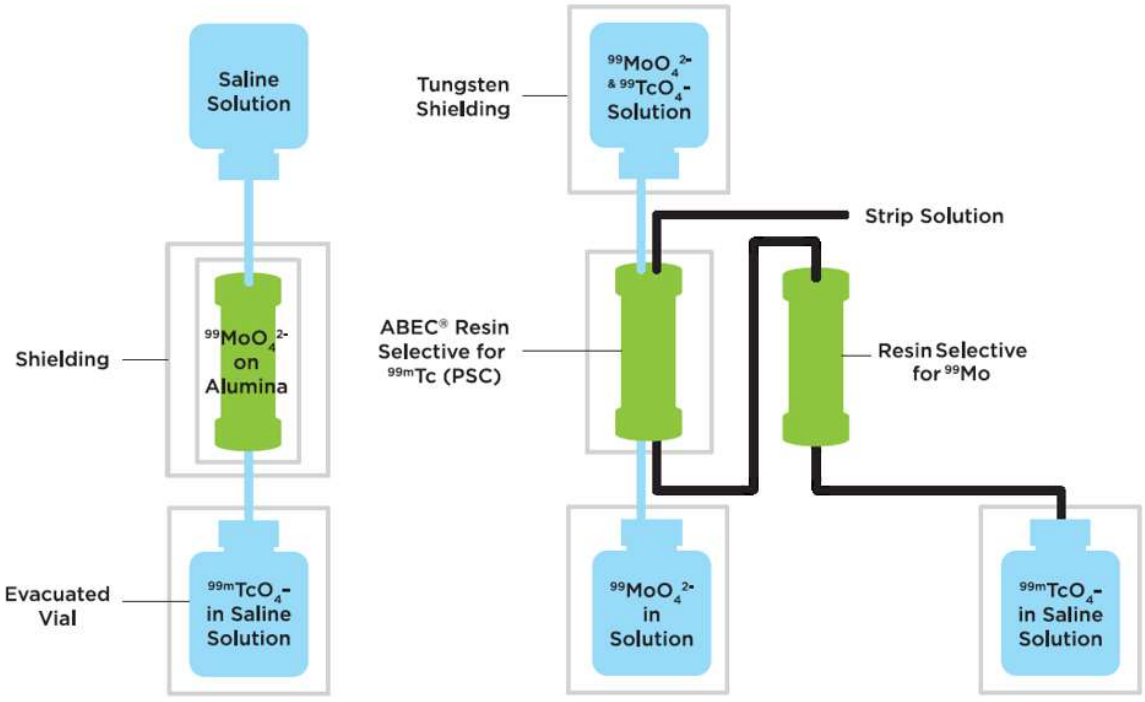

Figure 4-1. Comparison of traditional ion-exchange column (left) and a generic multicolumn selectivity inversion generator (right); adapted from Horwitz and Bond [1]

One method used for capturing LSA generator waste solutions is through solidification of the waste with superabsorbent polymers (SAPs). The waste stream from LSA generators is highly alkaline, comprising primarily aqueous NaOH solution, so alkaline SAPs are used. In a typical LSA generator, fresh containers with ~350 g of dry polymer collect up to 3.5 L of used Mo solution (~200 elutions), at which point the containers are replaced. The final waste matrix contains around 10 mL of waste solution per gram of dry polymer and each waste containiner may hold up to several grams of Mo.

The SAP composition is a mixture of two hydrogel copolymers consisting of crosslinked poly(acrylamide-co-acrylic acid). An example of the poly(acrylamide-co-acrylic acid) structure is depicted in Figure 4-2 [2]. These commercially available polymers are commonly used for their superabsorbent qualities and ability to sequester harmful multivalent cations. The ratio of comonomers is often tuned to achieve the desired gel properties. In general, the non-ionic acrylamide monomers add mechanical strength, allowing the hydrogel beads to retain their spherical shape. Acrylate monomers participate in hydrogen bonding and enhance the absorption capacity for liquid solutions. The molecular weights of the polymer and its crosslinkers allow for additional tunability of its features. Longer (high-molecular-weight) crosslinkers between chains allow for greater swellability compared to shorter (low-molecular-weight) crosslinkers.

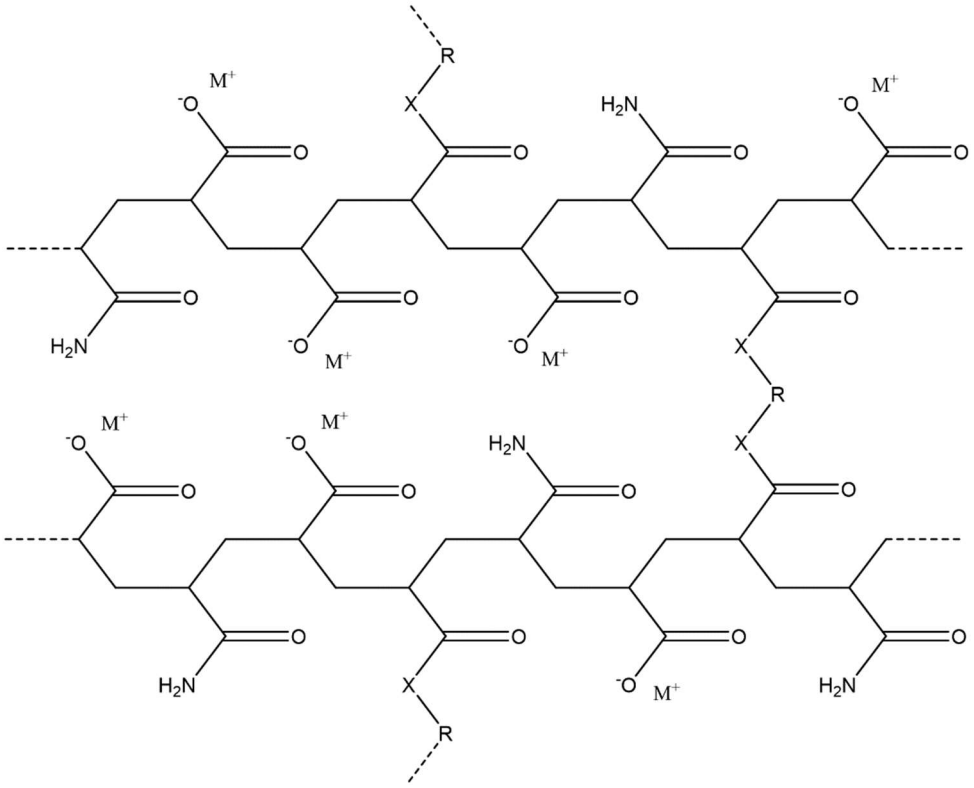

Figure 4-2. Poly(acrylamide-co-acrylic acid) polymer network. M+ = Na+, R = CH2, and X = NH or O

Poly(acrylamide-co-acrylic acid) is an atactic, weakly anionic polyelectrolyte containing ionizable groups that are able to dissociate in aqeuous media [3]. The dissociation of positive counterions in solution creates a high charge density along its backbone, which allows repulsive forces between charged groups to extend the polymer chain. Water capture is facilitated by hydrogen bonding within the three-dimensional framework of crosslinked chains. As a result, anionic hydrogels are able to absorb 100 to 1000 times their mass of neutral- to high-pH aqueous solutions.

Hydrogen bonding in hydrogels can be disrupted by the neutralization of the charged groups. In anionic hydrogels, high-ionic-strength and high-acid conditions greatly reduce the absorption capacity for water. Decreasing the pH environment of a fully swollen anionic hydrogel can result in the collapse, or deswelling, of the gel and release of absorbed

solution [2]. It is important to consider the deswelling behavior when recovering absorbed Mo solutions, which are highly alkaline.

A poly(acrylamide-co-acrylic acid) chain is typically synthesized by solution or suspension polymerization using the desired ratio of monomeric subunits in a mixture. However, the copolymer can also be derived from homogeneous polyacrylamide following the partial hydrolysis of amide moieties [4]. Amide groups will hydrlyze to carboxyl groups under both alkaline and acidic conditions through, for example, the reactions [5]

$$CH_3CONH_2 + NaOH \rightarrow CH_3COONa + NH_3 \quad (1)$$

$$CH_3CONH_2 + H_2O + HCl \rightarrow CH_3COOH + NH_4^+Cl^- \quad (2)$$

The result of amide hydrolysis of polyacrylamide is the partial or complete conversion to polyacrylate and release of ammonia. Partial degradation of the NSB polymer is apparent in SAP waste (pH ~14), which offgasses ammonia.

The high charge density in anionic hydrogels enables the binding and sequestration of various multivalent cations (e.g., Ca^{2+}, Co^{2+}, Al^{3+}, MoO_2^{2+}) following the dissociation of positive counterions (Na^+, K^+) [6]. Polymers with carboxyl groups ($-COO^-$) can precipitate as M^{2+}-polyacrylates (eg. M = Ca, Mg, Ba) [7] [8]. Precipitation is due to metal-bridged complexing that takes place between two neighboring monomers along an individual chain, causing the polymer backbone to shrink. This effect is known as counterion condensation or “salting out,” and results in flocculation of metal-polymer aggregates. Flocculation of dissolved metals makes polyacrylate useful for wastewater treament [5].

Hydrogels that precipitate through complexation with multivalent cations show limited resolubilization in aqueous solutions. This feature may be leveraged for phase separation in NSB. Divalent counterions show strong affinity for polyacrylates in saline solutions and have been generally classified in the order [3] $Mg^{2+} < Ca^{2+} < Ba^{2+} < Mn^{2+} < Co^{2+} < Ni^{2+} < Cd^{2+} << Cu^{2+}$. However, dissolved metals typically show reduced binding to

polyacrylate in matrices of high acidity and ionic strength [9]. One exception to this rule is metals that form complexes in acidic solutions. The molybdenyl oxocation MoO_2^{2+} that forms at pH < 0 may therefore coprecipitate with polyacrylate [10]. The use of a complexing acid such as HCl can preclude the formation of MoO_2^{2+}, favoring the chloro-complex MoO_2Cl_2.

The extraction of Mo from the polymer will still require purification steps to remove Na and K before Mo is recycled to ammonium heptamolybdate (AHM). One method available to accomplish this purification leverages the extractability of MoO_2Cl_2 in HCl using the neutral extracting ligand tri-n-butyl phosphate (TBP) [11]. Our group has previously optimized this process in the recycling of source Mo targets (MOEX process), which achieves quantitative Mo recoveries and excellent Na and K decontamination [12]. The MOEX process was recently implemented in large-scale, rapid processing schemes using countercurrent centrifugal contactors [13]. Mo is recovered in ammonium hydroxide, which is evaporated to form solid AHM. The AHM powder is heated in a furnace, where it is converted to Mo metal. An investigation into the continous recycling of K_2MoO_4 source material is ongoing and is presented in a separate report.

Typical LSA generator waste containers may contain up to several-gram quantities of enriched Mo metal. It is important to develop recycling strategies to convert this Mo back to AHM for the production of new targets for irradiation. The purpose of this study is to provide an efficient method for the recovery of enriched Mo from SAP gel waste. Preliminary data on solvent extraction and column chromatographic separation of Mo recovered from NSB are also presented.

4. 3 Experimental

4. 3. 1 Reagents

All chemicals were purchased from Fisher Scientific and used as received. Hydrochloric acid was trace-metal grade, and all water was deionized and purified to >18 MΩ-cm. When impurities were being measured, glassware was acid-washed thoroughly

prior to use. Simulated LSA generator waste solutions consisted of NaOH, KOH, NaCl, and Mo^{6+} at pH 14.3. Brilliant Blue FCF (2-[[4-[ethyl-[(3-sulfonatophenyl)methyl]amino]phenyl]-[4-[ethyl-[(3-sulfonatophenyl)methyl]azaniumylidene]cyclohexa-2,5-dien-1-ylidene]methyl]benzenesulfonate) was also added, which is used in commerical LSA generator waste gels. The pH of all solutions was determined by titration with phenolphthalein using standardized NaOH or HCl.

SAPs were obtained in dry polymer form and as a gel containing true waste solution. When preparing LSA waste simulant from dry SAP, the simulant solution was added using a ratio of 10 mL/g polymer and allowed to equilibrate for 12–24 hours. The mixture underwent a color change from blue to pink during the equilibration period, with a final pH around 14. Metal concentrations were determined by inductively coupled plasma mass spectrometry (ICP-MS).

4. 3. 2 Polymer Deswelling

Small-scale experiments were performed using either a glass fritted vacuum filtration apparatus with a glass-wool prefilter with 2-µm pore size, or Milllipore low-binding Durapore PVDF membrane centrifuge tubes with 0.22-µm pore size. SAP gel was added to sample containers by mass; then deswelling solutions were added at an approximately 1:1 volume ratio. The mixture was stirred or vortexed thoroughly and allowed to settle for at least one hour to allow equlibration, during which time no further changes to the mixture were apparent. Samples were then filtered or centrifuged for 5 min at 2500 rpm to separate liquid and solid phases.

Reactions on a larger scale were performed in open glass beakers with overhead stirring to allow offgassing of ammonium chloride. The solid phase settled to the bottom of the container and tackified together, forming a cake. This mixture was filtered over a medium glass frit under full vacuum. The solid phase was then immediately washed or soaked in HCl solution to recover the remaining Mo. Liquid phases that were turbid after

filtration were filtered again, using a 0.45-µm PVDF filter. The ingrowth of various impurities was determined by ICP-MS and compared to a system blank of trace-metal-grade HCl, which was collected through the same filtration apparatus. Temperature measurements were recorded using a Teflon-coated k-type thermocouple.

Polymer deswelling was quantified in terms of the deswelling ratio (DR) shown in Eq. 3, where m_s is the weight of the swollen polymer and m_d is the weight of the final dry state [14]:

$$DR(\%) = 100\ x\ \frac{m_s - m_d}{m_s} \quad (3)$$

Mo recoveries were measured using ^{99}Mo radiotracer obtained from a commercial ^{99}Mo/^{99m}Tc generator (Lantheus Medical Imaging). Solid and liquid phases were transferred to 20-mL liquid scintillation vials prior to counting. Gamma counting of ^{99}Mo was performed on either an HPGe detector (Ortec) or a NaI gamma counter (Perkin Elmer), using the 740-keV peak.

4. 3. 3 Purification of Recovered Mo

Solvent extraction experiments were performed using the effluent recovered from SAP gel acidified to 5M HCl. This solution was added to an organic phase of 30% (v/v) TBP in tetrachloroethylene (TCE). The mixture was vortexed continuously for 20 min and centrifuged at 2000 rpm for 5 min. The organic phase was stripped using 3M NH_4OH (NH_3-basis), mixed for 5 min, and centrifuged. All aquous-phase volumes were recorded and Mo concentrations were determined by ICP-MS.

Chromatography experiments were done using commercial TBP resin (Triskem Inc.) with 50- to 100-µm particle size. Resin was dry packed into columns with 10-mm inner diameter and 20-µm-porosity polyethylene frits. The packed resin was pre-conditioned with 3 bed volumes of 5M HCl for at least 12 hours to ensure proper wetting. Gravity flow rates (approximately 1–2 mL/min) were used. Aliquots of the eluates were

collected in 4-mL polypropylene gamma-counting tubes or 20-mL liquid scintillation vials and counted as previously described.

4. 4 Results and Discussion

4. 4. 1 Deswelling Experiments

The plot in Figure 4-3 summarizes the key findings from deswelling experiments. The characteristics of SAP gel were investigated by adding HCl or brine solutions of monovalent (Na^{+}) or divalent (Ca^{2+}) cations. The purpose of these experiments was to determine conditions under which the maximum volume of Mo solution was desorbed from the gel and how they relate to Mo recovery. A second important consideration was the solid-phase characteristics after precipitation. In each case, the supernatant phase contained organic material leached from SAPs, which was evident from the effluent color and the turbidity of the solution. Therefore, purification of the effluent to remove dissolved organics was required regardless of the added solution.

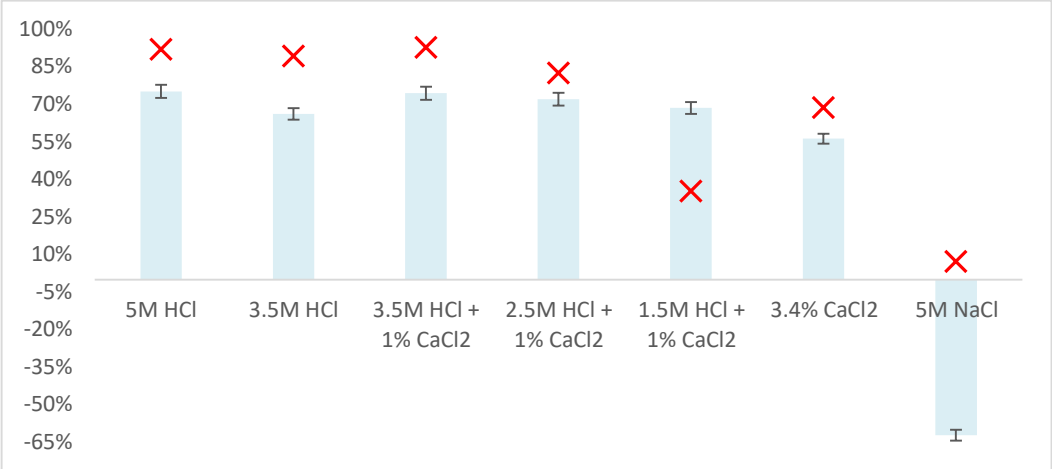

Figure 4-3. Deswelling of SAP hydrogel (columns) and Mo recovery (red X symbols) using HCl and $CaCl_2$. Concentrations correspond to the composition of solutions added to SAP gel (1:1 v/v)

In general, gel treated with HCl decreased in mass and settled to the bottom of the sample vial, where it formed a tackified precipitate. The polymer collapses because of neutralization of charges along the polymer chain by protonation or cation exchange with Ca^{2+}. Precipitation reactions appeared to reach equilibrium within 15 min, after which the mass of the precipitate remained constant. Gels treated with HCl concentrations of 5M or greater were similar to each other in their solid-phase characteristics. At concentrations lower than 5M HCl, the gel did not fully deswell and remained adherent to container surfaces. Gel treated with $CaCl_2$ brine formed a dense, white solid phase, indicating the precipitation of Ca-polyacrylate. As expected, the NaCl brine was mostly absorbed by the polymer, resulting in an overall increase in gel mass. The absorption of NaCl brine shows that SAP waste gel is below its swelling capacity for high-ionic-strength solutions.

Ca^{2+} and HCl were both effective at deswelling the hydrogel and releasing the Mo to the liquid phase (Figure 4-4). Maximum Mo recoveries (93%) and gel deswelling ratios (75%) were obtained from samples treated with ≥3.5M HCl, irrespective of $CaCl_2$ content. Below the maximum deswelling ratio, adding 1% $CaCl_2$ to HCl resulted in improved deswelling compared to $CaCl_2$-free solutions, but not improved Mo recovery.

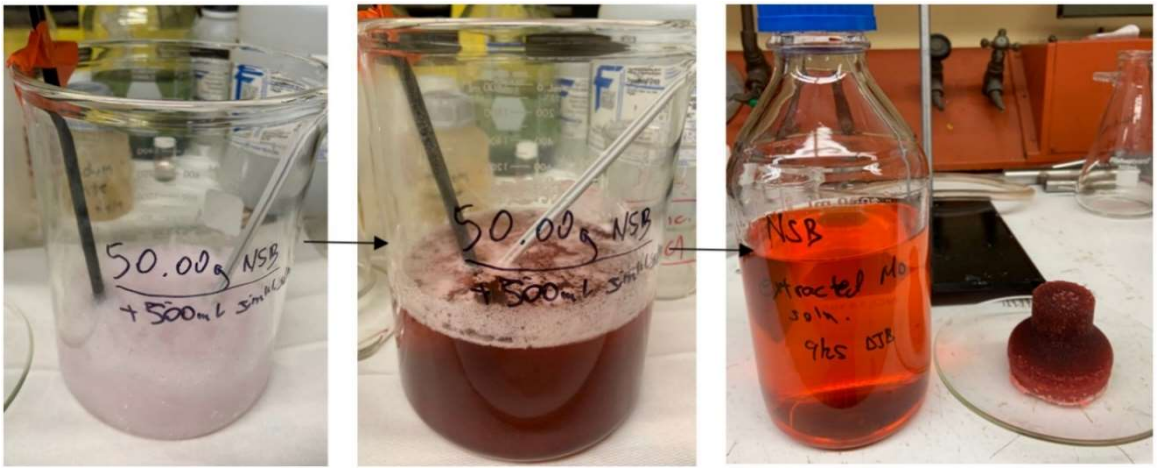

Figure 4-4. Simulated LSA generator waste gel (left), gel treated with HCl (middle), and the resulting liquid and solid phases after filtration (right)

While the addition of $CaCl_2$ did not improve Mo recovery in HCl solutions, its effect on the precipitate characteristics may be useful in the larger-scale processing of the gel. Ca precipitation produced denser and less adherent gel precipitates. This characteristic

could help to simplify waste handling and reduce surface contamination on laboratory equipment. In addition, $CaCl_2$ may be used to remove organic material that is leached to the aqueous stream during deswelling. This idea follows a similar principle used in wastewater treatment processes, where polyacrylates are used to remove metal contaminants by flocculation. However, adding $CaCl_2$ could produce undesired downstream effects, which were not investigated in this study. For example, Ca^{2+} may partition into the Mo fraction and affect the purification of Mo. $CaCl_2$ was therefore excluded from further experiments.

4. 4. 2 Mo Recovery with HCl

Mo recovery as a function of HCl concentration (0.5-10M) was further explored without added $CaCl_2$. The data in Figure 4-5 show that more than 90% of Mo can be extracted from the polymer using HCl concentrations of 3M or greater; above 3M HCl, the differences are minimal. The liquid matrix obtained is similar to that used in MOEX processing (≥5M HCl) [12]. Therefore, strong HCl solutions were used for all remaining

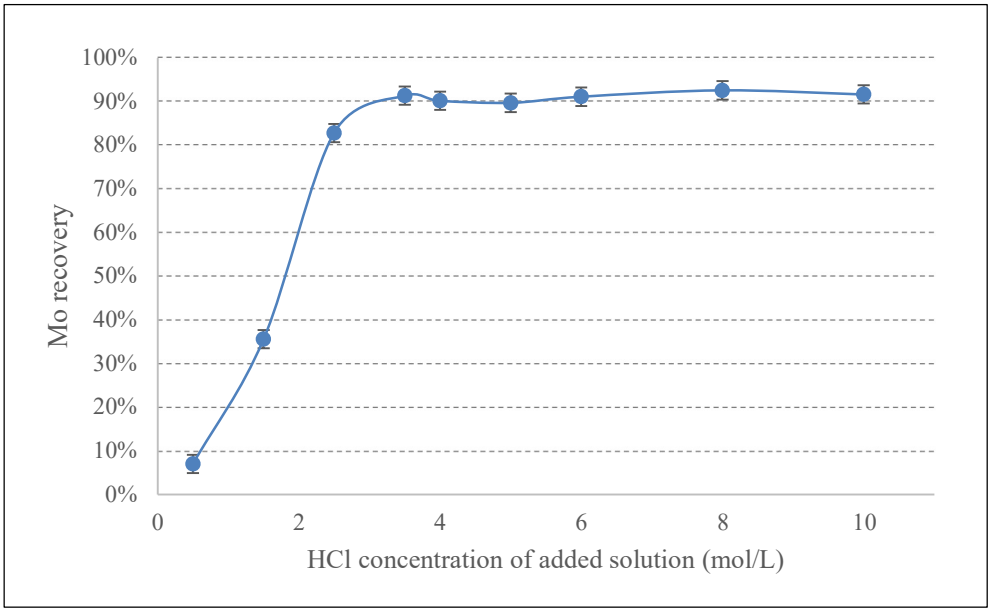

Figure 4-5. Total Mo recovery from SAP gel versus HCl concentration, after 1 hour equilibration time at room temperature. The HCl concentration represents the solution added to the gel, since the resulting mixture is a complex matrix

experiments. The final acidity of SAP gel when treated with 11M HCl is around 5M H^+, as determined by titration.

Washes of the gel were measured to determine the Mo recoveries per wash volume. Data in Table 4-1 show that the majority of Mo is carried in the effluent during the first filtration. Mo recovery (75%) is consistent with the gel deswelling ratios under these conditions (75%), indicating that Mo was solvated by HCl and minimally associated with the precipitated polymer. Consecutive HCl washes were able to remove most of the remaining Mo. The solid phase contained the remaining Mo (7%).

Table 4-1. Mo recovery from SAP gel treated with 10M HCl. A 5-g sample of 99Mo-spiked SAP simulant gel was deswelled with 5 mL of HCl for a 1 hour equilibration time prior to vacuum filtration

	Mo
Effluent	74.9%
Wash 1 – 2 mL, 5M HCl	11.4%
Wash 2 – 2 mL, 5M HCl	5.4%
Wash 3 – 2 mL, 5M HCl	1.5%
Total Mo recovered	**93.2%**

Figure 4-6 shows the kinetics of Mo extraction from the gel after acidification with 11M HCl in a 1:1 volume ratio. The data show that the bulk of the Mo extraction occurred very rapidly, with 89% of the Mo in the liquid phase after the first 2 min of contact time. This recovery rate parallels the rate of gel precipitation from deswelling experiments. However, when solid phases were then soaked in 5M HCl for an additional 12 hours, near-quantitative Mo recoveries were obtained.

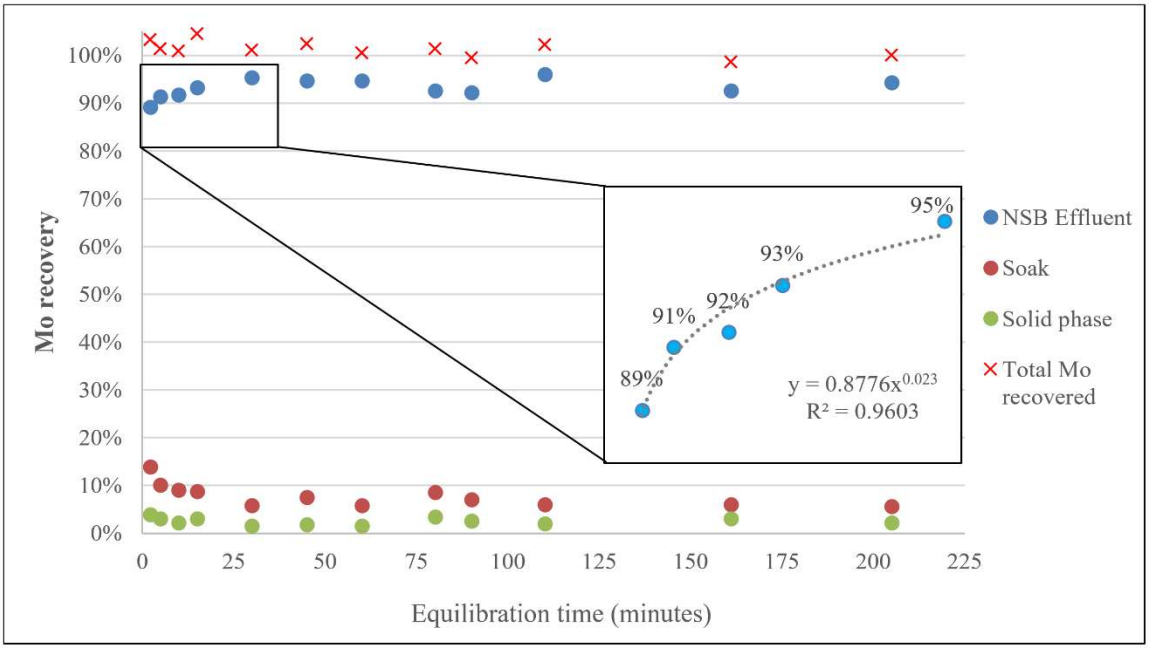

Figure 4-6. Mo recovery from SAP gel using concentrated HCl with different equilibration times. The mixture was vortexed intermittently, then filtered and washed at the corresponding time point. Each solid phase was then subjected to a 12-h soak in 5M HCl to recover the remaining Mo

Extraction equilibrium was reached within 30 min of contact time with HCl. The slow equilibration time is most likely caused by the diffusion-limited exchange of Mo through the dense polymer, which rapidly shrinks during the first 2 min of contact with HCl. Extended equilibration times in concentrated HCl caused signs of acidic degradation of the polymer after several days. It is possible that very high HCl concentrations cause the scission of the CH_2-CHR-CH_2 backbone and dissolution of low-molecular-weight fragments [15]. It is important to minimize the degradation of the polymer, which would complicate downstream purification processes. Therefore, soaking was done in 5M HCl, which produced no apparent signs of polymer degradation by 72 hours.

Table 4-2 shows the average values for Mo recovered after the mixture reached equilibrium (in ≥ 30 min). It can be seen that the majority of Mo is released from the polymer during the first HCl contact. Roughly 6–12% of Mo is left in the solid phase after the first HCl contact. Soaking the solid phase in 5M HCl led to extraction of most of the remaining Mo and reduced Mo losses to around 2%.

Table 4-2. Average equilibrium values for Mo recovery at each stage

	Mo Recovery ± S.D.
Effluent + washes	94.1% ± 1.3%
5M HCl soak	6.6% ± 2.4%
Solid phase	2.4% ± 0.7%
Total recovery	**100.7% ± 1.2%**

Overall, the data suggest that Mo can be nearly quantitatively separated from the bulk of the organic polymer using strong HCl. Two contacts of the gel with strong HCl, one 11M-HCl deswelling period and one 5M-HCl soak, were able to recover 98–100% of the Mo. However, as previously mentioned, the effluent from this reaction contains small amounts of organic contaminants derived from the SAP mixture. This is evident from the effluent color and occasional turbidity of recovered solutions. Mo must be separated from organic material prior to target fabrication. Preliminary experiments on the removal of organic contaminants will be discussed in later sections of this report.

4. 4. 3 Scaled-up Processing of LSA waste gel

A large 600-g batch of simulated LSA waste was acidified with 11M HCl to test the scaled-up process. Solution volumes and other reaction characteristics were recorded. Results from these experiments are shown in Table 4-3 and Figure 4-7.

Table 4-3. Volumes and deswelling ratio (DR) from a 600-g waste batch treated with HCl

	Mass (g)	Volume (L)
Initial NSB polymer	50.00	-
Simulant solution	548	0.50
Total starting gel	598	
11M HCl	-	0.55
5M HCl washes	-	0.04
Total volume of starting solution	-	1.09
Recovered liquid phase	-	1.00

Recovered solid phase	126.5	-
DR (%)	79%	

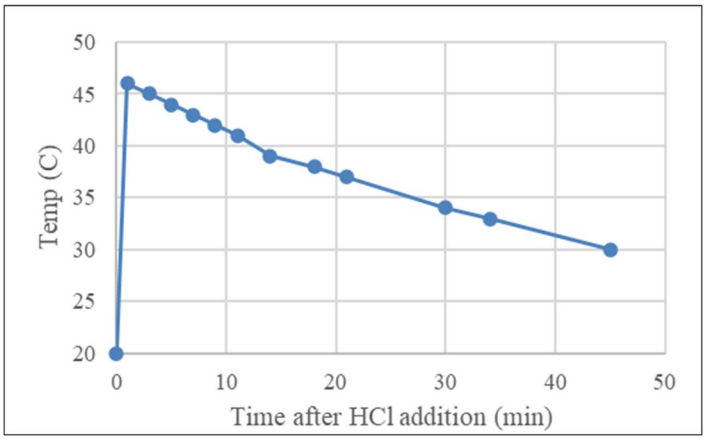

Figure 4-7. Solution temperature recorded during deswelling of 600-g SAP gel with concentrated HCl

It was noticed during large-scale processing of NSB gel that adding HCl resulted in the release of heat and white vapor, and foam formation. The recorded temperature reached a maximum of 47°C. It is likely that heat release is mainly due to the exothermic reaction of acid-base neutralization. Vapor formation is the result of acidic degradation of amide groups of the polymer, generating a carboxylic acid group and free ammonium ion. Liberated gaseous ammonia reacts with HCl fumes to produce white ammonium chloride gas following the reaction

$$NH_{3(g)} + HCl_{(g)} \rightarrow NH_4Cl_{(g)} \quad (4)$$

Hydrolysis of amide groups likely occurs on the acrylamide monomers but may also occur on crosslinkers between chains, resulting in the de-crosslinking and release of water-soluble polyacrylate fragments. However, the solid phase appeared to remain undissolved as a tackified precipitate. The overall reduction in SAP gel mass was 79%. The gel precipitate can be air-dried over several days to further reduce its mass, resulting in a low-activity, compact waste form.

4. 4. 4 Impurities

The purity of the extracted Mo product will be affected by contaminants accumulated from the LSA generator systems or from the SAP mixture. The tabulated results from the ICP-MS analysis of simulated and true waste are displayed in Table 4-4. Data from these samples were compared with a system blank using trace-metal-grade HCl filtered through the same apparatus.

Table 4-4. Metal impurities detected by ICP-MS after treatment of SAP waste gel (simulated and true waste) with concentrated HCl. Uncertainty associated with ICP-MS detection is ±10%

	Concentration (ppm)		
Element	Simulated Waste Solution	Effluent from Simulated Waste Gel (60-g Sample)	Effluent from SAP Waste Gel (55-g Sample)
Mo	3370	1400	1030
Na	55100	35200	34700
K	3910	1690	2120
P	ND[a]	4.48	9.13
Zn	ND	0.73	0.20
Sn	ND	0.18	0.19
Cu	ND	0.16	0.06
Mn	ND	0.09	0.04
Cr	ND	0.09	0.06
Ni	ND	0.07	0.05
Cs	ND	0.02	0.02
Zr	ND	0.01	0.01
B	ND	ND	ND
Al	ND	ND	ND
Ti	ND	ND	ND
Nb	ND	ND	ND
Si	ND	ND	ND
Ca	ND	ND	ND
Fe	ND	ND	ND
Cd	ND	ND	ND
Sb	ND	ND	ND
W	ND	ND	ND

[a] ND –below detectable limits.

The overall similarity between the simulated and true waste effluents indicates that the prepared simulant provides a very good approximation of true waste conditions. As expected, high concentrations of Na and K from the waste solution (NaOH, KOH) were leached from the SAP mixture. Another source of Na is the Na^+ counterions from Na-polyacrylate, which were likely replaced by acidic protons to form polyacrylic acid. The presence of Cs, Zr, and stainless steel corrosion products may significantly affect the radiochemical purity of recycled Mo upon irradiation, if these impurities are not removed. The final mass of Mo recovered per gram of SAP gel was 2.3 mg (simulant) and 1.9 mg (true waste gel). Judging from the true waste recovery, 1.9 g of Mo can be recovered per-kg waste gel using this method.

4. 4. 5 Solvent Extraction of Recovered Mo

Large-scale liquid-liquid extraction of Mo in HCl has been previously developed by Argonne for the recycle of enriched Mo material and is discussed in the literature [12], [13]. In strong HCl solutions, Mo can be extracted quantitatively using 30% TBP in TCE. This process achieves good decontamination with respect to Na and K, both of which are present at g/L levels in solutions recovered from SAP. The effluent contains ~5M HCl, 1.5M Na^+, 0.05M K^+, dissolved brilliant blue dye, and other organics. Table 4-5 shows Mo loss after solvent extraction of the effluent. The data show that there is minimal direct interference from organic contaminants with the extraction of Mo by TBP (98% recovery).

Table 4-5. Mo losses (± S.D.) during solvent extraction of Mo from recovered LSA waste solution, acidified to 5M acid concentration using HCl

	Volume (L)	Mo Lost (%)	Mo conc. (mM)
SAP effluent	0.820	-	19.5
Acidified solution	1.049	-	15.2
Stripped solution	1.049	2% ± 1%	14.8

The loss of a few percent of Mo is due to the formation of a solid third phase at the aqueous-organic interface after mixing. The thin interfacial film shown in Figure 4-8 appeared in all experiments where effluents from SAP extraction were used. It appears to be the result of the aggregation of amphiphilic organic molecules suspended in the aqueous solution. The film was easily removed by spatula in small-scale experiments. However, it would interfere with large-scale automated processing schemes where centrifugal contactors or mixer-settler-type extraction may be used.

Numerous approaches to removing these organic contaminants were tried (e.g., filtration, centrifugation, pH-adjustment, solvent exchange, pre-contacted organic phase), but they were not able to adequately separate dissolved organics to prevent third-phase formation. Therefore, extraction chromatography using TBP resin was briefly investigated as an alternative to solvent extraction which may avoid the problems associated with third-phase formation. Additionally, the use of TBP resin could simplify the procedure to separate Mo from the remaining organic material, concentrate Mo on the column, and elute it into ammonium hydroxide solution.

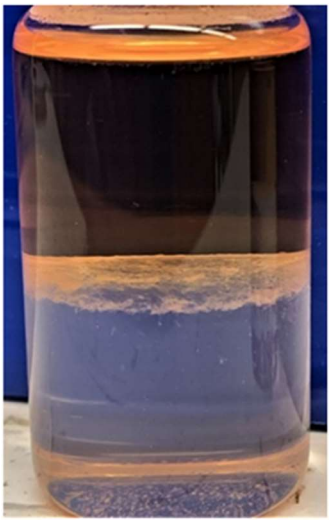

Figure 4-8. Contacting effluent from SAP waste with 30% TBP in TCE resulted in third-phase formation at the aqueous-organic interface

The preliminary results from a 1-g TBP resin column are presented in Figure 4-9. The data suggest that the resin is highly effective at concentrating Mo from the complex

feed matrix (SAP-derived) and eluting concentrated Mo. The sharp elution of Mo by NH_4OH suggests fast kinetics of MoO_2Cl_2 conversion to MoO_4^{2-}, which is consistent with the stripping behavior of Mo in solvent extraction. A separate column experiment confirmed this result and further suggested that the loading capacity of TBP resin for Mo in HCl is between 31 and 36 mg Mo/g TBP resin. However, fundamental studies will be needed to determine resin characteristics before designing a full-scale column.

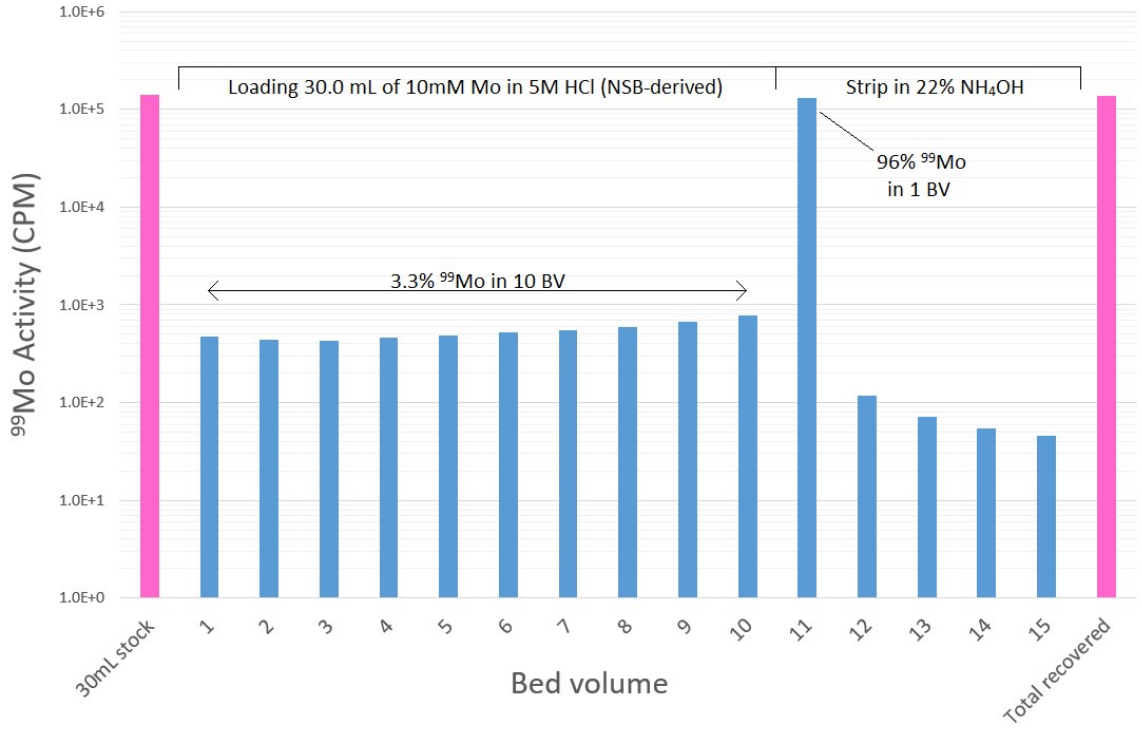

Figure 4-9. Loading and elution profiles from TBP resin (1.0 g resin) column chromatography of 10 mM Mo in 5 MHCl + 1.5M Na+. Bed volume (BV) was approximately 3.0 mL

The reason why a few percent of Mo was lost during the loading stage is unclear. One possible explanation is that unanchored TBP molecules are washing out through the column with the liquid phase. This problem could be corrected with more thorough washing of the resin before loading. But the determination of optimal feed conditions such as HCl concentration, flow rate, and weight distribution values were not in the scope of this report and will be presented in a separate work.

Mo was loaded onto the TBP column and directly eluted into NH_4OH. The product was evaporated and washed with 100% ethanol to produce a crystalline Mo product that

was verified by X-ray diffraction. Evaporation of Mo in excess NH_4OH will produce the AHM product, which is insoluble in ethanol. Alternatively, the loaded column may be washed with HCl to remove adsorbed organics and then eluted to produce a clear NH_4OH product. Quantitative analysis and optimization of these steps will be necessary to obtain the AHM product with the desired purity and yield.

4. 5 Conclusion

The chemical flow sheet in Figure 4-10 depicts the proposed Mo recycle process and recovery yields. The proposed process results in very high Mo recoveries from SAP-solidified LSA waste, in a chemical form that is readily recycled into new targets. The extraction of Mo from SAPs can be achieved by contacting the gel with strong HCl solutions. A strong acidic environment collapses the hydrogel, which densifies into a solid phase and releases the absorbed solution. Using HCl prevents molybdenyl coprecipitation with the polymer, owing to formation of neutral chloro-complexes that are freely released to the liquid phase. Near-quantitative Mo recoveries can be obtained after two HCl contacts (deswelling + soak). The solid waste mass of precipitated polymer constitutes 75% of the initial SAP mass and can be subsequently air-dried to produce a low-activity, compact waste form.

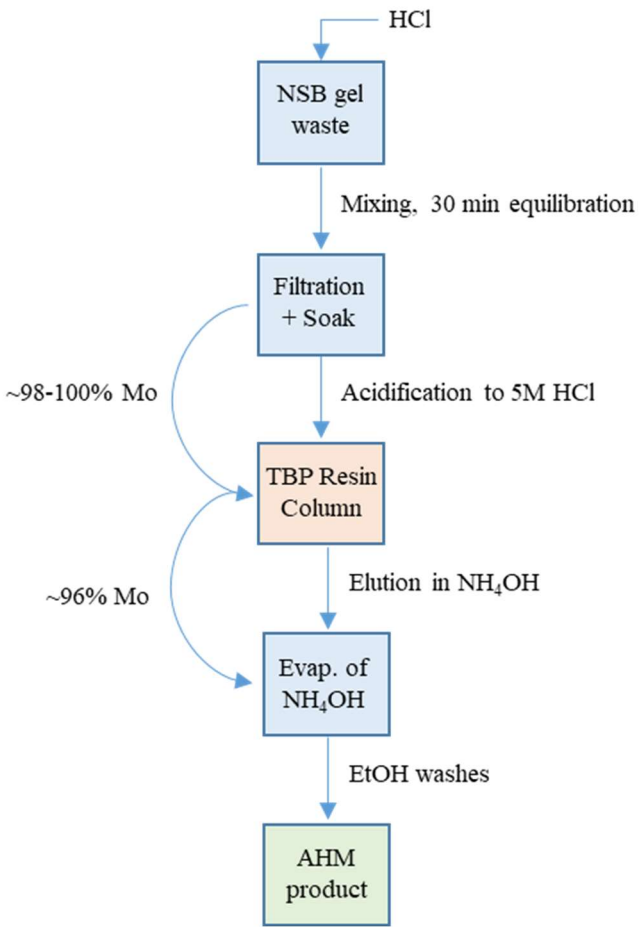

Figure 4-10. Proposed flow chart for the recovery of Mo from LSA waste solidified inn SAPs, with stepwise recovery yields

The use of high concentrations of HCl with SAPs resulted in the leaching out of small amounts of organic impurities. This leaching may be due to amide hydrolysis of crosslinker groups, or to chain scission. Organic molecules with surfactant properties then accumulate in the liquid phase and cause the formation of an interfacial third phase during solvent extraction. Various techniques were tested to separate the dispersed organic material from recovered solutions, including activated charcoal chromatography, nanofiltration, centrifugation, pH-controlled precipitation, Ca^{2+} precipitation, and pre-contacting with an organic phase. However, these techniques were not sufficient to avoid

the formation of a third phase, which prevents the use of large-scale solvent extraction methods.

Preliminary experiments using extraction chromatography with TBP resin showed promising progress toward resolving the problems associated with the third phase. Mo was adsorbed on the resin and eluted (96%) in a very low volume of NH_4OH. Mo can then be crystallized as AHM and washed with ethanol to remove remaining organic material.

4. 6 References

[1] E. P. Horwitz and A. H. Bond, "Purification of radionuclides for nuclear medicine: The multicolumn selectivity inversion generator concept," Czechoslov. J. Phys., vol. 53, no. S1, pp. A713–A716, 2003.

[2] M. J. Zohuriaan-Mehr and K. Kabiri, "Superabsorbent polymer materials: A review," Iranian Polymer Journal, vol. 17, no. 6, pp. 451–477, 2008.

[3] I. Sabbagh and M. Delsanti, "Solubility of highly charged anionic polyelectrolytes in presence of multivalent cations: Specific interaction effect," Eur. Phys. J. E, vol. 1, no. 1, pp. 75–86, 2000.

[4] R. S. Tomar, I. Gupta, R. Singhal, and A. K. Nagpal, "Synthesis of poly (acrylamide-co-acrylic acid) based superaborbent hydrogels: Study of network parameters and swelling behaviour," Polym. - Plast. Technol. Eng., vol. 46, no. 5, pp. 481–488, May 2007.

[5] B. Xiong et al., "Polyacrylamide degradation and its implications in environmental systems," npj Clean Water, vol. 1, no. 1, p. 17, Dec. 2018.

[6] J. D. Stahl, M. D. Cameron, J. Haselbach, and S. D. Aust, "Biodegradation of superabsorbent polymers in soil," Environmental Science and Pollution Research, vol. 7, no. 2, pp. 83–88, 2000.

[7] R. Schweins and K. Huber, "Collapse of sodium polyacrylate chains in calcium salt solutions," The Eur. Phys. J. E, vol. 5, pp. 117–126, 2001.

[8] M. Elsharafi, C. Chancellor, C. Kirby, and J. T. Ok, "Hydrochloride acid effect on the PH value of the superabsorbent polymer (SAP) solutions," Int. J. Petrochem. Sci. Eng., vol. 1, no. 2, pp. 21–26, 2016.

[9] S. Schiewer, “Modelling complexation and electrostatic attraction in heavy metal biosorption by Sargassum biomass,” in 16th Intl. Seaweed Symp., Developments in Hydrobiology, vol. 137. Springer, Dordrecht, 1999.

[10] J. J. Cruywagen and J. B. B. Heyns, “Molybdenum(VI) equilibria at high perchloric acid concentration,” Polyhedron, vol. 19, no. 8, pp. 907–911, 2000.

[11] P. Tkac, M. A. Momen, A. T. Breshears, M. A. Brown, and G. F. Vandegrift, “Molybdenum(VI) Coordination in Tributyl Phosphate Chloride Based System,” Ind. Eng. Chem. Res., vol. 57, no. 16, pp. 5661–5669, 2018.

[12] P. Tkac, M. A. Brown, A. Momen, K. E. Wardle, J. M. Copple, and G. F. Vandegrift, “MOEX: Solvent extraction approach for recycling enriched 98Mo/100Mo material,” Sep. Sci. Technol., vol. 53, no. 12, pp. 1856–1863, 2018.

[13] P. A. Kozak, P. Tkac, K. E. Wardle, M. A. Brown, and G. F. Vandegrift, “Demonstration of the MOEX process using additive-manufacturing-fabricated annular centrifugal contactors," Solvent Extraction and Ion Exchange, vol. 38, no. 1, pp. 120–131, 2020.

[14] Y. Wang et al., “Chitosan cross-linked poly(acrylic acid) hydrogels: Drug release control and mechanism,” Colloids Surfaces B Biointerfaces, vol. 152, pp. 252–259, Apr. 2017.

[15] Y. Pei, L. Zhao, G. Du, N. Li, K. Xu, and H. Yang, “Investigation of the degradation and stability of acrylamide-based polymers in acid solution: Functional monomer modified polyacrylamide,” Petroleum, vol. 2, no. 4, pp. 399–407, Dec. 2016.

CHAPTER 5 SUMMARY

The use of alternative technolgies to produce ^{99}Mo has recently achieved small-scale commerical production in the US. As the use of these technolgies progresses, efficient and economic radiochemical separation schemes are required. This disseration provides a brief look at the chemical science supporting ^{99}Mo development and contributes some fundamental and practical studies on the recycling and purification strategies for acclerator-produced ^{99}Mo.

The first of these studies (chapter 2) addresses the fundamental nature of Mo chemical speciation during large-scale recycling of Mo targets. In aqueous acidic solutions, the interesting chemistry of Mo gives rise to a series of complex simultaneous equilibria resulting in self-assembly of several polyoxometalate species that have been traditionally difficult to characterize. Many studies devoted the identification of polymolybdate complexes were performed in mildly acidic solutions (pH 2-6) where large polyanions, such as $[Mo_8O_{26}]^{4-}$, $[Mo_7O_{24}]^{6-}$, $[HMo_7O_{24}]^{5-}$, and $[Mo_{36}O_{112}(H_2O)_{16}]^{8-}$ occur as a result of Brønsted acid-base condensation-addition processes. At pH<0, as proton activity increases, the stability of Mo polyoxoanions decreases. At very high acidities, dinuclear cations of Mo(VI) show a strong tendency to form with characteristic UV absorption band at ~245nm. UV sepctra of concentrated Mo solutions were taken between 0.1-300mM Mo in 0.5-11M HCl to characterize Mo speciation during MOEX solvent extraction. In this work, it was shown that at 0.1mM Mo and 0.5–11 M HCl, monomeric Mo(VI) species predominate and the total contribution from dimeric species is below 1%. As the Mo concentration increases up to 300mM, absorbance spectra show the characteristic peak attributed to O-Mo-O bridging of cationic Mo dimers. Results from the equilibrium modeling and factor analysis of UV data revealed three major dimeric species present in HCl. The doubly and triply charged $Mo_2O_5^{2+}$ and $HMo_2O_5^{3+}$ cations, perviously determined in $HClO_4$ by other others, were stable in HCl solutions less than 4M. In addition, strong evidence was found for another species forming between 4-6M HCl. Based on equilibrium modeling, the singly chlorinated dinuclear cation $HMo_2O_5Cl^{2+}$ is the most likely species forming in these conditions, existing in relevant abundance even as high as 6M HCl at 300mM Mo.

Furthermore, it was demonstrated that for MOEX-relevant conditions (300mM Mo and 5M HCl) about 40% of Mo atoms exist in dinuclear form.

The development of a well-defined model system is required for understanding the behavior of Mo at high concentrations in acid solutions. The presense of cation Mo dimers does not directly effect the extraction efficiency of Mo during MOEX. Instead, this research provides a better understanding of the fundamental chemistry of molybdenum and presents formation constants that may be useful for chemical engineering applications or, for example, where alternative extraction methods might be used. It has also been known for many years that various elements can be incorporated into polynuclear structures forming heteroatomic structures. In Mo chemistry, heteropolymolybdate complexes can occur as mixed-valence Mo^{VI}-O-Mo^{V} entities such as $[MO^{VI}_{126}Mo^{V}_{28}O_{426}H_{14}(H_2O)_{70}]^{14-}$ (molybdenum blue) or with other elements like $[Se^{IV}Mo_6O_{21}(O_2CCH_2NH_3)_3]^{2-}$, $[As^{III}Mo_6O_{21}(O_2CCH_2NH_3)_3]^{3-}$, $[Bi^{III}Mo_6O_{21}(O_2CCH_2NH_3)_3]^{3-}$. Therefore, understanding Mo chemistry during repeated recycles of enriched $^{98/100}$Mo targets may improve our understanding of the ingrowth and propogation of metal impurities during industrial production of ^{99}Mo.

An especially important element to detect and separate from Mo prior to target irradiation is Re. Due to their similar chemistries, Re is found chiefly with copper ores containing molbdenite (MoS_2) where its exists as a lattice substitute (ReS_2) at about 0.02–0.20 wt% and thus is a common impurity in commercial Mo. Separation and detection of Re from Mo targets is essential for ensuring the radiopurity of accelerator-produced ^{99}Mo via neutron capture ^{98}Mo(n,γ)^{99}Mo. The two naturally occuring isotopes ^{185}Re (37.5%) and ^{187}Re (62.6%) have large thermal neutron absorption cross sections and produce short-lived neutron-activation products ^{186}Re ($T_{1/2}$ = 90.6 hr) and ^{188}Re ($T_{1/2}$ = 16.9 hr). The importance of detection and removal of Re from MoO_3 target material has been noted during the production of ^{99}Mo, where the presense of ^{186,188}Re neutron-activation products is observed. Therefore, efficient detection and purification strategies must be established to ensure the purity of Mo batches from commerically available Mo material and between consecutive recycles of targets. Two such methods were developed in this work (chapter

3) for the separation and detection of ultratrace Re in Mo targets. Using solvent extraction or extraction chromatography, Re dissolved in 4M H_2SO_4 can be quantitatively removed from Mo with a separation factor of about 3,300. Extraction of Re increases with H_2SO_4 concentration, reaching a distribution ratio of 207 at 4M H_2SO_4. Owing to excellent Re extraction, SF for Re/Mo increased with acid concentration from 100 to 1000 between 1 and 2 M H_2SO_4 to >1,000 for 4 M H_2SO_4 and above. The developed chromatographic method provides improved separation of Re from Mo compared to solvent extraction. Ultrahigh-purity MoO_3 powder samples were tested in roughly 1-g quantities by solvent extraction and column chromatography and showed close agreement in the determination of Re content. Detection limits in ICP-MS analysis were improved using matrix-matching to result in final values of L_D = 0.1 ng Re/g Mo and L_Q = 0.3 ng Re/g Mo for Re in bulk Mo samples. These values offer greatly enhanced detection of Re in solid Mo target material by a factor of about 5×10^4. These methods ensure that Re content in Mo targets can be quantified at very low levels to ensure the radiopurity of the ^{99}Mo product. By bypassing post-irradiation radiochemical separations of $^{186/188}$Re, time-consuming processing schemes may be altogether avoided and the delivery of ^{99}Mo to the customer be expedited.

Use of modern, low specific activity ^{99}Mo/^{99m}Tc generators in hospitals and radiopharmacies can result in the loss of unirradiated enriched $^{98/100}$Mo to the generator waste stream. This is not a problem when natural Mo targets are used. But the recycling of enriched Mo is of great practical importance for commerical ^{99}Mo producers. Despite during each milking, generator systems can lose roughly ~1% of eMo into waste stream, netting a cumulative loss of ~20-30% of eMo material into the waste. Typically, the waste stream is composed of NaOH and saline (NaCl) solution with small amounts of K_2MoO_4 in 5M KOH. This waste stream is solidified in a waste container using a proprietary “superabsorbent polymer”. The final work of this dissertation (chapter 4) proposese a simple chemical recycling process that results in very high Mo recoveries from superabsorbant polymer (SAP)-solidified waste from low specific activity generators.

Extraction of Mo from SAPs can be achieved by contacting the gel with strong HCl solutions. A strong acidic environment collapses the hydrogel, which densifies into a solid phase and releases the absorbed solution. Using HCl prevents molybdenyl coprecipitation with the polymer, owing to formation of neutral chloro-complexes that are freely released to the liquid phase. Near-quantitative Mo recoveries can be obtained after two HCl contacts (deswelling + soak). The solid waste mass of precipitated polymer constitutes 75% of the initial SAP mass and can be subsequently air-dried to produce a low-activity, compact waste form. The use of high concentrations of HCl with SAPs resulted in the leaching out of small amounts of organic impurities. This leaching may be due to amide hydrolysis of crosslinker groups, or to chain scission. Organic molecules with surfactant properties then accumulate in the liquid phase and cause the formation of an interfacial third phase during solvent extraction. Various techniques were tested to separate the dispersed organic material from recovered solutions, including activated charcoal chromatography, nanofiltration, centrifugation, pH-controlled precipitation, Ca^{2+} precipitation, and pre-contacting with an organic phase. However, these techniques were not sufficient to avoid the formation of a third phase, which prevents the use of large-scale solvent extraction methods. Preliminary experiments using extraction chromatography with TBP resin showed promising progress toward resolving the problems associated with the third phase. Mo was adsorbed on the resin and eluted (96%) in a very low volume of NH_4OH. Mo can then be crystallized as AHM and washed with ethanol to remove remaining organic material.